Advances in Anatomy
Embryology and Cell Biology
191

Anton B. Tonchev · Tetsumori Yamashima
George N. Chaldakov

Distribution and Phenotype of Proliferating Cells in the Forebrain of Adult Macaque Monkeys After Transient Global Cerebral Ischemia

Springer

Reviews and critical articles covering the entire field of normal anatomy (cytology, histology, cyto- and histochemistry, electron microscopy, macroscopy, experimental morphology and embryology and comparative anatomy) are published in Advances in Anatomy, Embryology and Cell Biology. Papers dealing with anthropology and clinical morphology that aim to encourage cooperation between anatomy and related disciplines will also be accepted. Papers are normally commissioned. Original papers and communications may be submitted and will be considered for publication provided they meet the requirements of a review article and thus fit into the scope of "Advances". English language is preferred.

It is a fundamental condition that submitted manuscripts have not been and will not simultaneously be submitted or published elsewhere. With the acceptance of a manuscript for publication, the publisher acquires full and exclusive copyright for all languages and countries.

Twenty-five copies of each paper are supplied free of charge.

Manuscripts should be addressed to

Prof. Dr. F. **BECK**, Howard Florey Institute, University of Melbourne,
Parkville, 3000 Melbourne, Victoria, Australia
e-mail: fb22@le.ac.uk

Prof. Dr. F. **CLASCÁ**, Department of Anatomy, Histology and Neurobiology,
Universidad Autónoma de Madrid, Ave. Arzobispo Morcillo s/n, 28029 Madrid, Spain
e-mail: francisco.clasca@uam.es

Prof. Dr. M. **FROTSCHER**, Institut für Anatomie und Zellbiologie, Abteilung für Neuroanatomie,
Albert-Ludwigs-Universität Freiburg, Albertstr. 17, 79001 Freiburg, Germany
e-mail: michael.frotscher@anat.uni-freiburg.de

Prof. Dr. D. E. **HAINES**, Ph.D., Department of Anatomy, The University of Mississippi Med. Ctr.,
2500 North State Street, Jackson, MS 39216-4505, USA
e-mail: dhaines@anatomy.umsmed.edu

Prof. Dr. H.-W. **KORF**, Zentrum der Morphologie, Universität Frankfurt,
Theodor-Stern Kai 7, 60595 Frankfurt/Main, Germany
e-mail: korf@em.uni-frankfurt.de

Prof. Dr. E. **MARANI**, Department Biomedical Signal and Systems, University Twente,
P.O. Box 217, 7500 AE Enschede, The Netherlands
e-mail: e.marani@utwente.nl

Prof. Dr. R. **PUTZ**, Anatomische Anstalt der Universität München,
Lehrstuhl Anatomie I, Pettenkoferstr. 11, 80336 München, Germany
e-mail: reinhard.putz@med.uni-muenchen.de

Prof. Dr. Dr. h.c. Y. **SANO**, Department of Anatomy,
Kyoto Prefectural University of Medicine,
Kawaramachi-Hirokoji, 602 Kyoto, Japan

Prof. Dr. Dr. h.c. T.H. **SCHIEBLER**, Anatomisches Institut der Universität,
Koellikerstraße 6, 97070 Würzburg, Germany

191
Advances in Anatomy Embryology and Cell Biology

A. B. Tonchev · T. Yamashima
G. N. Chaldakov

Distribution and Phenotype of Proliferating Cells in the Forebrain of Adult Macaque Monkeys after Transient Global Cerebral Ischemia

With 65 Figures and 11 Tables

Springer

Anton B. Tonchev, Dr.
George N. Chaldakov, Dr.

Division of Cell Biology
Department of Forensic Medicine
Varna University of Medicine
55 Marin Drinov str.
9002 Varna
Bulgaria

e-mail: atontchev@yahoo.com
chaldakov@yahoo.com

Tetsumori Yamashima, Dr.

Department of Restorative Neurosurgery
Division of Neuroscience
Kanazawa University Graduate School of Medical Science
Takara-machi 13-1
Kanazawa 920-8641
Japan

e-mail: yamashim@med.kanazawa-u.ac.jp

ISSN 0301-5556
ISBN 978-3-540-39613-0 Springer Berlin Heidelberg New York

Editor: Simon Rallison, Heidelberg
Desk editor: Anne Clauss, Heidelberg
Production editor: Nadja Kroke, Leipzig
Cover design: WMX Design Heidelberg
Typesetting: LE-TEX Jelonek, Schmidt & Vöckler GbR, Leipzig
Printed on acid-free paper SPIN 11688396 27/3150/YL – 5 4 3 2 1 0

List of Contents

Preface

Most of the investigations described in the present paper were performed at the Department of Restorative Neurosurgery, Graduate School of Medical Sciences, Kanazawa University, Kanazawa, Japan, and some were carried out in the Division of Cell Biology, Varna University of Medicine, Varna, Bulgaria. The adult monkey cell proliferation project was initiated to provide information in non-human primates relevant to clinical conditions in humans. The proliferation patterns seen in adult monkey brains after global ischemia are just a step toward a deeper understanding of the molecular and cellular mechanisms that specify cell fate in postischemic primate telencephalon. Additional studies in monkeys are necessary to identify primate-specific brain repair mechanisms occurring after ischemic insults and other injuries, focusing on focal ischemic models as focal stroke is more common than global ischemia in humans.

At the same time, the model of global cerebral ischemia provides an excellent opportunity to study the regenerative capabilities of distant from one another telencephalic regions after a common for all insult. Thus, we initially investigated global cerebral ischemia, and we are now analyzing in-depth the molecular determinants involved in modulating cellular responses. We hope the data described in this paper may trigger further interest in non-human primate neurogenesis research. We are grateful to those who supported us during these studies. Hideyuki Okano, Kazunobu Sawamoto, Masahiko Watanabe, Nobuyuki Takakura, Luigi Aloe and Marco Fiore provided stimulating and critical discussions. Masao Yukie, Hiroshi Yamamoto, Ivan Stankulov and Peter Ghenev were always enthusiastic in their support. We express our gratitude to Liang Zhao and Xiangdi Wang for their excellent technical assistance. We are also indebted to Kiyoko Wada, Eiko Sakaguchi and Penka Filipova for secretarial assistance. We thank Ron Mathison for critically reading parts of the manuscript. Finally, our special thanks go to our families for their unwavering support.

Abbreviations

BDNF	Brain-derived neurotropic factor
bFGF	Basic fibroblast growth factor
BrdU	Bromodeoxyuridine
CA	*Cornu Ammonis*
CNP	2′,3′-Cyclic nucleotide 3′-phosphodiesterase
CNS	Central nervous system
DG	Dentate gyrus
DGL	Dentate granule cell layer
EGF	Epidermal growth factor
GAD	Glutamic acid decarboxylase
Gadd45	Growth arrest and DNA damage inducible gene 45
G-CSF	Granulocyte colony-stimulating factor
GDNF	Glial cell line-derived neurotrophic factor
GFAP	Glial fibrillary acidic protein
Ham56	Human alveolar macrophage 56 antigen
HB-EGF	Heparin-binding EGF-like growth factor
Iba1	Ionized calcium binding adapter molecule 1
IGF-1	Insulin-like growth factor-1
IT	Inferior temporal cortex
ITG	Inferior temporal gyrus
MTG	Middle temporal gyrus
NeuN	Neuronal nuclei
PHG	Parahippocampal gyrus
PHR	Parahippocampal region
PSA-NCAM	Polysialylated neural cell adhesion molecule
RMS	Rostral migratory stream
SCF	Stem cell factor
SDF-1α	Stromal cell-derived factor-1α
SGZ	Subgranular zone
STG	Superior temporal gyrus
SVZ	Subventricular zone
VEGF	Vascular endothelial growth factor
TUC4	TOAD/Ulip/CRMP 4
TUNEL	Terminal deoxynucleotidyltransferase (TdT)-mediated UTP nick end labeling

1 Introduction

1.1 Studies on Cell Proliferation in Adult Primate Brain

Until a few decades ago, a central postulate in neuroscience had been that the adult mammalian brain was unable to regenerate its neurons (Ramon y Cajal 1928). Although early studies reporting mitoses in postnatal (Hamilton 1901) and adult (Allen 1912) rat brain suggested the existence of postnatal progenitor cells in the adult mammalian central nervous system (CNS), it was not until the demonstration of de novo-generated cells (e.g., Schultze and Oehlert 1960) with tritiated (H^3)-thymidine was the potential of the adult CNS to replace some of its neurons confirmed. While at first mainly nonneuronal cells were investigated for H^3-thymidine labeling (Messier et al. 1958; Altman 1962a), a series of studies in the 1960s by Joseph Altman and co-workers was the first to show that de novo generation of neurons occurs in the hippocampus and possibly in other regions of the adult mammalian brain (Altman 1962b, 1963; Altman and Das 1965, 1966). Altman's results in rodents were confirmed in the next decades by Michel Kaplan and his collaborators (Kaplan and Hinds 1977; Kaplan 1981; Kaplan and Bell, 1983; 1984) as well as in birds by Fernando Nottebohm and coworkers (Goldman and Nottebohm 1983; Paton and Nottebohm 1984; reviewed by Nottebohm 2002).

These H^3-thymidine marker studies in lower mammals raised the question as to whether neuronal replacement by immature (progenitor) cells also occurs in adult primate brain. Studies reporting the presence of mitotic cells in the subependymal layer (also referred to as subventricular zone, SVZ) of the lateral ventricle of adult monkey brain (Lewis 1968; Kaplan 1983) suggested the presence of immature cells in adult primate CNS whose progeny could potentially be glial or neuronal cells, and thus prompted for a further investigation. Subsequent experiments performed in the laboratory of Pasko Rakic demonstrated renewal of oligodendrocytes, astrocytes, microglia, and vascular cells in a dozen of postpubertal monkeys injected with H^3-thymidine, but failed to detect evidence for neuronal replacement in any of the major brain subdivisions studied: neocortex, hippocampus, olfactory bulb, basal ganglia, thalamus, retina, cerebellum, brain stem, and spinal cord (Rakic 1985a, b). H^3-thymidine incorporation was detected in the nuclei of progenitor-like cells or astrocytes in the hippocampus, but not in neurons (Eckenhoff and Rakic 1988). Thus, adult neurogenesis was assumed not to occur in primate CNS, although with the introduction of new investigative tools this conclusion has been reversed.

The first advance came with the visualization of DNA synthesis immunohistochemically using bromodeoxyuridine (BrdU) (Miller and Nowakowski 1988). The second significant advance was the identification of new markers that allowed neurons to be distinguished from glia and that more precisely determined the developmental stage of cell populations (reviewed by Pevny and Rao 2003). These

techniques, now used in combination, permitted the determination of the "birthday" of a selective cell phenotype, such that the generation of new neurons in at least two regions of the adult rodent brain—the hippocampal dentate gyrus (DG) and SVZ—was convincingly demonstrated (reviewed by Gage et al. 1998; Garcia-Verdugo et al. 1998; Gage 2000). In primates, BrdU staining in adult monkey SVZ (McDermott and Lantos 1991) supported previous work with H^3-thymidine (Kaplan 1983). Subsequently, double-labeling experiments using BrdU and various cell markers provided evidence for the addition of new neurons to adult monkey DG (Gould et al. 1998; Gould et al. 1999a; Kornack and Rakic 1999) and olfactory bulb (Kornack and Rakic 2001a; Bedard et al. 2002a). Importantly, incorporation of BrdU in DG neurons was detected in the hippocampus of adult humans up to 781 days after BrdU injection (Eriksson et al. 1998). As a consequence, the dogma that no new neurons are added to the adult brain needed to be reconsidered (Gross 2000).

While the presence of neurogenesis in adult monkey DG and olfactory bulb is now generally accepted, its existence outside these regions remains controversial. Reports of neuronal renewal in normal monkey neocortex (Gould et al. 1999b, 2001; Bernier et al. 2002) were challenged (Kornack and Rakic 1999b; Koketsu et al. 2003), and a similar controversy exists for rodents, with both the absence (Magavi et al. 2000) and presence (Dayer et al. 2005) of neurogenesis in normal neocortex being claimed. Adult neurogenesis in the striatum (Bedard et al. 2002b) and amygdala (Bernier et al. 2002) of monkeys has been proposed. While studies in monkeys mostly involve normal animals, one report showed alterations of monkey DG progenitor proliferation after stress (Gould et al. 1998), thus demonstrating the ability of primate precursors to respond to changes in the environment. In addition, several papers have reported in vitro neurogenesis in human hippocampus (Roy et al. 2000), olfactory bulb (Pagano et al. 2000), and cortex (Nunes et al. 2003).

1.2 Methodological Considerations in Detecting Cell Proliferation

For practical purposes the methods used to study cell proliferation can be divided into two groups: (1) those that allow labeling of both dividing cells and their postmitotic daughter cells; and (2) those that selectively identify dividing cells but cannot identify their postmitotic progeny.

The H^3-thymidine and BrdU methods label both dividing cells and their progeny. These chemicals become incorporated into DNA of dividing cells during the S phase of the cell cycle, and are carried into the daughter cells. However, strictly speaking H^3-thymidine and BrdU indicate DNA synthesis, but do not clearly prove that cell division has occurred (Nowakowski and Hayes 2001). This distinction is important as there are several instances when BrdU (or H^3-thymidine) can be incorporated into DNA by nonmitotic processes such as DNA repair (Rakic 2002a, b), apoptosis (Katchanov et al. 2001; Kuan et al. 2004), or the development of polyploidy (Yang et al. 2001). As cell proliferation is frequently studied using

BrdU under conditions causing cell injury that may involve one or more of the nonmitotic processes (see next section for details), it is crucial to perform experiments that distinguish between mitotic and nonmitotic BrdU incorporation (Nowakowski and Hayes 2001; Rakic 2002a, b).

Recombinant retroviruses have become a useful tool for labeling proliferating cells and their descendants. Integration of the retroviral genome into the host cell requires a passage through the M phase, and therefore most retroviruses only successfully integrate in mitotic cells (Luskin 1993; reviewed by Cepko et al. 1998). Because of their unique features, retroviruses are suitable for the labeling of neural precursor cells and their progeny, and they can also be used for gene delivery into cells (Kageyama 2003). In contrast to BrdU immunohistochemistry, the retrovirus system does not require fixation and thus can be used with living cells. The recording of neuronal electrophysiological activity in adult-generated neurons would represent a direct proof of functional neurogenesis in vivo (van Praag et al. 2002; Carleton et al. 2003).

A second group of histochemical methods identifies cells that divide at a certain moment of time but cannot trace their offspring. In addition to the simplest of these methods—detection of mitotic figures in routinely stained histological sections (e.g., Lewis 1968)—several marker proteins, revealed by immunohistochemistry, visualize proliferating cells. Two commonly used markers are Ki67 and phosphohistone H3. The antigen Ki67 is present in all phases of the cell cycle except G_0, and the transition from a proliferative to nonproliferative state is rapidly followed by its disappearance, which makes it an excellent tool to determine the proliferating cell fraction in a given cell population (Scholzen and Gerdes 2000). In contrast to BrdU, which can be incorporated into DNA only during S phase, Ki67 is expressed also in G_1, G_2, and M phases. Furthermore, since Ki67 is an endogenous cell antigen, it does not require external application (e.g., in the form of injection) as in the case of BrdU or H^3-thymidine (Kee et al. 2002). Therefore, Ki67 is particularly suitable for studies in humans. The phosphorylated form of histone H3 (phosphohistone H3) is selectively expressed in the M phase (Hendzel et al. 1997; Strahl and Allis 2000) and consequently stains fewer proliferating cells than Ki67 (Tonchev et al. 2003b). However, because of its selective expression in the M phase, phosphohistone H3 is an unequivocal mitotic marker, while Ki67, like BrdU, can be expressed in nonmitotic cells with certain types of injury (Kuan et al. 2004). Other immunohistochemically identifiable proliferation markers include molecules involved in the regulation of cell cycle and DNA replication, and these are reviewed elsewhere (e.g., Saeger 2004).

1.3 Cell Proliferation in Rodent Brain After Ischemia

In the widely used rodent models, various conditions or factors affecting the proliferation and differentiation of neural progenitor cells have been described. Adult brain injury, which has been most intensively studied, can activate an endogenous

program of neurogenesis and gliogenesis (reviewed by Kuhn et al. 2001; Hallbergson et al. 2003; Parent 2003; Lie et al. 2004). Cerebral ischemia, as the most common cause of brain damage, has received considerable attention.

Two types of circulatory perturbations contribute to different types of ischemic injury to the brain (reviewed by Lipton 1999): (1) stroke (a complete occlusion of a cerebral artery) irreversibly kills the neurons in its core region and severely damages others in the penumbral region; and (2) reversible circulatory arrest, with a transient total stop of cerebral blood flow, selectively kills vulnerable cell populations. These clinical conditions can be studied in animals, with focal ischemic models replicating stroke and global ischemic models replicating cardiac arrest.

Early studies on postischemic cellular proliferation using H^3-thymidine were confined to glial cell regeneration (Du Bois et al. 1985). The first demonstration of increased neurogenesis in adult mammalian brain after ischemia was a study by Liu et al. (1998) showing increased postischemic neurogenesis in hippocampal DG in a model of transient global cerebral ischemia in gerbils. Lui et al. (1998) demonstrated that global ischemia increased cell proliferation 12-fold (as measured by BrdU incorporation) in the subgranular zone (SGZ) of DG with a peak in the second postischemic week. Investigation of the long-term fate of BrdU-positive ($BrdU^+$) cells revealed that over half of them acquired a neuronal phenotype in the dentate granule cell layer (DGL) of DG, while a smaller fraction had become astrocytes in the CA4 sector. These observations were repeated in mice (Takagi et al. 1999) and rats (Kee et al. 2001), confirming generalized postischemic, neurogenic enhancement among various rodent species. Kee et al. (2001) demonstrated that ischemia increases the quantity of adult-generated neurons in DGL, but does not modify neuronal differentiation. Importantly, the $BrdU^+$ cells in SGZ were identified as neural progenitor cells (Yagita et al. 2001), and the gradual increase in the expression of the marker indicates a stepwise cellular maturation before integration into the DGL (Iwai et al. 2002). This observation supports the conclusion that $BrdU^+$ neurons in DGL are derived from $BrdU^+$ progenitors in SGZ, and further confirmation was obtained using a retroviral vector (Tanaka et al. 2004). The use of a retroviral vector (Tanaka et al. 2004) also demonstrated that adult-generated neurons after ischemia are able to extend dendrites into the molecular layer of DG as is seen in normal animals (van Praag et al. 2002).

Studies on the regulation of DG neurogenesis after global ischemia led to a surprising result. A neurotrophin—brain-derived neurotrophic factor (BDNF)—was known for its stimulatory effect on SVZ progenitor proliferation and neuronal differentiation under normal conditions (Zigova et al. 1998; Pencea et al. 2001a; Benraiss et al. 2001) and a similar effect on DG progenitors would be deduced to exist after ischemia. However, Larsson et al. (2002) found that BDNF actually suppressed postischemic DG neurogenesis. Accordingly, blockade of BDNF receptor increased the number of adult-generated DG neurons after ischemia (Gustafsson et al. 2003). These results are important as they suggest that the potential neuroprotective agents may have differential effects on progenitor cell proliferation and

differentiation depending on the region and type of injury. Thus, the effects of every agent on a particular progenitor cell population need to be carefully addressed in each model of disease.

As transient ischemic injury is detrimental for the pyramidal neurons of the hippocampal CA1 sector, while in DG it causes little or no damage (Kirino 1982; Pulsinelli et al. 1982; Smith et al. 1984), the above-mentioned studies could not provide evidence that the new neurons replace neurons that had died. Similarly, although global ischemia was demonstrated to activate progenitor cells and neurogenesis in the other well-recognized germinative zone, SVZ (Iwai et al. 2003), evidence for replacement in the SVZ/olfactory bulb pathway has not been shown either. However, the CA1 sector that is vulnerable to ischemia represents a good model for testing whether endogenous neural progenitors are capable of postischemic neuronal replacement in vivo. Combining BrdU infusion with retroviral injections, Nakatomi et al. (2002) reported that a limited number of CA1 neurons can be regenerated by endogenous progenitors. Furthermore, after an intracerebroventricular infusion of basic fibroblast growth factor (bFGF) and epidermal growth factor (EGF), the increase in the number of progenitor-generated CA1 neurons was sufficient to ameliorate postischemic neurological deficits as the new CA1 pyramidal cells integrated into circuitry and expressed functional synapses (Nakatomi et al. 2002). Subsequent experiments in adult (Schmidt and Reymann 2002; Bendel et al. 2005) and neonatal (Daval et al. 2004) animals support these observations and suggest that the rodent brain possesses an endogenous ability to repair damage to hippocampal CA1 neurons. However, a note of caution should be expressed as ischemia can trigger a nonmitotic incorporation of BrdU and positive Ki67 signals in CA1 neurons as a result of cell cycle activation prior to cell death (Kuan et al. 2004). A false interpretation of neurogenesis is possible.

In addition to global ischemic models, cell proliferation and neurogenesis have also been studied in models of focal ischemic injury such as seen with ligation of the middle cerebral artery. Initial studies revealed that focal ischemic infarction in one hemisphere triggered progenitor cell proliferation in the ipsilateral and/or contralateral SVZ and SGZ (Jin et al. 2001; Zhang et al. 2001), but only the ipsilateral progenitors survived in the long term (Takasawa et al. 2002). Further studies refined our understanding of stroke-induced neurogenesis in three important aspects. First, neuronal replacement, as suggested by Nakatomi et al. (2002) in the CA1 sector, occurs since progenitor cells residing in SVZ migrate after an ischemia toward the adjacent striatum where they differentiate into medium spiny neurons—the cell type killed by ischemia (Arvidsson et al. 2002; Parent et al. 2002). Second, a variety of stimuli and agents affect postischemic neuronal generation, and these include growth factors/cytokines such as bFGF (Yoshimura et al. 2001), EGF (Teramoto et al. 2003), heparin-binding EGF-like growth factor (HB-EGF; Jin et al. 2002a; Sugiura et al. 2005), vascular endothelial growth factor (VEGF; Sun et al. 2003), stem cell factor (SCF; Jin et al. 2002b), insulin-like growth factor-1 (IGF-1; Dempsey et al. 2003), glial cell line-derived neurotrophic factor (GDNF; Dempsey et al. 2003), granulocyte colony-stimulating factor (G-CSF; Shyu et al.

2004; Schneider et al. 2005), and stromal cell-derived factor-1α (SDF-1α; Imitola et al. 2004), neurotransmitters such as nitric oxide (Keynes and Garthwaite 2004) and glutamate (Arvidsson et al. 2001), and conditions such as environmental enrichment (Komitova et al. 2005a), physical exercise (Komitova et al. 2005b), and ionizing radiation (Raber et al. 2004). Third, the preservation of stroke-activated neurogenesis, albeit at a lower level (Jin et al. 2004; Darsalia et al. 2005), is clinically relevant as stroke occurs more frequently in aged humans.

Interestingly, SVZ progenitor migration that is normally directed to the olfactory bulb was shown to be redirected toward the ischemic cortex (Jin et al. 2003). This exciting finding accords with a previous report of neurogenesis in ischemic neocortex (Jiang et al. 2001), but this issue remains controversial (Arvidsson et al. 2002). Furthermore, ischemia can increase neuronal differentiation and symmetric divisions of SVZ progenitors (Zhang et al. 2004). Electrophysiological investigation of postischemic precursors revealed that an ischemic stimulus shifts their current profile from passive toward a complex physiologic phenotype (Kronenberg et al. 2005), thus providing electrophysiological evidence for activation.

While all of the above-mentioned studies were performed using adult models, the effects of focal ischemia on SVZ or SGZ precursor cells were also investigated in neonatal animals. Unilateral hypoxic–ischemic injury elicited an increase of $BrdU^+$ cells in ipsilateral hippocampus, mainly DG, and the number of $BrdU^+$ neuronal cells was also increased in DG, while the number of oligodendrocytes decreased (Bartley et al. 2005). Ischemia also upregulated progenitor cell proliferation in neonatal SVZ, peri-infarct striatum (Plane et al. 2004), and cortex (Fagel et al. 2006). However, a more severe insult had the opposite effect, reducing the ability of SVZ to generate progenitors (Levison et al. 2001).

To date, over 100 papers have been published addressing the issue of postischemic neurogenesis, and the reader is referred to a number of recent reviews for further information and analysis on the topic (Sharp et al. 2002; Kokaia and Lindvall 2003; Felling and Levison 2003; Lindvall and Kokaia 2004; Abrahams et al. 2004; Zhang et al. 2005; Lichtenwalner and Parent 2006).

1.4 Global Cerebral Ischemia in Primates

The detrimental effects of global ischemic injury following circulatory arrest on the human brain had long been recognized (Neubuerger 1954), but a better understanding of the pathology required the development of appropriate nonhuman primate models (Brierley et al. 1969; Wolin et al. 1971; Nemoto et al. 1977). While these early studies reported on cortical and striatal pathology, the discovery of delayed neuronal death in rodent hippocampus after global ischemia (Kirino 1982; Pulsinelli et al. 1982; Smith et al. 1984) triggered interest as to whether a similar phenomenon might occur in the primate brain.

Zola-Morgan et al. (1986) were the first to report a CA1 sector lesion in a patient who had suffered from a transient global ischemic insult during cardiac

surgery. Subsequently, the same research group presented three additional human cases with hippocampal (mainly CA1) lesions (Rempel-Clower et al. 1996). The common neuropathological finding among these four patients was the bilateral disappearance of CA1 accompanied by memory deficits. These initial findings were confirmed histologically (Petito et al. 1987) as well as by magnetic resonance imaging (Fujioka et al. 2000). These human studies confirmed the clinical significance of delayed neuronal death, and further evaluation of this phenomenon in monkey models was required.

Applying a nonsurgical model, i.e., hypotension induced by neck cuffing as described previously by Nemoto et al. (1977), Zola-Morgan and coworkers (1992) reported a marked neuronal loss in CA1 sector and partial loss in CA2 and CA4 sectors of six monkeys with accompanying memory loss. Thus, the hippocampus is a focal site of cerebral ischemia, and damage limited to it is sufficient to impair memory (Zola-Morgan et al. 1992). Using an alternative approach—surgical occlusion of all eight major arteries supplying blood to the brain—Tabuchi et al. (1992, 1995) obtained similar results, and showed that an occlusion lasting 15 min produced damage that was limited to the hippocampus.

The mechanisms involved in the pathogenesis of primate ischemic neuronal death are gradually being elucidated. By performing both in vitro and in vivo studies, Yamashima et al. (1994, 1996) demonstrated calcium and phosphoinositide activation in postischemic CA1 neurons prior to necrotic cell death. Furthermore, the calcium-dependent protease calpain was upregulated in dying CA1 neurons (Yamashima et al. 1996) and was localized to the lysosomal membrane, which was disrupted after ischemia (Yamashima et al. 1998). As the lysosomal enzymes of cathepsin family were also activated in CA1 neurons after ischemia (Kohda et al. 1996), a link between calpain-induced lysosomal disruption and subsequent cytosolic release of cathepsins was proposed—the "calpain-cathepsin" hypothesis of delayed CA1 neuronal necrosis (Yamashima et al. 1998; 2003; reviewed by Tontchev and Yamashima 1999; Yamashima 2000). Based on this hypothesis, application of drugs inhibiting cathepsin activity blocked the development of CA1 neuronal death (Tsuchiya et al. 1999). Another lysosomal protease, DNAse II, and the cytosolic caspase-activated DNAse were also upregulated after ischemia (Tsukada et al. 2001), and thus were implicated in the calpain–cathepsin hypothesis.

Oxidative neuronal damage also contributes to delayed neuronal death after global cerebral ischemia as demonstrated by studies in humans (Love et al. 1998, 1999).

The existence of an established monkey ischemic model in our laboratory together with the data in adult rodents prompted us to investigate whether transient global cerebral ischemia activates neural progenitor cells residing in several regions of adult monkey telencephalon. In addition, we aimed to quantify this activation and determine the phenotype of descendant brain cell types generated by the progenitors in postischemic monkeys.

2
Materials and Methods

2.1
Animal Subjects

All experimental and surgical procedures were approved by the Animal Care and Ethics Committee of Kanazawa University. The subjects of our investigations were female Japanese macaque monkeys (*Macaca fuscata*). These were kept in air-conditioned cages sized approximately 1 m on a side. The monkeys were allowed free access to water and were daily fed with artificial animal food, and fruits or vegetables. In total, tissues from 29 monkeys were included in the present study: one monkey was neonatal (14 days old, sacrificed on postnatal day 14; P14), while the rest of the monkeys were sexually mature (age of 5–13 years).

The adult monkeys underwent transient, complete, whole brain ischemia ($n = 18$) or sham surgery ($n = 10$) according to a surgical procedure previously introduced (Yamashima et al. 1996, 1998, 2000). The monkeys were incubated under slow induction of general anesthesia, then intubated and maintained with artificial ventilation of 1% halothane in 40% O_2 and 60% N_2O. During the experiment, lactated Ringer's solution was infused, and arterial blood pressure was monitored. Body temperature was monitored with a rectal probe, and was kept within 37±0.5°C using a warming blanket. The sternum was removed under sterile conditions, and the innominate and left subclavian arteries were exposed in the mediastinum. Under the normotension of 80–100 mmHg, the two arteries were clipped with vascular clamps for 20 min. After the onset of ischemia, the monkeys showed pupil dilation and a rise of the mean arterial blood pressure by at least 60–70 mmHg. The effectiveness of clipping was demonstrated by an almost complete absence (<1.0 ml/100 g brain/min) of cerebral blood flow being monitored by laser Doppler (Vasamedics, St. Paul, MN, USA). After recirculation, the monkeys became normotensive gradually. Upon extubation, the monkeys gradually regained consciousness and were returned to their cages. The neonatal monkey was not operated. The sham surgery was performed as the chest was opened but the vessel clipping was not performed. The duration of anesthesia was the same as for the ischemic subjects.

2.2
Bromodeoxyuridine Infusion Protocol

BrdU (5-bromo-2′-deoxyuridine) was purchased from Sigma-Aldrich Japan (Tokyo, Japan), and was dissolved in saline with 0.007 N NaOH at a concentration of up to 10 mg/ml. BrdU was intravenously injected in the saphenous vein as each injection was at a dose of 100 mg/kg. The neonatal monkey received two injections: one on the day of birth, and one on P14. Of the 28 adult monkeys, 22 received 5 injections on five consecutive days, and were sacrificed on various periods after the last BrdU injection. Based on these periods, two monkey groups emerged: a group with short-term survival after BrdU, the monkeys within which

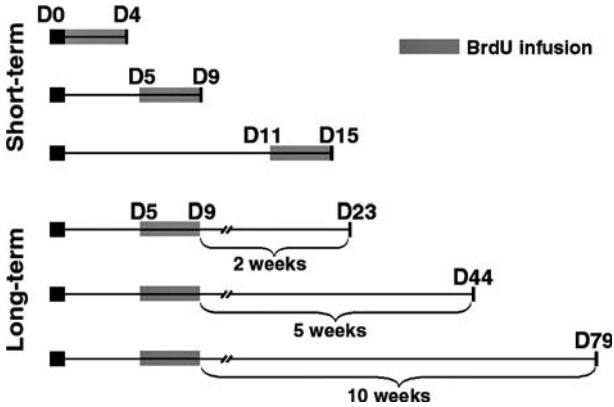

Fig. 1 Scheme of the BrdU infusion protocol (the duration of BrdU infusion is depicted by a *gray bar*). Surgery was performed on day 0 (*D0*), and the monkeys of the short-term survival group ("*short-term*") were killed on days 4, 9, and 15 (*D4*, *D9*, *D15*). The monkeys of the long-term survival group ("*long-term*") were injected during days 5–9 and killed on days 23, 44, and 79 (2, 5, and 10 weeks after BrdU, respectively)

were sacrificed 2 h after the fifth BrdU injection, and a long-term survival group, the monkeys within which were sacrificed 2–10 weeks after BrdU (Fig. 1). The monkeys of the short-term survival group ($n = 12$) were sacrificed on days 4 ($n = 3$), 9 ($n = 3$), and 15 ($n = 3$) after ischemia or on days 4 ($n = 1$) and 9 ($n = 2$) after the sham operation. The animals of the long-term survival group ($n = 10$) received BrdU injections on days 5–9 after surgery and were sacrificed 2, 5, and 10 weeks after the last injection, i.e., on days 23 ($n = 2$), 44 ($n = 2$), and 79 ($n = 2$) after ischemia or on days 23 ($n = 2$) and 44 ($n = 2$) after the sham operation.

2.3 Tissue Processing

At respective intervals as described above the monkeys were euthanized by lethal doses of sodium pentobarbital, the chest was opened, and intracardial perfusion of 0.5 l ice-cold saline with heparin was performed, immediately followed by 2.5 l of ice-cold solution of 4% paraformaldehyde in phosphate-buffered saline (PBS), pH = 7. The cranium was opened, and the brain was removed.

For histological analyses, brains were postfixed in 4% paraformaldehyde overnight at 4°C, then brains were sliced and cryoprotected in 30% sucrose solution in PBS containing 0.1% sodium azide, until respective tissues sank to the bottom. Then, tissue blocks were embedded in optimum cutting temperature (OCT) medium (Tissue-Tek, Sakura Finetech, Tokyo, Japan) and frozen at −70°C. Frozen 40-µm-thick sections were sequentially cut on a Leica CM3050 cryomicrotome and stored free-floating at −20°C in a cryopreservation buffer containing 25% ethylene glycol and 25% glycerol in 0.05 M phosphate buffer

until staining. The temporal lobe was cut in the coronal plane, the olfactory bulb—in the saggital plane, the frontal lobe—either coronally (right hemisphere) or horizontally (left hemisphere) as described (Tonchev et al. 2003a, b; 2005).

Additionally, tissues from 6 monkeys (3 controls and 3 killed on postischemic day 5) were embedded in paraffin and processed for routine histological analysis.

For electron microscopical analyses, the fixative was 2.5% glutaraldehyde followed by 1% osmium tetroxide for 1 h at 4°C, and embedding in an epon-araldite mixture (see below).

2.4 Immunohistochemistry

Prior to BrdU immunostaining, DNA was denaturated as free-floating sections were incubated in 50% formamide/50% 2×SSC buffer (0.3 M NaCl/0.03 M sodium citrate) at 65°C for 2 h, followed by 2 N HCl for 30 min at 37°C, as previously described (Kuhn et al. 1996). Subsequently, sections were washed in tris-buffered saline (TBS) (0.15 M NaCl, 0.1 M Tris-HCl, pH 7.5) containing 0.1% Triton X-100 (TBS-T). Nonspecific binding was blocked with TBS-T/10% normal serum (TBS-TB) for 30 min, prior to incubation with the primary antibodies diluted in TBS-TB at 4°C for 2 days. After washing (3×10 min), secondary antibodies were applied according to the species of the primary antibody for 2 h at room temperature in TBS-TB. Data details of primary or secondary antibodies are listed in Table 1.

For single-labeling by the immunoperoxidase method, respective primary antibodies were visualized with the ABC Elite kit (Vector; 1 h at room temperature) followed by washing in buffer and the color reaction using diaminobenzidine (DAB, Sigma-Aldrich, St. Louis, MO, USA) as chromogen (0.025% DAB and 0.03% H_2O_2 in TBS for 1–2 min). Then, the sections were mounted on glass slides and coverslipped under Entellan resin (Merck, Tokyo, Japan). For fluorescent immunostaining, the primary antibodies were visualized with antibodies conjugated to the following fluorochromes: Alexa Fluor-488, -546, -633 (Molecular Probes, Eugene, OR, USA), and tetramethylrhodamine isothiocyanate (TRITC; Jackson ImmunoResearch, West Grove, PA, USA). The DNA-binding dye propidium iodide (PI; Molecular Probes) was diluted in TBS (1:1000) and applied for 30 s as a nuclear counterstain for certain fluorescently labeled sections. Finally, the sections were coverslipped under Vectashield medium (Vector Laboratories, Burlingame, CA, USA) for fluorescence microscopy. Brain sections from a monkey untreated with BrdU, omission of primary antibodies, or incubation with irrelevant secondary antibodies served as negative controls.

2.5 Detection of DNA Damage and Degenerating Cells

DNA damage was evaluated by the terminal deoxynucleotidyltransferase (TdT)-mediated UTP nick end labeling (TUNEL) assay. Degenerating cells were stained by the Fluoro–Jade dye.

Table 1 List of primary and secondary antibodies used in the current study, and their details

Antibody against	Species, isotype	Dilution	Marker for (references)	Vendor
Primary				
Proliferation				
BrdU	Mouse IgG	1:100	DNA synthesis (Packard et al. 1973; Miller and Nowakowski 1988)	Becton Dickinson, San Jose, CA, USA
	Rat IgG	1:100		Harlan Sera-Lab, Loughborough, UK
Ki67	Mouse IgG	1:50	Proliferating cells (Scholzen and Gerdes 2000)	Novocastra, Newcastle, UK; DAKO
Phosphohistone H3	Rabbit IgG	1:50	Mitotic cells (Hendzel et al. 1997; Strahl and Allis 2000)	Cell Signaling, Beverly, MA, USA
Progenitor				
Musashi1	Rat IgG	1:100	Neural progenitors, astrocytes (Sakakibara et al. 1996; Sakakibara and Okano 1997; Kaneko et al. 2000)	Dr. Hideyuki Okano
Nestin	Mouse IgM	1:100	Neural progenitors, astrocytes (Lendahl et al. 1990; Miyata and Ogawa 1994; Duggal et al. 1997)	Dr. Masaharu Ogawa and Dr. Takaki Miyata
	Rabbit IgG	1:400		Chemicon, Temecula, CA, USA
βIII-Tubulin	Mouse IgG	1:300	Neuronal progenitors (Lee et al. 1990; Pencea et al. 2001b)	Sigma-Aldrich Japan K.K., Tokyo, Japan
	Rabbit IgG	1:500		Covance, Richmond, CA, USA
Doublecortin	Rabbit IgG	1:400	Neuronal progenitors (Gleeson et al. 1999; Francis et al. 1999; Mizuguchi et al. 1999)	Dr. Masashi Mizuguchi
	Goat IgG	1:200		Santa Cruz, Santa Cruz, CA, USA
Hu (HuC/HuD)	Mouse IgG	1:200	Neuronal progenitors (Okano and Darnell 1997; Wakamatsu and Weston 1997)	Molecular Probes, Eugene, OR, USA
PSA-NCAM	Mouse IgM	1:500	Neuronal progenitors (Seki and Arai 1993)	Dr. Tatsunori Seki
TUC4	Rabbit IgG	1:500	Neuronal progenitors (Quinn et al. 1999)	Chemicon

Table 1 (continued)

Antibody against	Species, isotype	Dilution	Marker for (references)	Vendor
Neuronal				
Neuronal nuclei (NeuN)	Mouse IgG	1:100	Neurons (Mullen et al. 1992)	Chemicon
GAD65/67	Rabbit IgG	1:400	γ-Aminobutyric acid (GABA)ergic neurons (Jongen-Relo et al. 1999)	Chemicon
Glial				
CNP	Mouse IgG	1:400	Oligodendrocytes (Kornack and Rakic 1999)	Chemicon
S100β	Mouse IgG	1:500	Astrocytes (Boyes et al. 1986)	Sigma
GFAP	Rabbit IgG	1:200	Astrocytes (Boyes et al. 1986)	Sigma
Iba1	Rabbit IgG	1:800	Microglia/macrophages (Imai et al. 1996; Ito et al. 1998)	Dr. Yoshinori Imai
CD68	Mouse IgG	1:25	Microglia/macrophages (Hulette et al. 1992)	DAKO, Carpinteria, CA, USA
Ham56	Mouse IgM	1:50	Reactive microglia, macrophages (Gown et al. 1986; Hulette et al. 1992)	DAKO
Other				
CD31	Mouse IgG	1:50	Endothelial cells	DAKO
Caspase-3 (activated)	Rabbit IgG	1:50	Apoptotic cells (Cooper-Kuhn and Kuhn 2002)	Cell Signaling
Gadd45	Rabbit IgG	1:100	DNA repair (Rich et al. 2000)	Santa Cruz

Table 1 (continued)

Antibody against	Species, isotype	Dilution	Marker for (references)	Vendor
Secondary				
Mouse IgG	Horse	1:30–1:100	Peroxidase detection	Vector, Burlingame, CA, USA
Rabbit IgG	Goat	1:100	Peroxidase detection	Vector
Goat IgG	Horse	1:100	Peroxidase detection	
Mouse IgG	Goat	1:100–1:400	Immunofluorescence detection	Molecular Probes
Mouse IgM	Goat	1:100	Immunofluorescence detection	Molecular Probes
Rabbit IgG	Goat	1:100–1:200	Immunofluorescence detection	Molecular Probes
Rat IgG	Goat	1:100–1:400	Immunofluorescence detection	Molecular Probes
Goat IgG	Donkey	1:100	Immunofluorescence detection	Molecular Probes
Rat IgG	Goat	1:50–1:200	Immunofluorescence detection	Jackson, West Grove, PA, USA
Goat IgG	Donkey	1:50–1:200	Immunofluorescence detection	Jackson

BrdU, bromodeoxyuridine; CNP, 2′,3′-cyclic nucleotide 3′-phosphodiesterase; GAD, glutamic acid decarboxylase; Gadd45, growth arrest and DNA damage inducible gene 45; GFAP, glial fibrillary acidic protein; Ham56, human alveolar macrophage 56 antigen; Iba1, ionized calcium binding adapter molecule 1; PSA-NCAM, polysialylated neural cell adhesion molecule; TUC4, TOAD/Ulip/CRMP4

The TUNEL assay was performed on free-floating sections using a kit (ApopTag in situ cell death detection kit; Intergen, Purchase, NY, USA) as described (Bondolfi et al. 2002) with some modifications. The sections were washed in TBS-T and then dehydrated in ascending ethanol/dH_2O series (50%, 70%, 90%, 5 min each) followed by 15 min incubation in 100% ethanol and rehydration in ethanol/dH_2O (90%, 70%, 50%, 5 min each). Then, the sections were equilibrated in proteinase K (PK) reaction buffer [100 mM Tris-HCl, 50 mM ethylenediaminetetraacetate (EDTA)] followed by PK (20 μg/ml, 15 min). PK was washed by several TBS-T rinses before the sections were incubated in equilibration buffer followed by TdT/reaction buffer mixture (15/85, ApopTag kit) at 37°C for 2 h. The reaction was visualized by sheep antidigoxigenin–fluorescein antibody in blocking solution (62/68, ApopTag kit) overnight at 4°C, followed by antisheep-Alexa Fluor 488 conjugated antibody in normal donkey serum for 2 h. DNAse pretreatment of the sections prior to the TdT step served as a positive control of the reaction specificity, while TdT omission—as a negative control. For TUNEL/NeuN/BrdU triple-labeling, the TUNEL assay was performed until the TdT step, then DNA was denatured, followed by digoxigenin visualization. After a positive TUNEL signal was confirmed on the next day, the sections were blocked in TBS-TB, and BrdU and NeuN were immunostained as already described (Tonchev et al. 2003a).

Fluoro–Jade staining was performed as described in Schmued and Hopkins (2000) with modifications (Butler et al. 2002). The sections were wet mounted onto microscope glass slides and air-dried for 30 min at 37°C in an oven. Then, the sections were pretreated for 5 min in absolute alcohol, followed by 3 min in 70% ethanol, 3 min in 50% ethanol, and 5 min in distilled water. The slides were then immersed in a solution of 0.05% $KMnO_4$ for 30 min at room temperature, and stained for 30 min in a solution of 0.001% Fluoro–Jade B (Chemicon, Temecula, CA, USA) in 0.1% acetic acid. Finally, the slides were then rinsed in distilled water, dried, cleared in xylene, and coverslipped.

2.6 Electron Microscopy

For conventional electron microscopy, processing was performed as described in Tsukada et al. (2001) and Yamashima et al. (2003). Small specimens of hippocampus were fixed with 2.5% glutaraldehyde for 2 h and subsequently with 1% osmium tetroxide in TBS for 1 h at 4°C, dehydrated in ascending ethanol series, incubated in propylene oxide (2 × 15 min); and finally embedded in epon-araldite mixture. Usually, between four and eight semithin (1 μm) sections were stained with toluidine blue for the light microscopic observation. After trimming upon observation of toluidine blue staining, the ultrathin sections were stained with uranyl acetate (10 min) and lead citrate (5 min) for the electron microscopic observation (JEM H-600, Hitachi, Tokyo).

For immunoelectron microscopy, processing was performed as described in Yamashima et al. (2004). Free-floating 40-μm-thick cryosections were stained using

the immunoperoxidase method with prolonged (at least 10 min) DAB reaction, and then fixed with 2.5% glutaraldehyde for 2 h, and with 1% osmium tetroxide in TBS for 1 h at 4°C, before dehydration and embedding in the epon–araldite mixture. After staining with toluidine blue for the light microscopic observation, the trimmed ultrathin sections were observed without ultrastructural staining to close up the DAB reaction or with minimal staining (uranyl acetate, 2 min; lead citrate, 1 min) to observe the background.

2.7 Image Acquisition and Analysis

Light microscopy of immunoperoxidase-stained sections was done on Axiovert S100 microscope (Carl Zeiss, Tokyo, Japan) and digitized by a 3-CCD (charge-coupled device) digital camera (Fujifilm, Tokyo, Japan) on a personal computer (Fujitsu, Tokyo, Japan). Only cells in a single focal plane were counted on a computer screen to avoid oversampling.

In the temporal lobe, we focused on the following structures (Fig. 2A): the (1) hippocampus proper (*cornu Ammonis*, CA) including its CA1–CA4 sectors (Lorente de No 1934); (2) SVZ of the inferior horn of the lateral ventricle (SVZi); (3) parahippocampal region (PHR), including the parahippocampal gyrus (PHG, van Hoesen 1982), and the perirhinal cortex, that is areas 35 and 36 of Brodmann (1905); (4) temporal neocortical areas, including the inferior temporal cortex (IT), a visual association cortex (Gross 1994), and the superior temporal gyrus (STG; area 22 of Brodmann) containing both primary and association auditory areas (Streitfeld 1980). In the frontal lobe, we focused on the following structures (Fig. 2B, C): the (1) SVZ of the anterior horn of the lateral ventricle (SVZa); (2) frontal neocortex; (3) striatum; (4) rostral migratory stream (RMS), a pathway from SVZa to the olfactory bulb, was investigated on horizontal sections (Fig. 2C). The olfactory bulb itself was also investigated on saggital sections, and its anatomical nomenclature was defined as described previously (Alonso et al. 1998).

$BrdU^+$ cells were evaluated on a series of every 12th section through the regions of interest in the following manner: (1) in DG, SVZi and olfactory bulb, the total number of $BrdU^+$ cells were counted and divided by the total area for each section (Tonchev et al. 2003a, b); (2) in CA, the number of $BrdU^+$ cells was counted within frames of 880 μm × 680 μm, which were placed within the proximal (adjacent to CA2), middle, or distal (adjacent to the subiculum) portions of the CA1 sector, and a single frame was placed within CA2 and CA3 (Fig. 2A, bottom panel); the frames encompassed the pyramidal, radiate, and lacunosum-moleculare layers; (3) in SVZa the number of $BrdU^+$ cells was counted within 800 μm × 100 μm grids placed in each of the five aspects of SVZa (dorsal, ventral, septal, caudate, and anterior) as outlined in Fig. 2B and C (bottom panels); (4) in cortical areas (IT, STG, PHR, frontal) and striatum, the number of BrdU-positive cells was counted separately in the gray and white matter within randomly chosen fields of 880 μm × 680 μm encompassing the neocortical layers (5 fields in gray matter and 2 fields in the

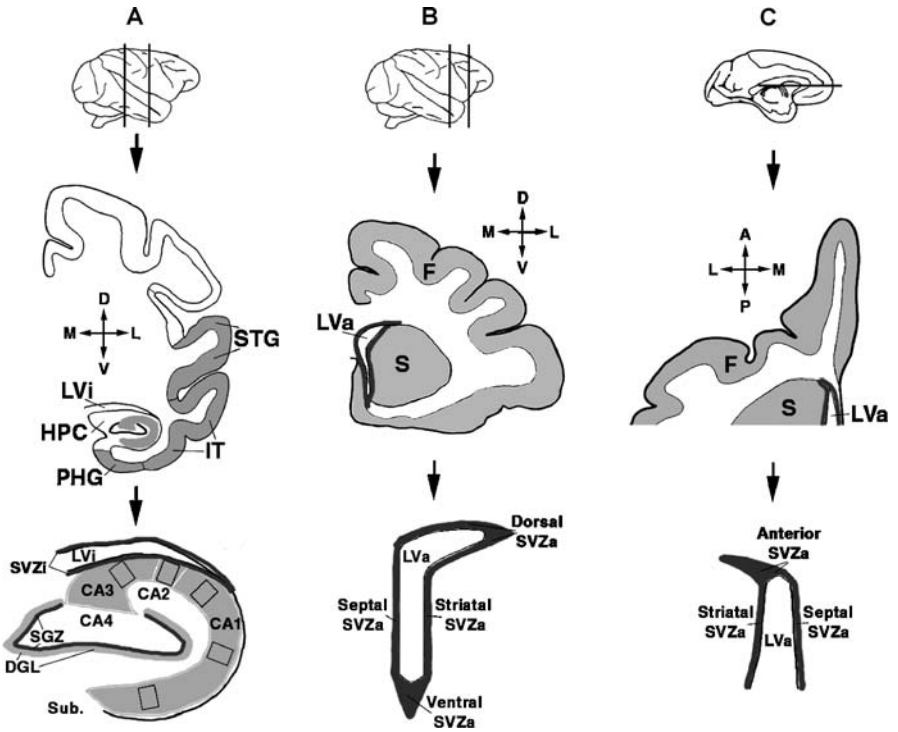

Fig. 2A–C Schematic maps of adult macaque monkey brain depicting regions of interest. **A** Lateral view on right hemisphere (*top panel*) with two vertical lines depicting the position of the hippocampus within the temporal lobe. Coronal view through the temporal lobe (*middle panel*) showing the relation of the hippocampal formation (*HPC*), parahippocampal gyrus (*PHG*), inferior temporal cortex (*IT*), superior temporal gyrus (*STG*), and inferior horn of the lateral ventricle (*LVi*). A detailed map of the hippocampal formation (*bottom panel*) including the CA1–CA4 sectors, dentate gyrus, of which the dentate granule cell layer (*DGL*) and the subgranular zone (SGZ) are shown, and the subiculum (*Sub.*). LVi and the subventricular zone along its walls (*SVZi*) are also depicted. **B** Lateral view on right hemisphere (*top panel*) with two vertical lines depicting region of the frontal lobe sampled for analysis. Coronal view through the frontal lobe (*middle panel*) showing the relation of the frontal cortex (*F*), striatum (*S*), and the anterior horn of the lateral ventricle (*LVa*). The subventricular zone along the walls of LVa (*SVZa*) is depicted in *dark gray*. Scheme of SVZa (*bottom panel*) showing its four aspects as seen on a coronal view: dorsal, striatal, septal, and ventral SVZa. **C** Lateral view on left hemisphere (*top panel*) with a line depicting the position of the horizontal map (*middle panel*). The relation of the frontal cortex (*F*), striatum (*S*), and the anterior horn of the lateral ventricle (*LVa*) as seen on a horizontal section are shown. SVZa is depicted in *dark gray*. Scheme of SVZa (*bottom panel*) showing its three aspects as seen on a horizontal view: anterior, striatal, and septal SVZa. Directions: *M*, medial; *L*, lateral; *D*, dorsal; *V*, ventral; *A*, anterior; *P*, posterior

white matter). SGZ and SVZ were defined as 50-μm bands immediately adjacent to the hilar surface of the granule and ependymal cell layers, respectively.

Cells positive for NeuN, TUNEL, and Fluoro–Jade were evaluated in grids of 800 μm × 500 μm (CA1) or 800 μm × 1,000 μm (neocortex and striatum). Areas were determined by public domain software (ImageJ; http://rsb.info.nih.gov/ij). The number of positive cells was divided by the respective area (total area or frame area). Thus, single-labeled cells for any marker were quantified densitometrically (cells/mm^2). Densities were averaged to obtain a mean density value for each region/animal group.

Double- and triple-labeling for BrdU and/or various markers was verified using confocal laser scanning microscopy (LSM 510, Carl Zeiss, Tokyo, Japan) on at least five anatomically matched sections per animal as at least 100 positive cells were evaluated for each marker. Alexa Fluor 88 was assigned to the green channel, either TRITC or Alexa Fluor 546 was assigned to the red channel, and Alexa Flour 633 was assigned to the blue channel. "Multiple-tracking" mode, where each fluorochrome is scanned separately and sequentially, was used to avoid the chance of signal transfer among channels. Z sectioning at 0.5- to 1-μm intervals was performed and optical stacks of at least 20 images were used for analysis. Digital three-dimensional (3D) reconstructions were created using Zeiss LSM software, version 2.3.

The assembly and brightness/contrast adjustments of all images were accomplished in Adobe Photoshop 5.0 (Adobe Systems, Mountain View, CA, USA).

2.8 Statistical Analysis

Data were expressed as the mean±standard error of the mean (SEM). Differences between means were determined using one-way analysis of variance (ANOVA) followed by the Tukey–Kramer post hoc comparison and two-sided t test. For comparing percentages, nonparametric tests were also applied (Mann–Whitney, Kruskal–Wallis). Differences were considered significant when $p < 0.05$.

3 Results

Ischemia caused damage to the monkey brain, which was most evident in the hippocampal CA1 sector, in accordance with previous findings (Zola-Morgan et al. 1992; Tabuchi et al. 1992; Yamashima et al. 1996, 1998). Staining for the TUNEL assay characteristic for DNA damage in CA1 revealed a marked increase of positive cells on day 4 after ischemia, with a subsequent sharp decrease on days 9 and 15 (Fig. 3A, B). Double-staining with the neuronal marker NeuN demonstrated that TUNEL was positive in CA1 neurons. The use of Fluoro–Jade, a marker of degenerating cells (Schmued and Hopkins 2000), confirmed the TUNEL data. The number of Fluoro–Jade$^+$ cells was highest on day 4, declining at later time-points

white matter). SGZ and SVZ were defined as 50-μm bands immediately adjacent to the hilar surface of the granule and ependymal cell layers, respectively.

Cells positive for NeuN, TUNEL, and Fluoro–Jade were evaluated in grids of 800 μm × 500 μm (CA1) or 800 μm × 1,000 μm (neocortex and striatum). Areas were determined by public domain software (ImageJ; http://rsb.info.nih.gov/ij). The number of positive cells was divided by the respective area (total area or frame area). Thus, single-labeled cells for any marker were quantified densitometrically (cells/mm^2). Densities were averaged to obtain a mean density value for each region/animal group.

Double- and triple-labeling for BrdU and/or various markers was verified using confocal laser scanning microscopy (LSM 510, Carl Zeiss, Tokyo, Japan) on at least five anatomically matched sections per animal as at least 100 positive cells were evaluated for each marker. Alexa Fluor 88 was assigned to the green channel, either TRITC or Alexa Fluor 546 was assigned to the red channel, and Alexa Flour 633 was assigned to the blue channel. "Multiple-tracking" mode, where each fluorochrome is scanned separately and sequentially, was used to avoid the chance of signal transfer among channels. Z sectioning at 0.5- to 1-μm intervals was performed and optical stacks of at least 20 images were used for analysis. Digital three-dimensional (3D) reconstructions were created using Zeiss LSM software, version 2.3.

The assembly and brightness/contrast adjustments of all images were accomplished in Adobe Photoshop 5.0 (Adobe Systems, Mountain View, CA, USA).

2.8 Statistical Analysis

Data were expressed as the mean±standard error of the mean (SEM). Differences between means were determined using one-way analysis of variance (ANOVA) followed by the Tukey–Kramer post hoc comparison and two-sided t test. For comparing percentages, nonparametric tests were also applied (Mann–Whitney, Kruskal–Wallis). Differences were considered significant when $p < 0.05$.

3 Results

Ischemia caused damage to the monkey brain, which was most evident in the hippocampal CA1 sector, in accordance with previous findings (Zola-Morgan et al. 1992; Tabuchi et al. 1992; Yamashima et al. 1996, 1998). Staining for the TUNEL assay characteristic for DNA damage in CA1 revealed a marked increase of positive cells on day 4 after ischemia, with a subsequent sharp decrease on days 9 and 15 (Fig. 3A, B). Double-staining with the neuronal marker NeuN demonstrated that TUNEL was positive in CA1 neurons. The use of Fluoro–Jade, a marker of degenerating cells (Schmued and Hopkins 2000), confirmed the TUNEL data. The number of Fluoro–Jade$^+$ cells was highest on day 4, declining at later time-points

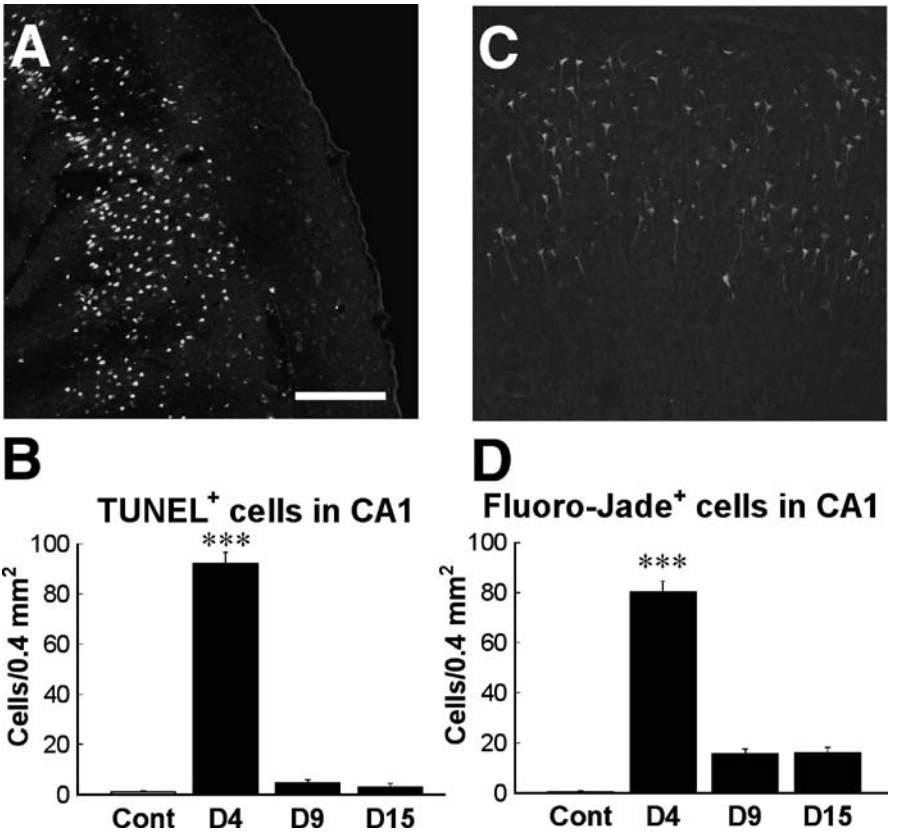

Fig. 3A–D Postischemic damage in CA1 on day 4. **A** Staining for the TUNEL assay showing numerous positive cells. **B** Statistical analysis of TUNEL$^+$ cells per frame of 0.4 mm^2 in CA1; $***p < 0.001$, one-way ANOVA followed by Tukey–Kramer post hoc. **C** Staining for Fluoro–Jade demonstrating similar pattern to the TUNEL stain. **D** Statistical analysis of Fluoro-Jade$^+$ cells per frame of 0.4 mm^2 in CA1; $***p < 0.001$, one-way ANOVA followed by Tukey–Kramer post hoc. *Scale bar* = 200 μm

(Fig. 3C, D). The density of Fluoro–Jade$^+$ cells on day 4 (80±4 per frame; Fig. 5F) was compatible with that of TUNEL$^+$ cells on day 4 (92±4 per frame; Fig. 3B, D). In contrast to CA, DG remained negative for Fluoro–Jade at all time-points (data not shown).

We then evaluated the neuronal cell loss on sections stained for the neuronal marker NeuN. Staining revealed a marked reduction of NeuN$^+$ cells in CA1 starting from day 4 that persisted at later time-points (Fig. 4). Some patchy cell loss was seen also in CA2, CA3, and CA4 (arrows in Fig. 4), while DG and subiculum did not exhibit cell loss. Statistical analysis of the number of NeuN$^+$ cells in frames placed in proximal, middle, and distal CA1 demonstrated a significant reduction of positive cells in all postischemic monkeys (Fig. 5, left column). Despite some reduction of

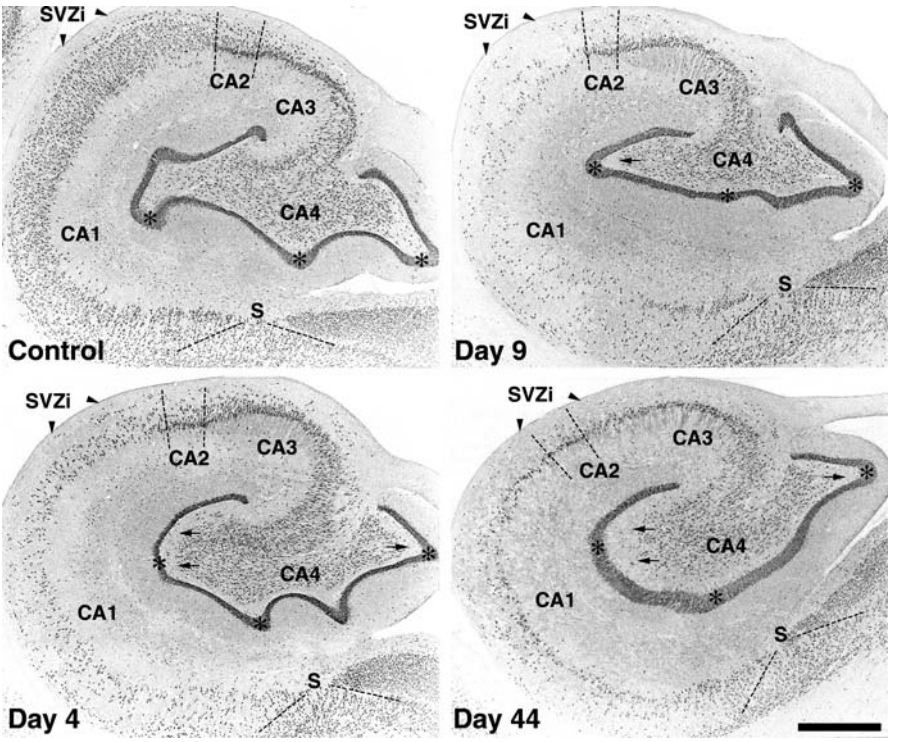

Fig. 4 Staining for NeuN in hippocampus sector of control, day-4, day-9, and day-44 monkeys. Note the marked reduction of positive cells in CA1 contrasting the overall normal appearance of the other sectors. Cell loss in CA4 is shown by *arrows*, while the SVZi adjacent to CA1 is depicted by arrowheads. *Asterisks*, DG; *S*, subiculum. *Scale bar* = 1 mm (*D*)

the density of $NeuN^+$ cells in CA2–CA4, statistically significant changes were not observed (Fig. 5, right column).

Cell damage was observed also in other brain regions. In the neocortex and striatum, ischemia significantly increased the density of $TUNEL^+$ cells on day 4, with a decline at subsequent time-points. In both neocortex and striatum, the positive cells were dispersed among the parenchyma, and the density of positive cells in these two regions (15–20 cells per frame of 0.8 mm^2) was lower compared to the density in CA1 (80–90 cells per frame of 0.4 mm^2). Accordingly, evaluation of neuronal cell loss by NeuN staining did not reveal any visible cell loss under low magnification. A high magnification inspection on routinely stained sections, however, revealed that a few of the neocortical neurons exhibited postischemic degenerative changes (Yoshida et al. 2002). In contrast, nearly all CA1 neurons showed features of degeneration including marked shrinkage and chromatolysis, and a slightly condensed or pyknotic nucleus (Yamashima et al. 1998; Yoshida et al. 2002). In the olfactory bulb, only a few $TUNEL^+$ cells were detected, and NeuN staining did not reveal cell loss.

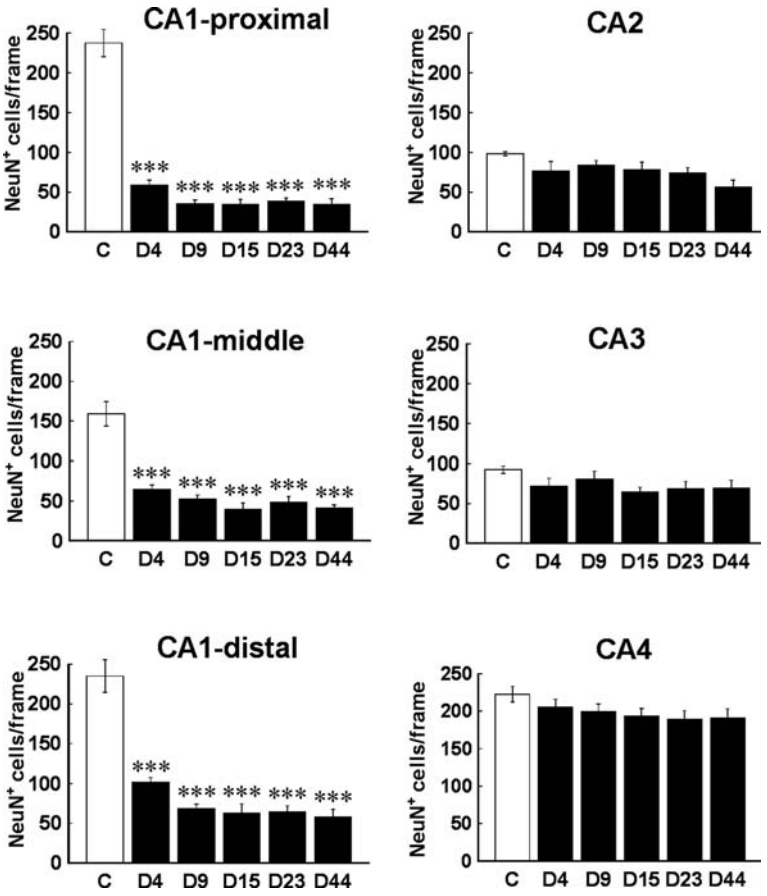

Fig. 5 Statistical analysis of NeuN$^+$ cells in the hippocampus. In CA1, cells were counted within frames placed in the proximal, middle, and distal CA1, while in CA2–CA4 a single frame was used (see Fig. 3A). Note the marked reduction of positive cells in CA1 (*left column* of graphs) contrasting the insignificant reductions in CA2–CA4 (*right column* of graphs). ***$p < 0.001$, one-way ANOVA followed by Tukey–Kramer post hoc

Overall, presented data show that our monkey model represents a paradigm of marked neuronal damage in CA1, mild to moderate damage in striatum, neocortex, and CA2–CA4, and minimal or absent damage in DG, PHR, and olfactory bulb (Yoshida et al. 2002). In this context of graded damage in different telencephalic regions we investigated the distribution, density, and phenotype of de novo-generated cells.

3.1 Hippocampal Formation

The hippocampal formation includes DG, the hippocampus proper including CA1–CA4 sectors (Lorente de No 1934) and the subiculum (van Hoesen 1982). Based on previous publications on postischemic cell proliferation in the rodent brain (e.g., Liu et al. 1998; Nakatomi et al. 2002), at first we focused our attention on DG and hippocampus proper.

3.1.1 Dentate Gyrus

Within DG, most $BrdU^+$ cells in all monkeys were localized to SGZ (Fig. 6). Ischemia led to a visible increase of $BrdU^+$ cells in DG, on postischemic days 9 and 15 (Fig. 6A). Quantitative analysis of the monkeys with short-term survival after BrdU showed that in either DG as a whole or separately within SGZ or DGL, the density of proliferating cells had a peak on day 9 (Fig. 7A). To investigate the long-term fate of these cells, BrdU was injected during postischemic days 5–9 (as for the day-9 monkeys), and respective monkeys were sacrificed 2 weeks, 5 weeks, or 10 weeks after BrdU, i.e., on postischemic days 23, 44, or 79 (Fig. 6B). Quantitative analysis of this monkey group showed that—similar to the short-term survival group—the density of $BrdU^+$ cells in postischemic monkeys was significantly greater than the density in respective control DG, DGL, or SGZ (Fig. 7B). The majority of $BrdU^+$

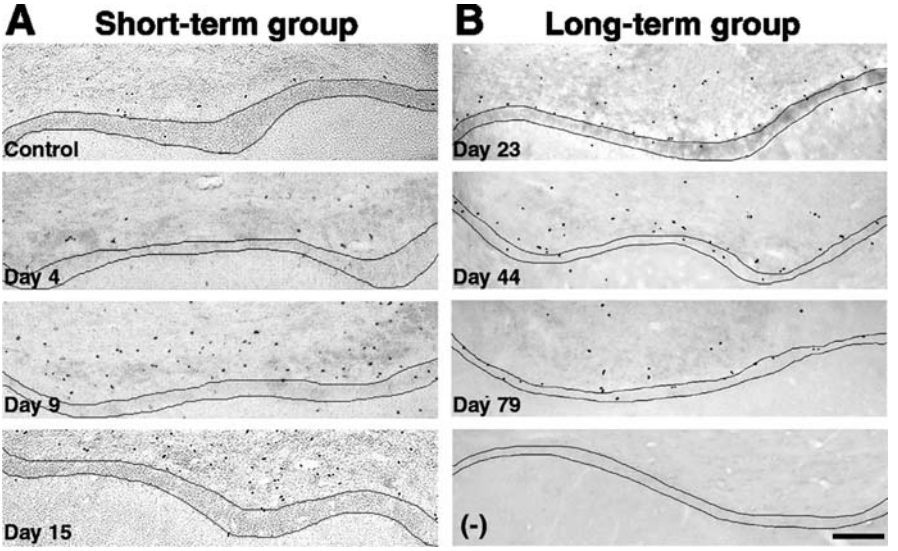

Fig. 6A, B Staining for BrdU in DG of the short-term (**A**) and long-term (**B**) monkey groups. DGL is outlined on each micrograph. A monkey not injected with BrdU served as a negative control (−). *Scale bar* = 200 μm

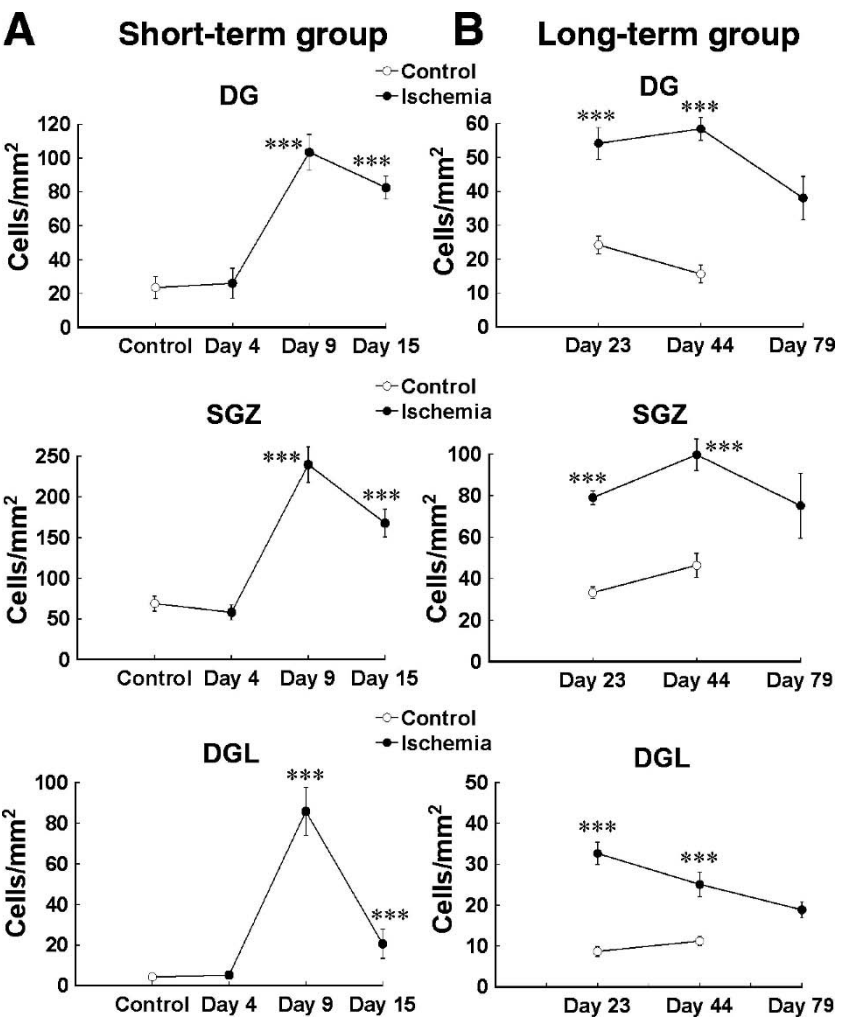

Fig. 7A, B Statistical analysis of the density of $BrdU^+$ in DG. **A** In the short-term survival group after BrdU, the density peaked on day 9. **B** In the long-term-survival monkey DG, density was significantly higher in postischemic compared to control brains. $***p < 0.001$ versus controls, one-way ANOVA followed by Tukey–Kramer *post hoc*

cells in both short- and long-term monkey groups were localized along the border between SGZ and the innermost layer of granule neurons. Many of these cells were frequently found in clusters, and quantitative study of the $BrdU^+$ cells clusters in SGZ showed a significantly greater density in the postischemic monkeys (Fig. 8A). Evaluation of the $BrdU^+$ cell distribution in DG revealed that beyond day 9 there was no increase in the proportion of $BrdU^+$ cells localized in DGL, as 70%–80% of the $BrdU^+$ cells in DG were localized in SGZ, 20%–30% in DGL, and only few cells in the molecular layer of DG (Fig. 8B).

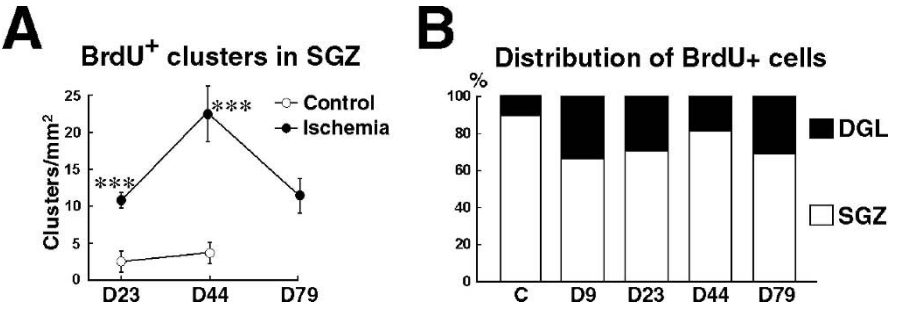

Fig. 8A, B Statistical analysis of the density of $BrdU^+$ cell clusters in SGZ (**A**) showed a significantly higher density in the postischemic monkey SGZ. Analysis of the distribution of $BrdU^+$ cells in DG (**B**) revealed that most $BrdU^+$ cells were found in SGZ while a much lower proportion—in DGL. ***$p < 0.001$, one-way ANOVA followed by Tukey–Kramer post hoc. *C*, control; *D*, day. *Scale bar* = 20 μm

In order to confirm the increased postischemic cell proliferation with an independent marker, we stained monkey brain sections for Ki67 (Kee et al. 2002). Ki67 immunohistochemistry confirmed that proliferation was increased on day 9 (Fig. 9B) as compared to control (Fig. 9A), and subsequently declined (Fig. 9C). The $Ki67^+$ cells were frequently grouped similarly to the $BrdU^+$ cells, in clusters or "doublets" (Fig. 9D, E). Double-labeling for BrdU and Ki67 demonstrated they stain the same cells (Fig. 9F). BrdU also colabeled with the mitotic marker phosphohistone H3 (Fig. 9G).

After observing the distribution and density of $BrdU^+$ cells in DG, we started evaluating their phenotype by combining BrdU with markers for progenitor cells or more mature cell types. As our first step, we explored the proteins Musashi1 and Nestin, markers of multipotent neural progenitors including neural stem cells (Kaneko et al. 2000; Lendahl et al. 1990). The $Musashi1^+$ cells and clusters in DG were localized mainly in SGZ (Fig. 10A), the zone with predominant $BrdU^+$ cell/cluster localization (Fig. 10B). Careful evaluation of $BrdU^+$ clusters revealed that many of them were also positive for Musashi1 at all time-points and within all monkeys (Fig. 10C, D; Table 2). The $BrdU^+/Musashi1^+$ cells were negative for the

Table 2 Percentages of colabeling of BrdU with markers for neural progenitors in DG. $BrdU^+$ cells were sampled for colabeling with either Musashi1 or Nestin as described in the text. Statistically significant differences between percentages were not detected

	Day 9		Day 23		Day 44		Day 79	
	Control	Ischemia	Control	Ischemia	Control	Ischemia	Control	Ischemia
Musashi1	42±6	45±7	36±6	47±8	44±8	49±7	NA	41±7
Nestin	23±5	20±5	25±6	28±5	30±7	26±4	NA	33±6

NA, not available

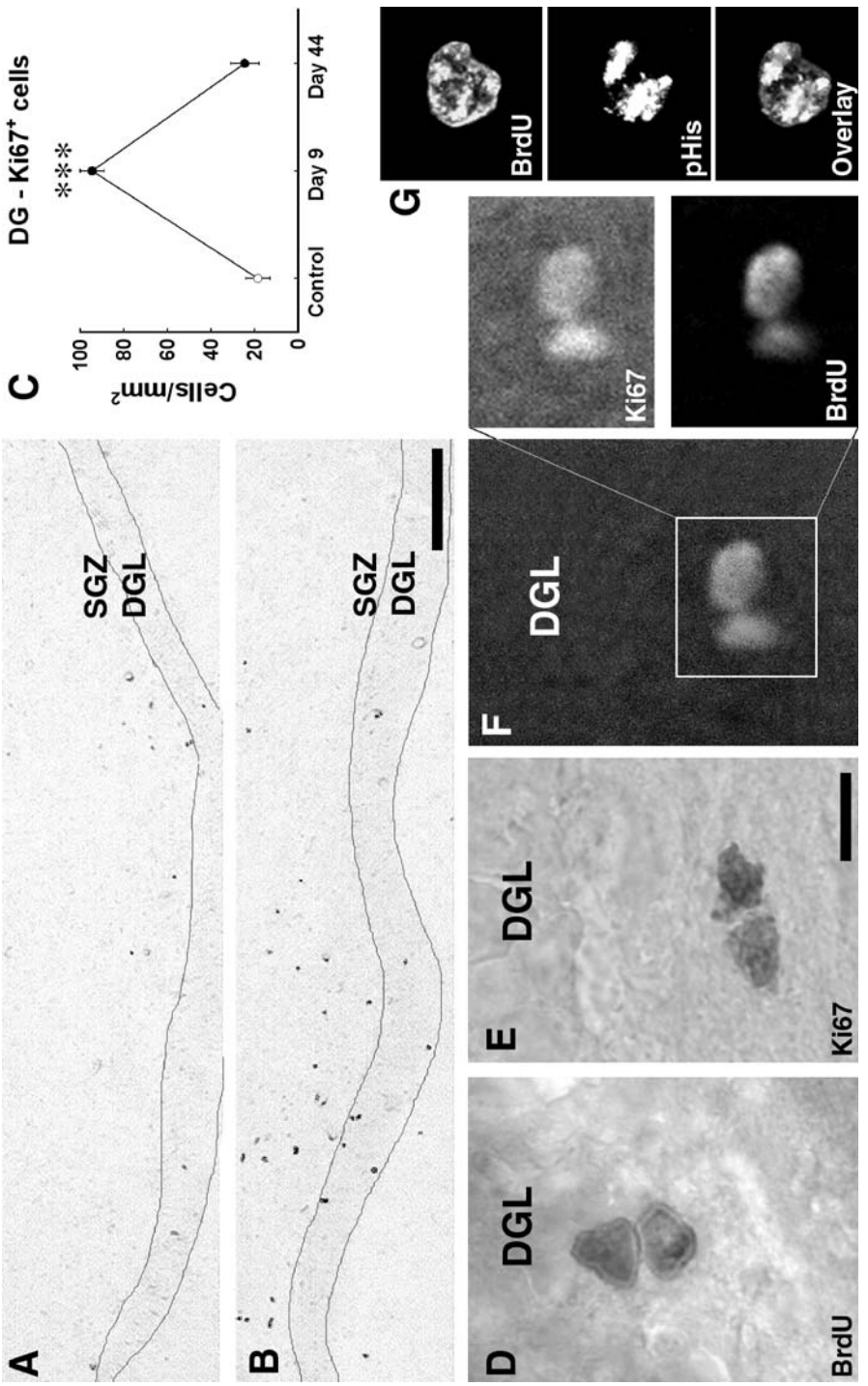
A
SGZ
DGL
B
SGZ
DGL
C
DG - Ki67+ cells
***
Cells/mm2
100
80
60
40
20
0
Control
Day 9
Day 44
D
DGL
BrdU
E
DGL
Ki67
F
DGL
Ki67
BrdU
G
BrdU
pHis
Overlay

Fig. 9A–G Low-power micrographs in monkey DG stained for Ki67 (**A, B**). Note the larger number of positive cells on day 9. **C** Quantitative analysis of the density of $Ki67^+$ cells in DG (***$p < 0.001$ versus control, one-way ANOVA followed by Tukey–Kramer post hoc). **D** $BrdU^+$ "doublet" in SGZ. **E** $Ki67^+$ "doublet" with a similar appearance as the $BrdU^+$ "doublet." **F** Double-staining of a "doublet" for BrdU and Ki67 in SGZ confirms they stain the same cells. **G** Double-staining for BrdU and phosphohistone H3 (pHis) in SGZ reveals a colabeled mitotic cell. *Scale bars* = 200 μm (**B**); 10 μm (**E**)

astrocyte marker glial fibrillary acidic protein (GFAP) although $BrdU^-$/$Musashi1^+$ cells were colabeled by GFAP (Tonchev et al. 2003a). Data of BrdU/Nestin coexpression resembled those of BrdU/Musashi1. Double-labeled cells in DG were located in SGZ (Fig. 11A), and observed in all monkeys (Table 2). The $BrdU^+$/$Nestin^+$ cells

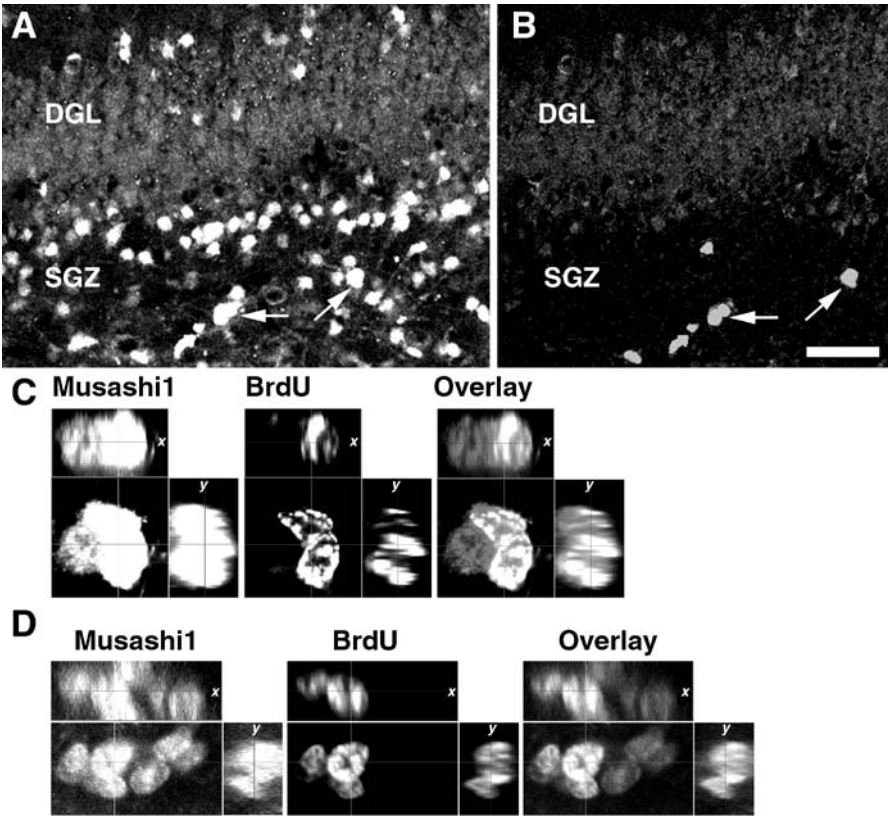

Fig. 10A–D Low-power micrographs in monkey DG stained for Musashi1 (**A**) and BrdU (**B**). Note numerous $Musashi1^+$ cells in SGZ, some of which appear double-labeled for BrdU (*arrows*). **C, D** High-power view of BrdU/Musashi1 colabeled clusters on days 9 (**C**) and 79 (**D**) with channel separation and 3D reconstructions in *x* and *y* axes. *Scale bar* = 50 μm

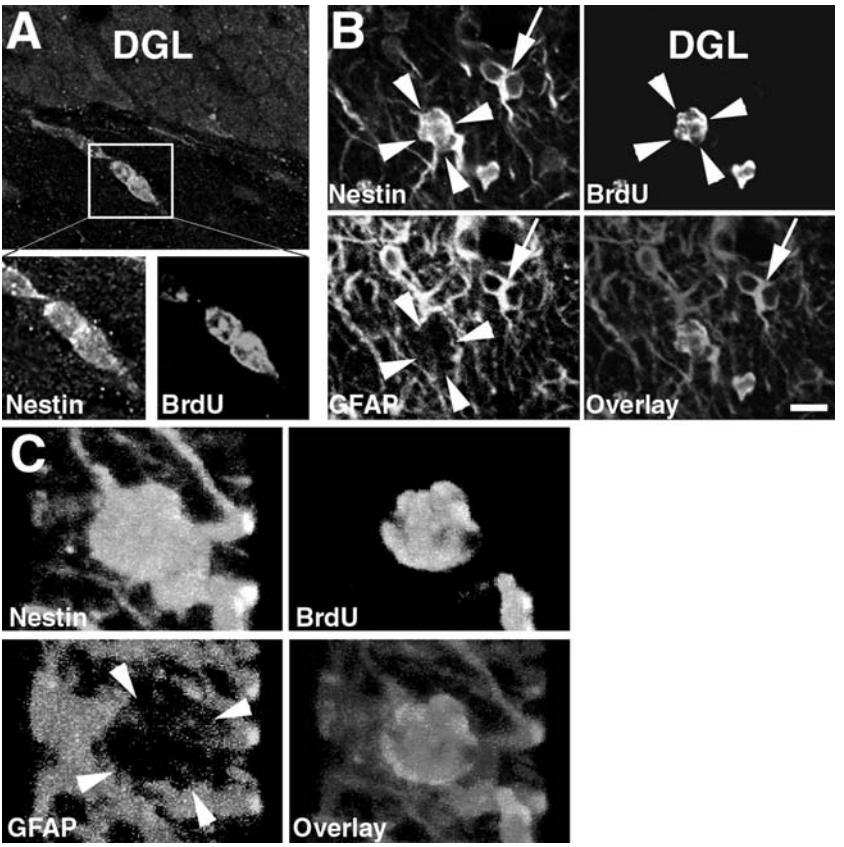

Fig. 11A–C **A** Double-staining for BrdU and Nestin in SGZ of control monkey with channel separation. Note a "doublet" stained by the two markers (*frame*). Nestin$^+$ cells that were colabeled by GFAP were negative for BrdU (*arrows*). **B** A BrdU$^+$/Nestin$^+$ cluster in day-9 SGZ is ensheathed by, but distinct from, GFAP$^+$ fibers (*arrowheads*). **C** Three-dimensional reconstruction of the cluster shown in **B** confirms it was encapsulated by GFAP$^+$ fibers (*arrowheads*), but the BrdU$^+$ cells were not colabeled for GFAP. *Scale bar* = 10 μm

were negative for the astrocyte marker GFAP (Fig. 11B, C; arrowheads) although BrdU$^-$/Nestin$^+$ cells were colabeled by GFAP (Fig. 11B; arrows). On average, 45%–50% of the BrdU$^+$ cells were colabeled for Musashi1 and 25%–30% were co-stained for Nestin. Statistically significant differences among the monkey groups were not observed (Table 2).

After investigating markers for neural progenitors, we evaluated putative BrdU expression in cells positive for markers of neuronal (i.e., committed to the neuronal lineage) progenitors: TUC4 (Quinn et al. 1999), Hu (Okano and Darnell 1997; Wakamatsu and Weston 1997), Doublecortin (Gleeson et al. 1999; Francis et al. 1999), βIII-tubulin (Lee et al. 1990; Pencea et al. 2001b), and PSA-NCAM

(Seki and Arai 1993). We did not find cells colabeled for BrdU and any of these markers in the control DG with short-term survival (day 4 or day 9 after sham operation). However, in the postischemic monkeys of the short- and long-term survival groups as well as in the controls with long-term survival, double-stained cells were observed (Fig. 12). These were localized in SGZ and extended processes parallel to the innermost layer of DGL granule neurons (Fig. 12A, C–E). The percentage of $BrdU^+$ cells coexpressing neuronal progenitor markers was 2%–3% in the postischemic monkeys with short-term survival, which was significantly higher than the

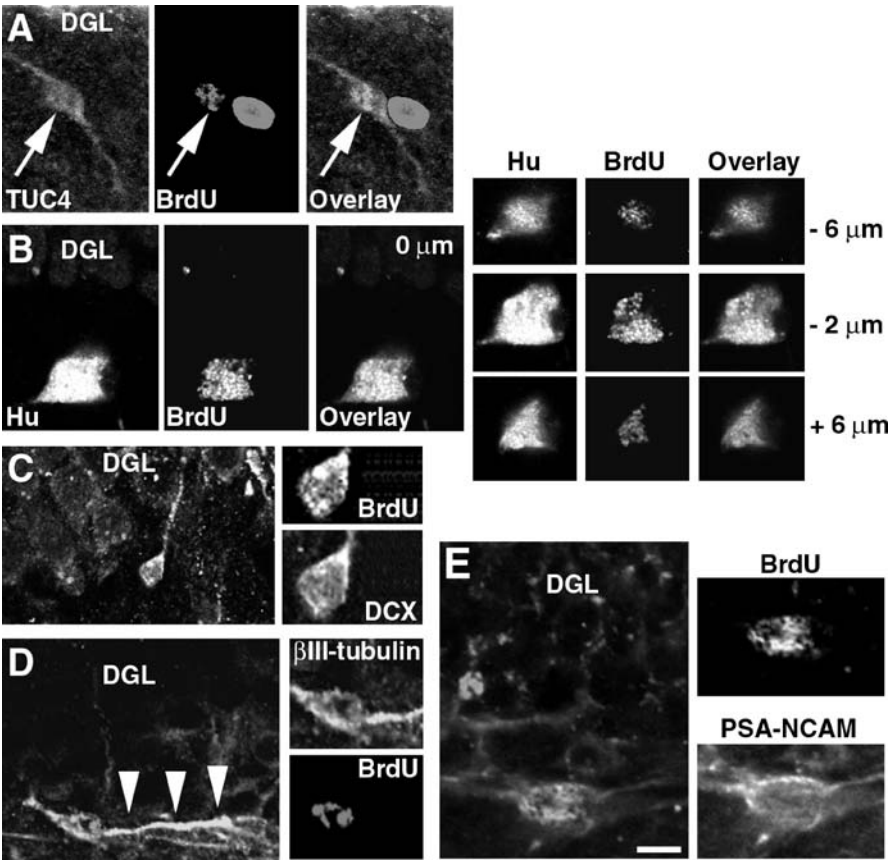

Fig. 12A–E Double-staining for BrdU and neuronal progenitor markers in SGZ. **A** An example of a BrdU/TUC4 double-stained cell (*arrows*) (day 9) adjacent to a $BrdU^+/TUC4^-$ cell. **B** A $BrdU^+/Hu^+$ cell (day 23) with serial scanning at various depths to confirm the colocalization of the two channels. **C** A cell double-stained for Doublecortin (DCX) and BrdU (day 15) shown with channel separation. **D** A cell double-stained for *β*III-tubulin and BrdU (day 9) extending processes parallel to DGL (*arrowheads*) is shown with channel separation. **E** A cell double-stained for PSA-NCAM and BrdU (day 44), extending processes parallel to DGL, is shown with channel separation. *Scale bar* = 10 μm

Table 3 Percentages of colabeling of BrdU with neuronal progenitor markers in DG. BrdU$^+$ cells were sampled for colabeling with any of βIII-tubulin, TUC4, Doublecortin, Hu, or PSA-NCAM as described in the text

	Day 9		Day 23		Day 44		Day 79	
	Control	Ischemia	Control	Ischemia	Control	Ischemia	Control	Ischemia
βIII-Tubulin	0	4±0.3*	6±2	8±3**	12±6	10±5**	NA	9±2**
TUC4	0	3±0.2*	6±2	9±3**	7±5	12±5**	NA	6±2**
Doublecortin	0	4±0.5*	7±3	9±5**	8±4	9±4**	NA	5±1**
Hu	0	1±0.5*	8±3	7±4**	10±5	8±3**	NA	3±2**
PSA-NCAM	0	3±0.8*	8±4	10±5**	8±4	9±6**	NA	6±2**

NA, not available *$p < 0.05$ versus control (day 9 sham operation); **$p < 0.05$ versus postischemic day 9; Kruskal–Wallis or Mann–Whitney tests

corresponding controls (Table 3). The percentages of colabeling rose to about 10% in the long-term survival group of postischemic monkeys, which was significantly higher than the short-term postischemic monkeys but not than control monkeys with a corresponding long-term survival after BrdU (Table 3).

We observed a gradual change of expression of markers on progenitor cells. Nestin was mainly expressed on multipolar cells in SGZ (Fig. 13A; arrowheads) and the few Nestin$^+$ cells extending processes in DGL were also positive for PSA-NCAM (Fig. 13A; arrows). The PSA-NCAM$^+$ cells were located in SGZ or within the 1–2 innermost layers of the granule cell, and many of these were double-positive for βIII-tubulin (Fig. 13B; arrows) while a few were negative for βIII-tubulin (Fig. 13B; arrowheads). Mature DGL neurons in deep granule layers or in SGZ/CA4 were PSA-NCAM/$^-$βIII-tubulin$^+$ (Fig. 13B; asterisks). Many βIII-tubulin$^+$ cells in deeper layers of DGL or in SGZ/CA4 exhibited a weak immunoreactivity and were positive for the mature neuronal marker NeuN (Fig. 13C; arrows). However, βIII-tubulin$^+$/NeuN$^-$ cells were also observed, and these had a strong βIII-tubulin immunoreactivity and location in SGZ/innermost layer of DGL (Fig. 13C; arrowheads). Thus, maturation appears to be associated with sequential expression of markers in the order Nestin, PSA-NCAM, βIII-tubulin, and then NeuN. This conclusion is also supported by the high percentage of BrdU$^+$ cells colabeled with Nestin (or Musashi1), with the percentage of co-staining decreasing for more mature markers (Tables 2 and 3).

The above data raise the question whether BrdU incorporation could be observed in mature DG neurons. To investigate this issue, we performed double-labeling for BrdU and the mature neuronal markers NeuN (Mullen et al. 1992) and glutamic acid decarboxylase (GAD) (Jongen-Relo et al. 1999). We did not find cells colabeled for BrdU and NeuN or GAD in the control DG with short-term survival (Fig. 14A). However, in the postischemic monkeys of the short- and long-term survival groups as well as in the controls with long-term survival, double-stained cells were observed (Fig. 14B–E). In the postischemic monkeys with short-term survival (e.g., day 9), the positive cells were within the innermost 2–3 layers of

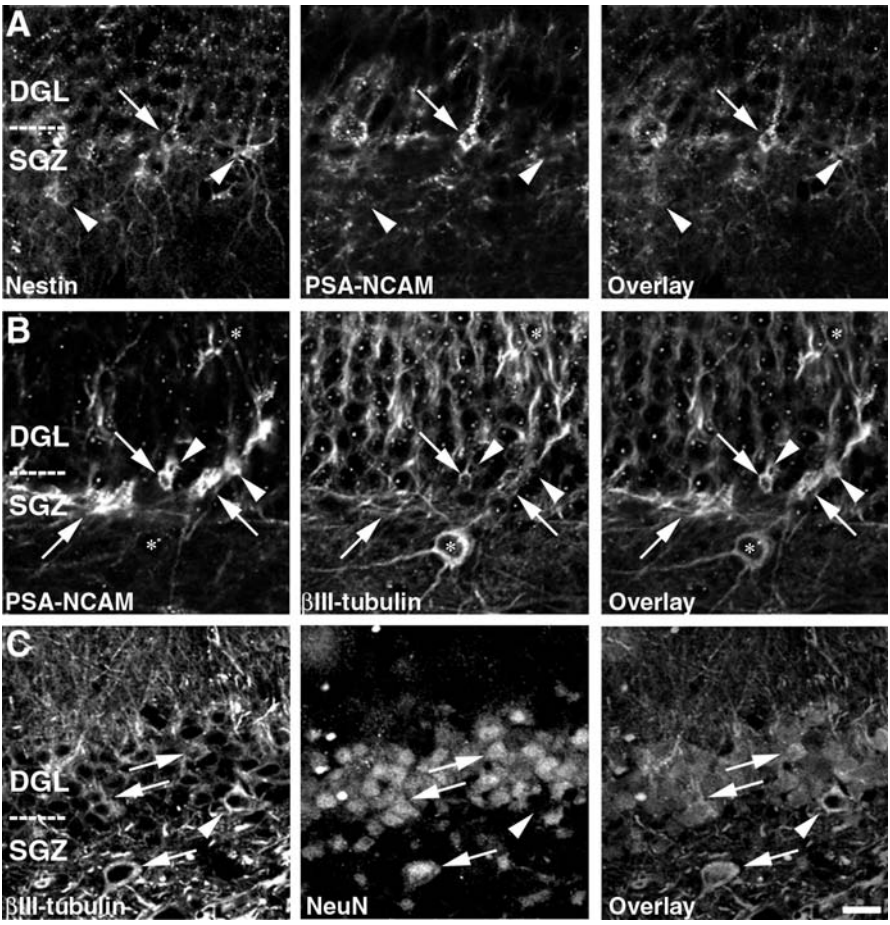

Fig. 13A–C Sequential expression of neural and neuronal progenitor markers in cells within DG. **A** The neural progenitor marker Nestin is expressed on cells negative for the neuronal progenitor marker PSA-NCAM (*arrowheads*), but a PSA-NCAM$^+$ cells extending a process toward DGL are weakly positive for Nestin (*arrows*). **B** PSA-NCAM/βIII-tubulin colabeling demonstrates the preferential localization of double-stained cells in SGZ (*arrows*), while mature βIII-tubulin$^+$ cells in CA4 or deep layers of DGL remain negative for PSA-NCAM (*asterisks*). PSA-NCAM$^+$/βIII-tubulin$^-$ cells (*arrowheads*) were also seen, adjacent to or in contact with PSA-NCAM$^+$/βIII-tubulin$^+$ cells. **C** NeuN/βIII-tubulin double-labeling showing that while most NeuN$^+$ cells were co-stained for βIII-tubulin (*arrows*), NeuN$^-$/βIII-tubulin$^+$ cells (arrowheads) were also observed (in SGZ). *Scale bar* = 20 μm

granule neurons (Fig. 14B), and we expected that over time we would find positive cells in deeper layers of DGL. However, we did not observe this, and even at the longest survival time studied the BrdU$^+$/NeuN$^+$ cells were located in the granule layers adjacent to SGZ (Fig. 14C–E). Serial scanning with the generation of 3D reconstructions confirmed the colocalization of NeuN or GAD with BrdU

Table 4 Percentages of colabeling of BrdU with mature neuronal markers in DG. $BrdU^+$ cells were sampled for colabeling with either NeuN or GAD as described in the text

	Day 9		Day 23		Day 44		Day 79	
	Control	Ischemia	Control	Ischemia	Control	Ischemia	Control	Ischemia
NeuN	0	2±1	5±2	6±3*	5±2*	7±3*	NA	8±3*
GAD	0	1±0.5	6±2	5±2*	5±2*	4±2*	NA	7±4*

NA, not available *$p < 0.05$ versus postischemic day 9, Kruskal–Wallis or Mann–Whitney tests

(Fig. 14D). The percentage of $BrdU^+$ cells coexpressing mature neuronal markers was 2% in postischemic monkeys of the short-term survival group. The percentages of colabeling rose to about 7%–8% in the long-term survival group, which was significantly higher than the short-term postischemic monkeys but not compared to control monkeys with a corresponding long-term survival after BrdU (Table 4).

Data showing the integration of newly generated neurons into the DG circuit came from experiments involving BrdU/βIII-tubulin colabeling. As reported above (Fig. 13C), βIII-tubulin is a marker of both neuronal progenitors and mature neurons. Furthermore, as the antigen is a cytoplasmic protein, this allows studying the direction of cellular processes extended by βIII-$tubulin^+$ cells (which is impossible for NeuN or Hu, for example, as they are nuclear antigens). We observed BrdU incorporation into βIII-$tubulin^+$ cells with features of mature neurons, i.e., not having a bipolar morphology but rather extending a single process in DGL (Fig. 15A; arrow). Confocal microscopy revealed that such cells established morphologically visible contacts with processes of neighboring $BrdU^-$/βIII-$tubulin^+$ neurons (Fig. 15A; arrowheads), which had a similar size and shape as compared to the $BrdU^+$/βIII-$tubulin^+$ cells. By immunoelectron microscopy, we observed the bipolar morphology of $BrdU^+$ neuronal progenitors (Fig. 15B), and cells with features of neuronal progenitors formed synaptic contacts (Fig. 15C). Such neuronal progenitors were frequently perivascular, and we proposed that they may originate from the vascular adventitia (Yamashima et al. 2004).

Taken together, the presented data suggest that the observation of BrdU incorporation into mature DG GABAergic neurons is not an artifact, but rather a result of sequential maturation of progenitors possibly arising from a Nestin/$Musashi1^+$ cellular pool.

In addition to neuronal cells, we also investigated for proliferation of glia. To label microglial cells we used the marker Iba1 that stains both nuclei and processes of microglia (Ito et al. 1998). Colabeling with BrdU showed that a proportion of the $BrdU^+$ cells in SGZ of the short-term survival monkey group were microglial cells (Fig. 16A; arrows) but not astrocytes (Fig. 16A; arrowheads). Furthermore, a significant proportion of $BrdU^+$ cells in DGL of long-term survival monkeys were $Iba1^+$ (Fig. 16B; arrows). However, the $BrdU^+$ clusters in SGZ remained negative for Iba1 (Fig. 16C). The percentage of $BrdU^+$ cells colabeled for Iba1 was 20%–30% in the postischemic monkeys, while 10%–15% in the controls.

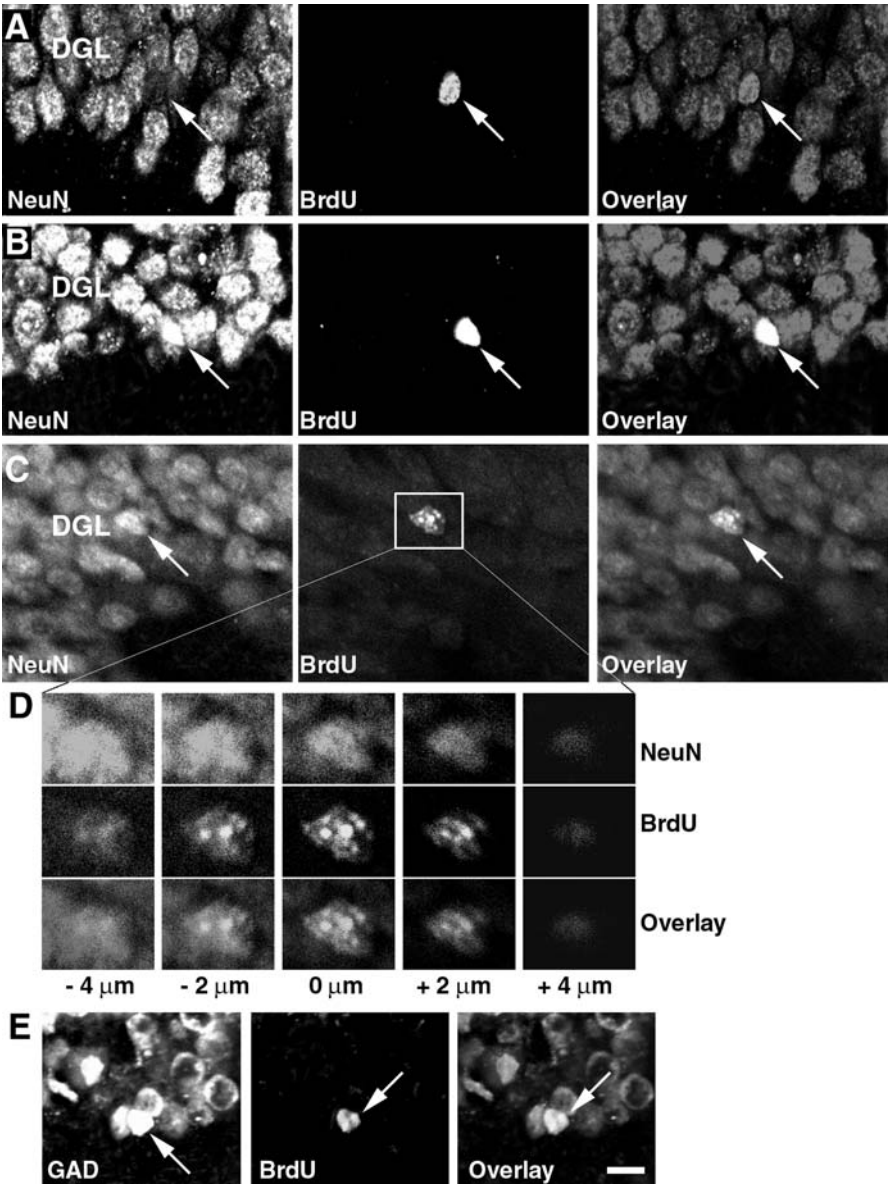

Fig. 14A–E Double-staining for BrdU and mature neuronal markers in DGL. **A** In control monkey DGL $BrdU^+$ cells (*arrows*) were distinct from $NeuN^+$ cells. **B** On day 9 after ischemia $BrdU^+/NeuN^+$ cells (*arrows*) were observed in the innermost layers of granule cells. **C** $BrdU^+/NeuN^+$ cells were seen up to day 79 (*arrows*). **D** The cell framed in **C** is shown in serial sectioning at various depths to confirm the colocalization of the two signals. **E** An example of cell double-stained for BrdU/GAD (*arrows*) on day 79. Scale bar = 10 μm

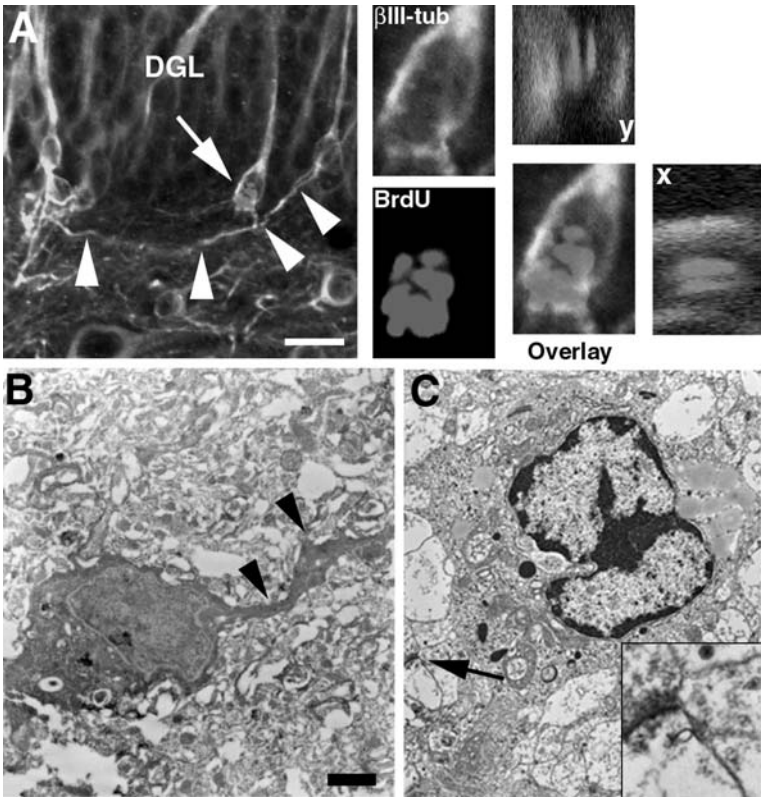

Fig. 15A–C **A** Double-staining for BrdU and βIII-tubulin (βIII-tub) on day 79 in DGL. Note the double-stained nucleus (arrow) as confirmed by channel separation with orthogonal projections (*right panel*). Furthermore, note the extension of cellular processes (*arrowheads*) of the BrdU$^+$/βIII-tubulin$^+$ cells toward neighboring BrdU$^-$/βIII-tubulin$^+$ cells. **B** BrdU immunoelectron microscopy in SGZ showing a positive cell extending process. Compare with Fig. 12D. **C** A putative neuronal progenitor cells forming in the vicinity of which a synaptic bouton is seen (*arrow*; magnified in the *inset*). *Scale bars* = 20 μm (**A**); 1 μm (**C**)

Although SGZ astrocytes remained negative for BrdU, we noticed a specific characteristic of these cells' existence in DG that, in our view, requires attention. In sections stained for the astrocyte marker S100β and counterstained by the nuclear dye PI, a S100β^+ cell band could be seen in SGZ that appeared more intensely stained compared to neighboring sectors such as DGL or CA4 (Fig. 17A, arrows). Comparison between control and ischemic DG did not show a visible increase in S100β immunoreactivity after ischemia (Fig. 17B, arrows). A more detailed examination of DG clearly demonstrated that SGZ contains a higher number of S100β^+ cells than adjacent sectors (Fig. 17C). Quantitative evaluation of S100β^+ cells within frames of 50 μm × 50 μm placed in SGZ, DGL, or the molecular layer of DG clarified this difference by showing that the density of S100β^+ cells in SGZ

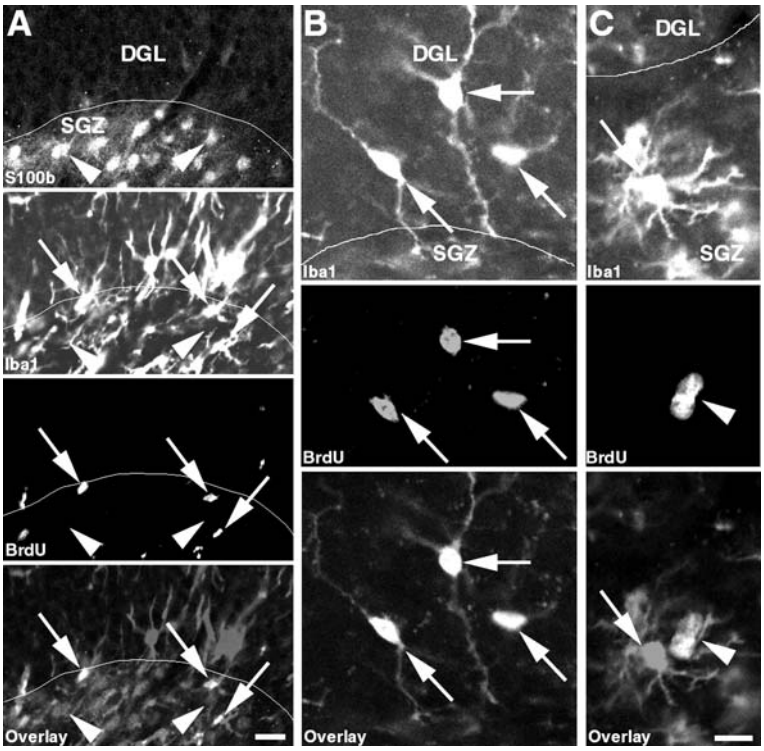

Fig. 16A–C Double-staining for BrdU and the microglial marker Iba1 in DG. **A** Triple-labeling for S100β, Iba1, and BrdU in day-4 DG demonstrates the presence of BrdU$^+$/Iba1$^+$ cells (*arrows*), while the S100β^+ cells (*arrowheads*) remain negative for BrdU. **B** Double-staining for Iba1 and BrdU in postischemic day-44 DGL demonstrates that many of the BrdU$^+$ cells in postischemic DG were microglia (*arrows*). **C** Double-staining for Iba1 and BrdU in postischemic day-79 SGZ shows a BrdU$^+$ "doublet" (*arrowhead*) that is distinct from an adjacent Iba1$^+$ cell (*arrow*). *Scale bars* = 20 μm (**A**); 10 μm (**C**)

was more than two times higher than in the other two layers of DG (Fig. 17D), with no statistical difference between control and day-9 postischemic DG. Like S100β^+ cells, the density of GFAP$^+$ cells in SGZ was higher than in DGL or in the molecular layer of DG (Fig. 17E). In contrast to monkeys, mice hippocampal sections stained for S100β (Fig. 18A) or GFAP (Fig. 18B) did not exhibit a marked difference between SGZ, the molecular layer of DG, and CA4 as regarding the density of positive cells. Thus, the accumulation of astrocytes in SGZ could be a phenomenon specific to the primate SGZ, whose significance is currently unknown and thus requires further investigations.

Ischemia also increased the BrdU incorporation into cells of blood vessel walls, and a vascular origin for at least some of the progenitor cells in DG could be deducted as reported previously (Yamashima et al. 2004).

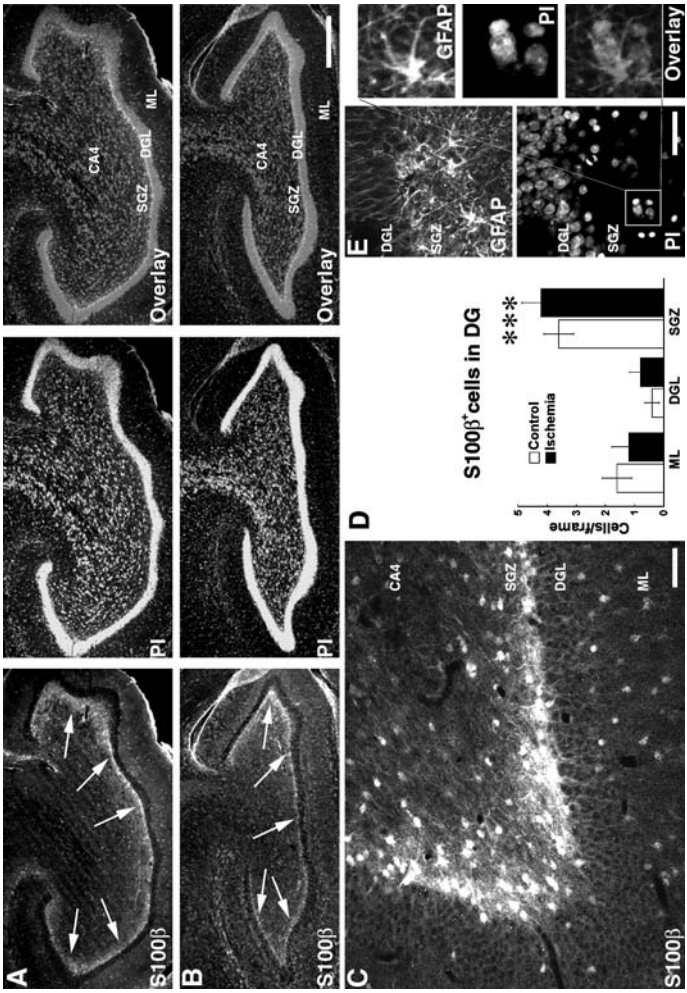

Fig. 17A–E Expression of astrocyte markers in adult monkey DG. **A** Low-magnification view of a control monkey section labeled for S100β, counterstained by PI and an overlay of the two channels. *Arrows* depict a high-intensity band of positive cells in SGZ. **B** Low-magnification view of postischemic day-9 monkey with a S100β^+ band (*arrows*). A visible difference in the intensity of S100β immunoreactivity between control and ischemic DG was not seen. **C** A higher magnification view of DG (day 9) confirms the differential distribution of S100β^+ cells among the subregions of DG. **D** Quantitative analysis of the density of S100β^+ cells in molecular layer (*ML*), DGL, and SGZ of DG. ***$p < 0.001$ versus ML or DGL, one-way ANOVA followed by Tukey–Kramer post hoc. **E** Staining for GFAP in DG confirms the density of astrocytes in SGZ. The framed area is shown with channel separation and depicts a PI$^+$ mitotic figure that is distinct from, although adjacent to, a GFAP$^+$ cells. *Scale bars* = 500 μm (**B**); 50 μm (**C**); 20 μm (**E**)

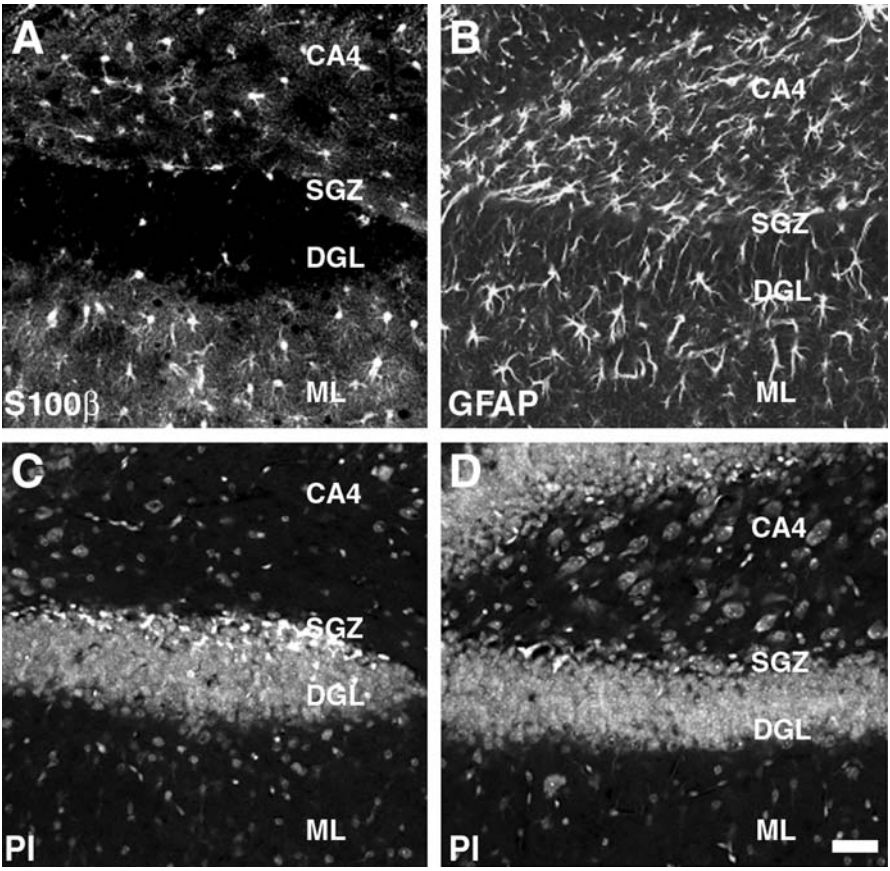

Fig. 18A–D Expression of astrocyte markers in adult mouse DG. **A** Staining for S100*β* demonstrates the lower density of positive cells in DGL as compared to neighboring DG layers. However, no difference could be seen among the molecular layer (*ML*), SGZ, and CA4 (PI counterstain is shown in **C**). **B** Stained for GFAP shows no difference in respect to the density of positive cells among ML, SGZ, and CA4 (PI counterstain is shown in **D**). *Scale bar* = 50 μm

3.1.2 Cornu Ammonis

Cells incorporating BrdU in CA1 were observed at all time-points, but their number was markedly increased in postischemic monkeys (Fig. 19). The $BrdU^+$ cells were homogeneously dispersed throughout the layers of CA. In CA2–3, an increase—similar to CA1—of proliferating cells was observed. In the control animals, the density of $BrdU^+$ cells was on average 10–20/mm^2 and increased approximately 10 times after ischemia (Fig. 20). The postischemic monkeys had significantly more $BrdU^+$ cells on days 23 and 44 compared to the controls (Fig. 20), and even

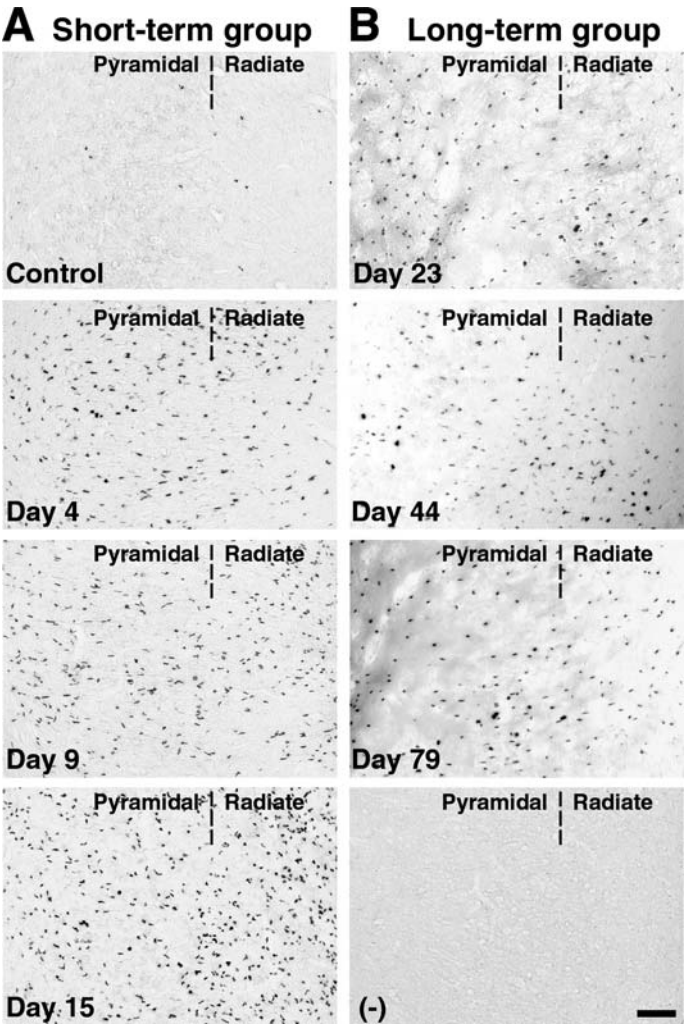

Fig. 19 Staining for BrdU in CA1 of short-term (**A**) and long-term (**B**) monkey groups. Note the marked increase of positive cells after ischemia and their homogeneous distribution between pyramidal and radiate cell layers. A monkey not injected with BrdU served as a negative control (−). The position of the visual field within *cornu Ammonis* corresponds to the middle portion of CA1 as shown in Fig. 3A). *Scale bar* = 100 μm

at the most distant postischemic time-point investigated (day 79) we calculated significantly more $BrdU^+$ cells in CA1 than in earlier time-points of sham-operated animals (such as day 23 or day 44). Significant differences between the short-term and the long-term postischemic monkey groups were not observed at an average cell density of 200 $BrdU^+$ cells/mm^2 in CA1, and 170 cells/mm^2 in CA2/3 (Fig. 20). Ischemia also increased the density of $BrdU^+$ cells in CA4, albeit at a much lower level than in CA1–3.

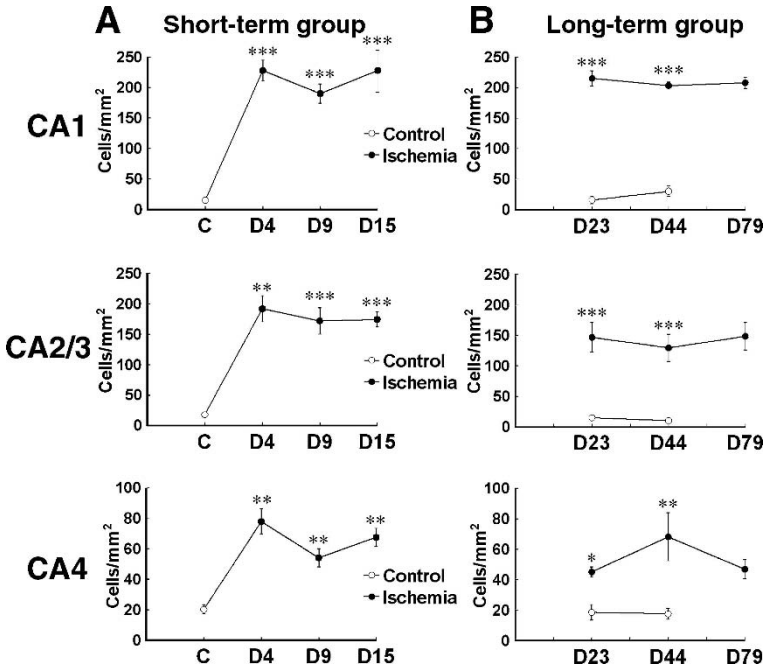

Fig. 20A, B Statistical analysis of the density of $BrdU^+$ cells in *cornu Ammonis*. **A** In the short-term survival group after BrdU the density peaked in the second postischemic week (days 9 and 15). **B** In long-term monkey group the density was significantly higher in postischemic compared to control brains. $*p < 0.05$, $**p < 0.01$, $***p < 0.001$, one-way ANOVA followed by Tukey–Kramer *post hoc*

Staining for independent proliferation markers such as Ki67 and phosphohistone H3 in CA1 confirmed the data acquired by BrdU staining (see Tonchev et al. 2003b for details). The percentage of colabeling between BrdU and Ki67 was almost complete, while the percentage of $BrdU^+$ cells co-stained for phosphohistone H3 was lower. This is reasonable as phosphohistone H3 is selectively expressed in the M phase (Hendzel et al. 1997; Strahl and Allis 2000), while Ki67 is expressed in all active phases of the cell cycle (Scholzen and Gerdes 2000; Kee et al. 2002).

Upon investigating the occurrence and distribution of proliferating cells in control and postischemic CA, we explored their phenotype. Evaluation of the $BrdU^+$ cells co-staining with the microglial marker Iba1 or the astrocytic marker S100β in the short-term survival group revealed that in control and postischemic day 4 CA1, only microglia but not astrocytes incorporated BrdU (Fig. 21A). However, in postischemic day 9 CA1 and at subsequent time-points, $BrdU^+$ astroglia were detected (Fig. 21B; arrowheads), although such cells were fewer than the $BrdU^+/Iba1^+$ microglia (Fig. 21B; arrows). Quantitative analysis revealed that the percentages of $BrdU^+$ cells expressing either Iba1 or S100β were significantly increased after ischemia at all time-points (Table 5). Furthermore, the percentage of $BrdU^+$ cells

Table 5 Percentages of colabeling of BrdU with glial markers in CA1. $BrdU^+$ cells were sampled for colabeling with Iba1, S100β, or CNP as described in the text

	Day 9		Day 23		Day 44		Day 79	
	Control	Ischemia	Control	Ischemia	Control	Ischemia	Control	Ischemia
Iba1	10±2	75±15***	8±4	78±18***	11±5	80±21***	NA	75±14
S100β	0	15±5***	2±1	12±5***	3±1	10±3***	NA	13±3
CNP	0	1±0.3	0,5	4±1*	0,5	3±1*	NA	4±2*

NA, not available ***$p < 0.001$, *$p < 0.05$ versus respective controls, Kruskal–Wallis, or Mann–Whitney tests

colabeled for Iba1 was significantly higher than the percentage of $BrdU^+$ cells colabeled for S100β (Table 5). An alternative astrocytic marker, GFAP, showed similar results to S100β (Fig. 21D).

Fig. 21A–D Glial proliferation in CA1 after ischemia. **A** Triple-staining for Iba1, S100β, and BrdU on postischemic day 4. Note that while Iba1 colabels with BrdU (*arrows*), S100β does not (*arrowheads*). The frame is magnified in the *lower panel* showing a $S100\beta^+$ cell that is tightly associated but distinct from two $Iba1^+$ cells. **B** Triple-staining for Iba1, S100β, and BrdU on postischemic day 15. Note that both Iba1 (*arrows*) and S100β (*arrowheads*) colabel with BrdU, but the $BrdU^+/Iba1^+$ cells are more numerous than the $BrdU^+/S100\beta^+$ cells. The image is representative also for day 9. **C** Proliferating $GFAP^+$ astrocytes coexpress Nestin on postischemic day 9 (*arrows*). Note their hypertrophy. **C** Proliferating $GFAP^+$ astrocytes coexpress Nestin on postischemic day 9 (*arrows*). Note their hypertrophy also. $BrdU^-/GFAP^+$ astrocytes colabeled for Nestin are seen (*arrowheads*). **D** Proliferating $GFAP^+$ astrocytes coexpress Musashi1 on postischemic day 15 (*arrows*). $BrdU^-/GFAP^+$ astrocytes colabeled for Musashi1 are also seen (*arrowheads*). *Scale bar* = 20 μm

Fig. 22A–F (on page 40) Microglial morphology and immunophenotypes. **A** Low-magnification view of control CA1 showing resting microglia with ramified morphology (the framed cells are magnified in the *inset*; the nucleus is depicted by an *arrowhead*). **B** Marked changes in postischemic day-4 CA1 as the microglia become ameboid and greatly increase their cell density. **C** Proliferating postischemic (day 9) $Iba1^+$ microglia coexpress CD68. **D** Proliferating postischemic (day 15) $Iba1^+$ microglia coexpress Ham56. **E** A globular cellular cluster is triple-labeled for Iba1, CD68, and Ham56 in postischemic (day 4) CA1. **F** A cluster with similar morphology seems to engulf $NeuN^+$ cells (*arrowheads*). *Scale bars* = 100 μm (**B**); 50 μm (**D**); 10 μm (**F**)

Fig. 23A–E (on page 41) Long-term fate of $BrdU^+$ cells in *cornu Ammonis* (for all images, BrdU is shown in the *left panel*). **A** Rod-shaped $Iba1^+$ microglia express BrdU in postischemic day-79 CA1 (*arrows*). **B** A few oligodendrocytes positive for CNP also colabeled with BrdU in the postischemic monkeys (micrograph from day-79 CA1). **C** Lack of colabeling of BrdU (*arrows*) with βIII-tubulin (day-44 CA1). **D** Lack of colabeling of BrdU (*arrowheads*) with NeuN (*arrows*) (day-44 CA1). **E** A cell that is positive for BrdU and Hu in CA4 (postischemic day 23) is depicted by arrows and shown in channel separation and orthogonal projections in the lower panel. *Scale bars* = 10 μm (**A, B, E**); 20 μm (**C**); 50 μm (**D**)

Reactive astroglia were positive for the intermediate filament protein Nestin (Fig. 21C) and the RNA-binding protein Musashi1 (Fig. 21D) and showed marked hypertrophy. On the other hand, different phenotypes of microglia were observed based on their expression of additional markers of activated microglia/macrophages: CD68 and Ham56. Simultaneously with their increased proliferation after ischemia, microglial cells changed their appearance from resting type with ramified morphology (Fig. 22A) to a rod-shaped or ame-

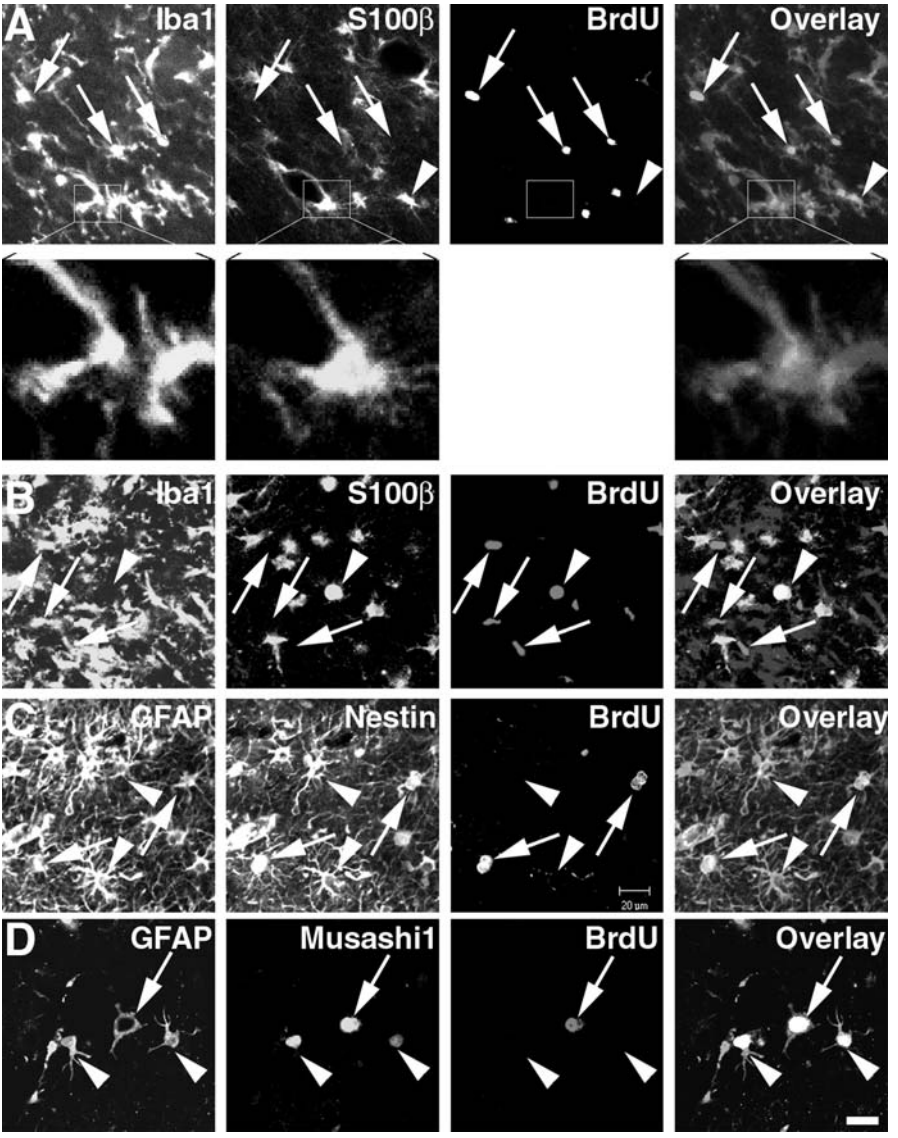

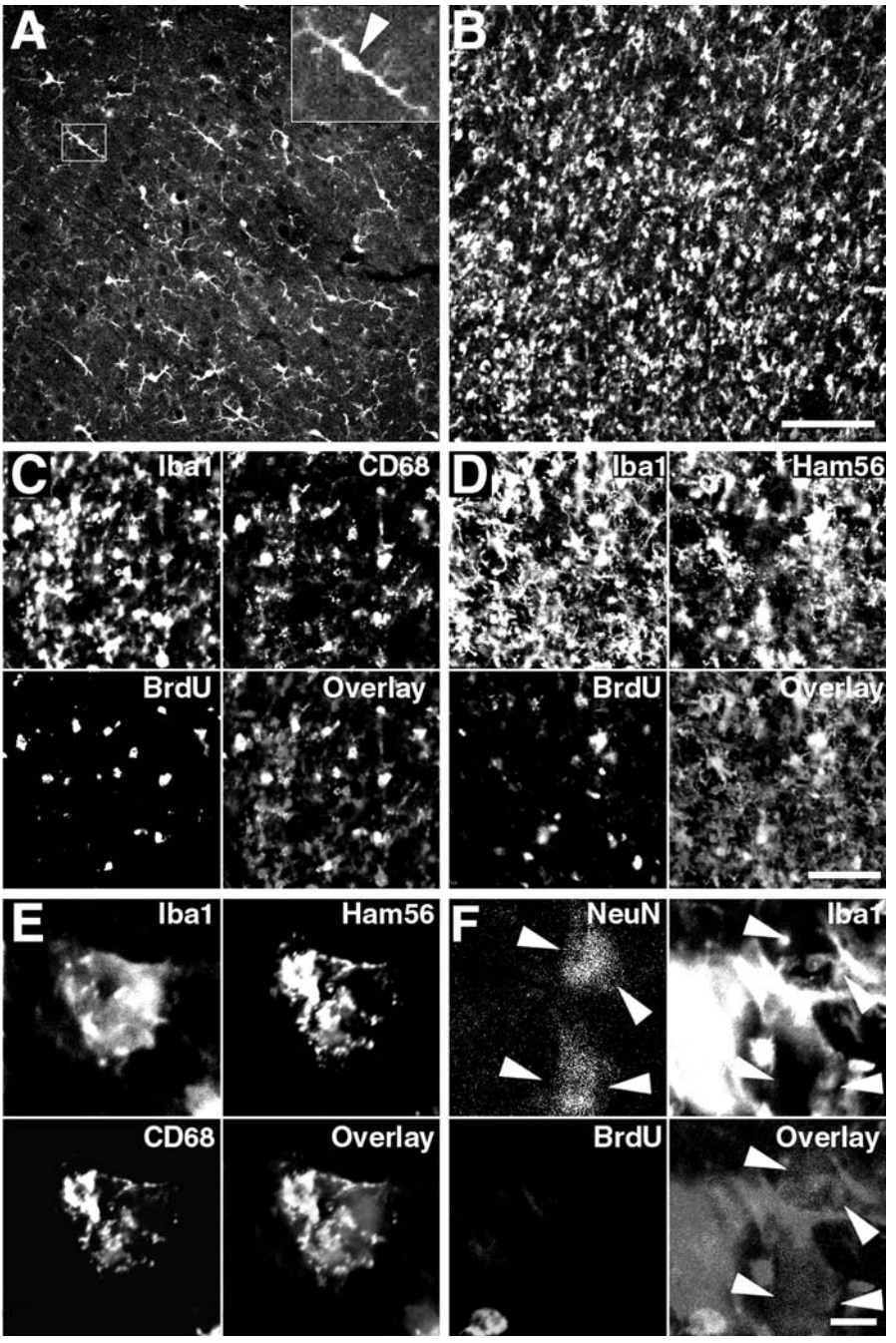
A
B
C
Iba1
CD68
BrdU
Overlay
D
Iba1
Ham56
BrdU
Overlay
E
Iba1
Ham56
CD68
Overlay
F
NeuN
Iba1
BrdU
Overlay

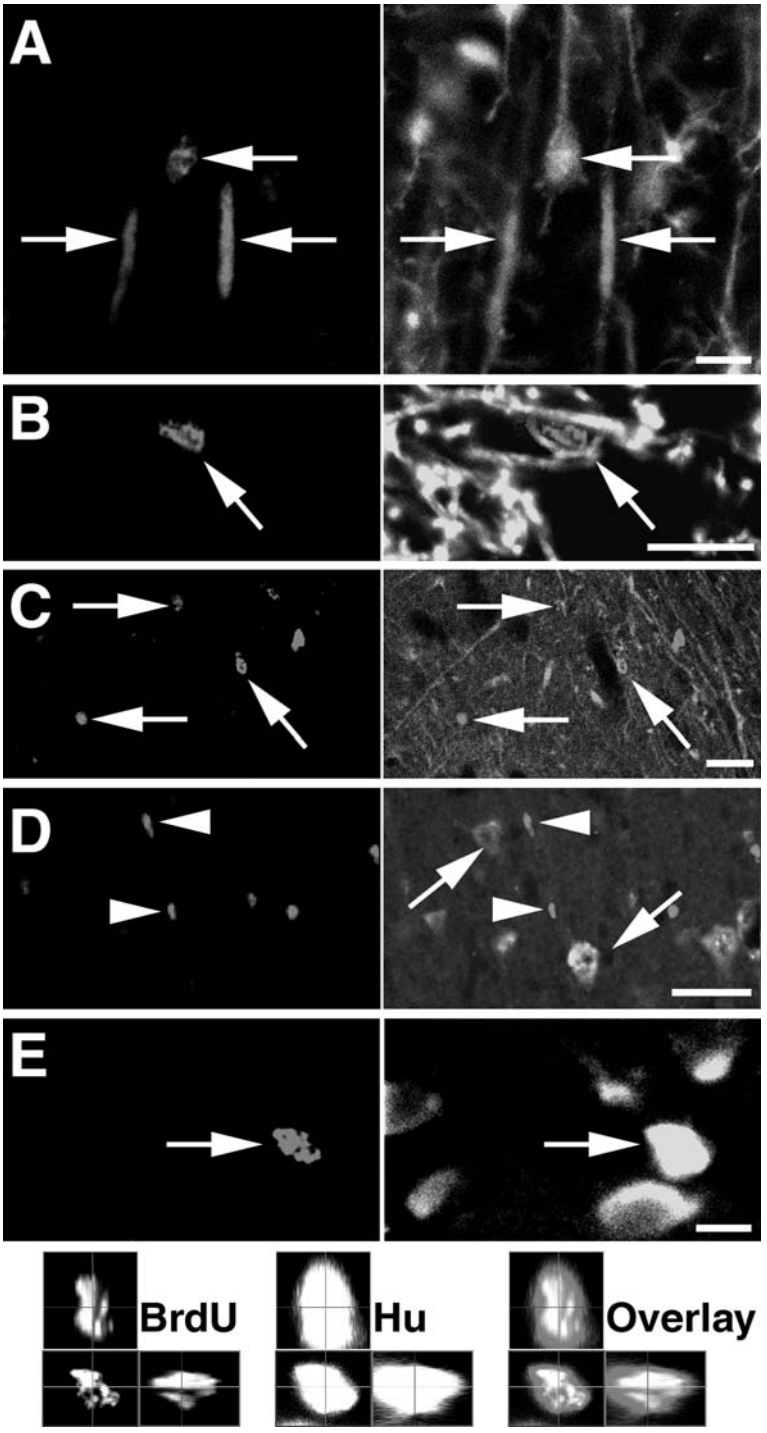
A
B
C
D
E
BrdU
Hu
Overlay

boid morphology of activated microglial/macrophages (Fig. 22B). Such cells coexpressed the markers CD68 (Fig. 22C) and Ham56 (Fig. 22D). Frequently, globoid aggregates were formed by activated microglia positive for Iba1, CD68, and Ham56 (Fig. 22E). These cells were typically found in the vicinity $NeuN^+$ neurons, which the microglia/macrophages seemed to engulf (Fig. 22F). While CD68 colabeled almost completely with Iba1, only 30%–40% of $Iba1^+$ cells coexpressed Ham56 in the postischemic monkeys, and none in the controls. Thus, the activated microglia/macrophages could be classified as $Iba1^+/CD68^+/Ham56^+$ or $Iba1^+/CD68^+/Ham56^-$.

In the long-term survival monkey group, microglia again represented the largest proportion of $BrdU^+$ cells (Fig. 23A; Table 5). In addition, a few 2′,3′-cyclic nucleotide 3′-phosphodiesterase $(CNP)^+$ oligodendrocytes incorporated BrdU in the postischemic monkeys (Fig. 23B; Table 5). In the control CA, we identified just 1–2 $BrdU^+/CNP^+$ cells representing about 0.5% of the $BrdU^+$ cells. Thus, in the control monkeys most of the $BrdU^+$ cells were of an unidentified phenotype.

Unlike the situation in DG, in CA none of the $BrdU^+$ cells coexpressed the neuronal markers βIII-tubulin (Fig. 23C) or NeuN (Fig. 23D) at any time-point or in any monkey group. A single $BrdU^+/Hu^+$ cell in postischemic CA4 was observed (Fig. 23E) suggesting a possibility for a very low level of neurogenesis in that sector.

3.1.3 Subiculum

Subiculum did not show significant differences compared to CA1. Ischemia tended to increase the $BrdU^+$ cells, particularly in the subicular part adjacent to neighboring CA1. The proliferating cells were microglia and a few were astrocytes. Neuronal or oligodendroglial cell proliferation was not observed.

3.2 Subventricular Zone of the Inferior Horn of the Lateral Ventricle

SVZi is adjacent to CA and the temporal lobe white matter. Because of this proximity, we were interested in whether this zone might contain progenitor cells and what would be their postischemic fate. Cells incorporating BrdU in SVZi were observed at all time-points, but their number was markedly increased after ischemia (Fig. 24). $BrdU^+$ cells were seen along both the inferior rim of SVZi (adjacent to CA) and the superior rim of SVZi (adjacent to the temporal white matter; Fig. 24). The $BrdU^+$ cells were typically located beneath the ependymal lining of the inferior horn of lateral ventricle, and in the short-term monkey group were single cells, or cells grouped in "doublets" or small clusters (3–4 cells) (Fig. 26A). In the long-term group, however, the $BrdU^+$ cells were not observed in aggregates (Fig. 27).

Statistical analysis demonstrated that the postischemic increase of $BrdU^+$ cells in the short-term monkey group was significant only on days 9 and 15, while the postischemic day-4 SVZi did not show statistically significant differences to

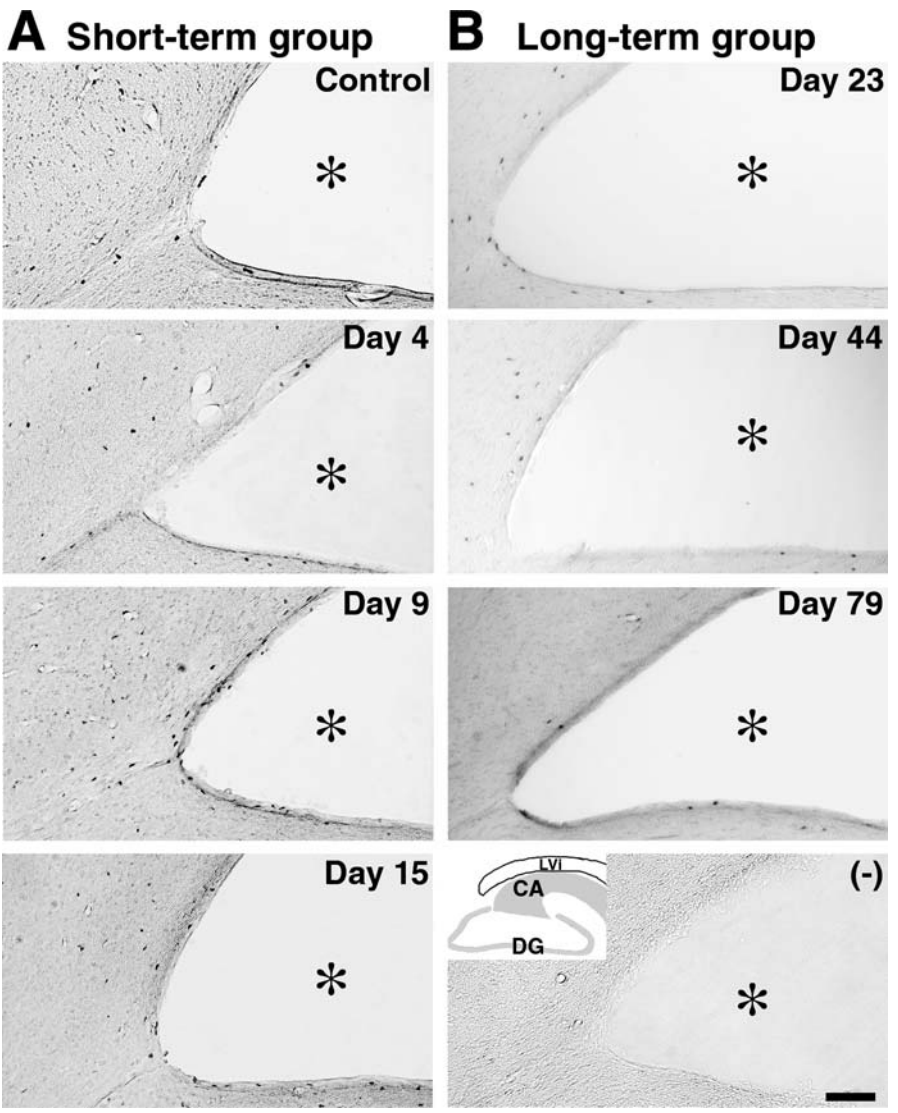

Fig. 24A, B Staining for BrdU in SVZi of short-term (**A**) and long-term (**B**) monkey groups. Note the increase of positive cells after ischemia. A monkey not injected with BrdU served as a negative control (−). The position of the visual field and its proximity to *cornu Ammonis* (CA) is schematically depicted in the *inset* of the negative control micrograph. *Asterisk*, lumen of the inferior horn of the lateral ventricle. *Scale bar* = 100 μm

the control (Fig. 25A). Within the long-term survival group, the postischemic monkeys had significantly more $BrdU^+$ cells on days 23 and 44 compared to the controls (Fig. 25B), and the day-79 monkeys had significantly more $BrdU^+$ cells than the day-44 controls (78±4 versus 35±10 cells/mm^2, $p < 0.001$, paired t test).

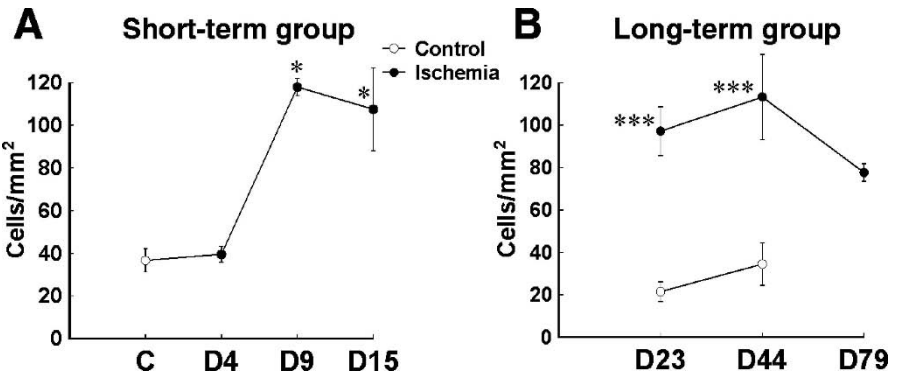

Fig. 25A, B Statistical analysis of the density of $BrdU^+$ cells in SVZi. **A** In the short-term survival group after BrdU the density was increased with statistical difference in the second postischemic week (days 9 and 15). **B** In long-term monkey group the density was significantly higher in postischemic compared to control brains. $*p < 0.05$, $***p < 0.001$ versus controls, one-way ANOVA followed by Tukey–Kramer *post hoc*

At the same time, a significant decrease of the density of $BrdU^+$ cells was observed on postischemic day 79 compared to postischemic day 44 (78±4 versus 113±20 cells/mm^2, $p < 0.01$, paired t test).

Analysis of cell marker expression by $BrdU^+$ cells revealed numerous $BrdU^+$/$Musashi1^+$ or $BrdU^+$/$Nestin^+$ cells along the inferior rim of SVZi (Fig. 26A, B). These cells were frequently in "doublets" or small clusters compatible with the results acquired by single BrdU immunostaining. Notably, the $BrdU^+$/$Musashi1^+$ and the $BrdU^+$/$Nestin^+$ cells were negative for the astrocytic marker GFAP (Fig. 26A; arrows), although $BrdU^-$/$Musashi1^+$ cells did co-stain with GFAP (Fig. 33A; arrowheads). A typical morphology of $BrdU^+$/$Nestin^+$ cells was a bipolar appearance with processes extended along and beneath the ependymal lining (Fig. 26B; arrowheads). BrdU incorporation into cells positive

Table 6 Percentages of colabeling of BrdU with progenitor cell markers in SVZi adjacent to CA1 sector. $BrdU^+$ cells were sampled for colabeling with any of Musashi1, Nestin, Doublecortin, or βIII-tubulin as described in the text

	Day 9		Day 23		Day 44		Day 79	
	Control	Ischemia	Control	Ischemia	Control	Ischemia	Control	Ischemia
Musashi1	35±6	44±8	26±8	37±10	41±13	46±9	NA	37±8
Nestin	19±5	20±6	17±6	31±9	27±11	32±12	NA	26±9
Doublecortin	0	3±1*	0	0	0	0	NA	0
βIII-Tubulin	0	2±1*	0	0	0	0	NA	0

NA, not available $*p < 0.05$ versus control (day 9 sham operation), Kruskal–Wallis or Mann–Whitney tests

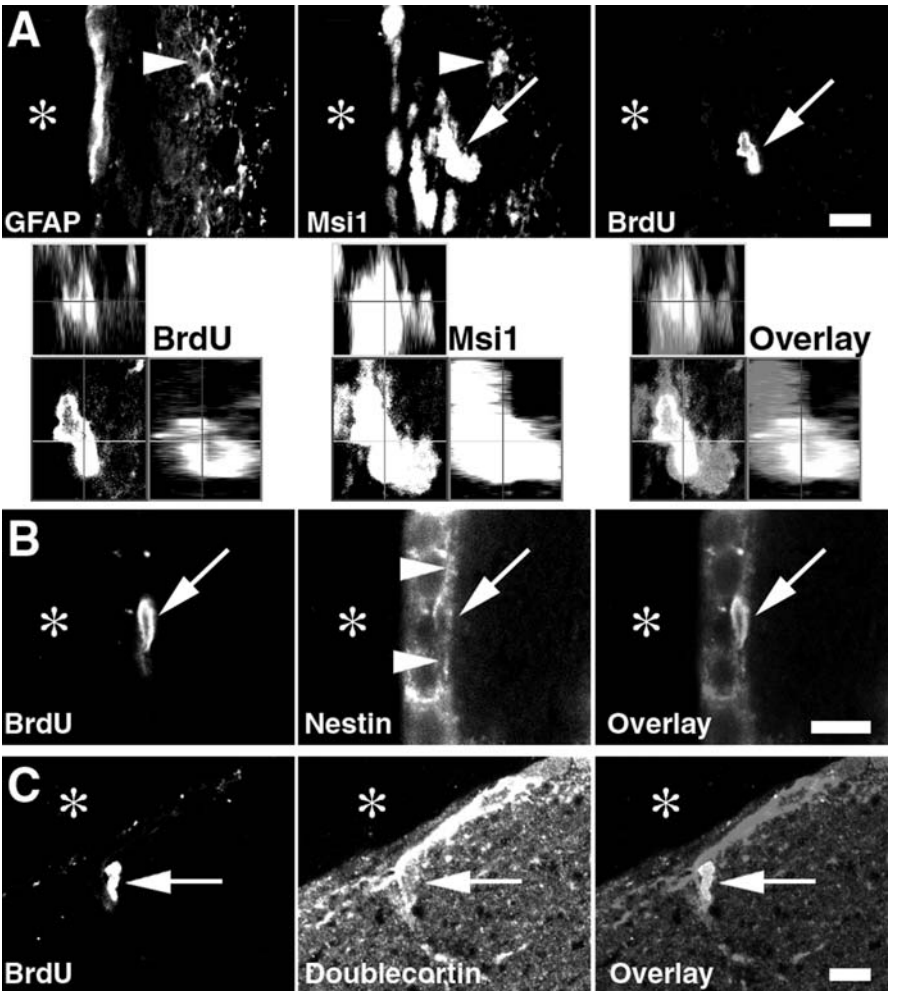

Fig. 26A–C Double-staining for BrdU and progenitor markers in SVZi of short-term monkey group. **A** A BrdU/Musashi1 double-stained cluster (*arrows*) is distinct from a neighboring Musashi1$^+$/GFAP$^+$ cell (*arrowheads*). High-magnification view of the cluster with channel separation and orthogonal projections is shown in the *lower panel*. The image is from a day-4 monkey. **B** Double-staining for BrdU and Nestin (day 9) showing a double-positive cell (*arrows*) extending processes (*arrowheads*) in subependyma. **C** A cell double-stained for BrdU and Doublecortin (day 9; *arrows*) exhibits a similar morphology and localization to the BrdU$^+$/Nestin$^+$ cell. *Asterisk*, lumen of inferior horn of the lateral ventricle. *Scale bars* = 10 μm

for neuronal progenitor markers such as Doublecortin was seen in the short-term survival group and their morphology was similar to that of the BrdU$^+$/Nestin$^+$ cells—subependymal localization with processes extended along the ependymal layer (Fig. 26C).

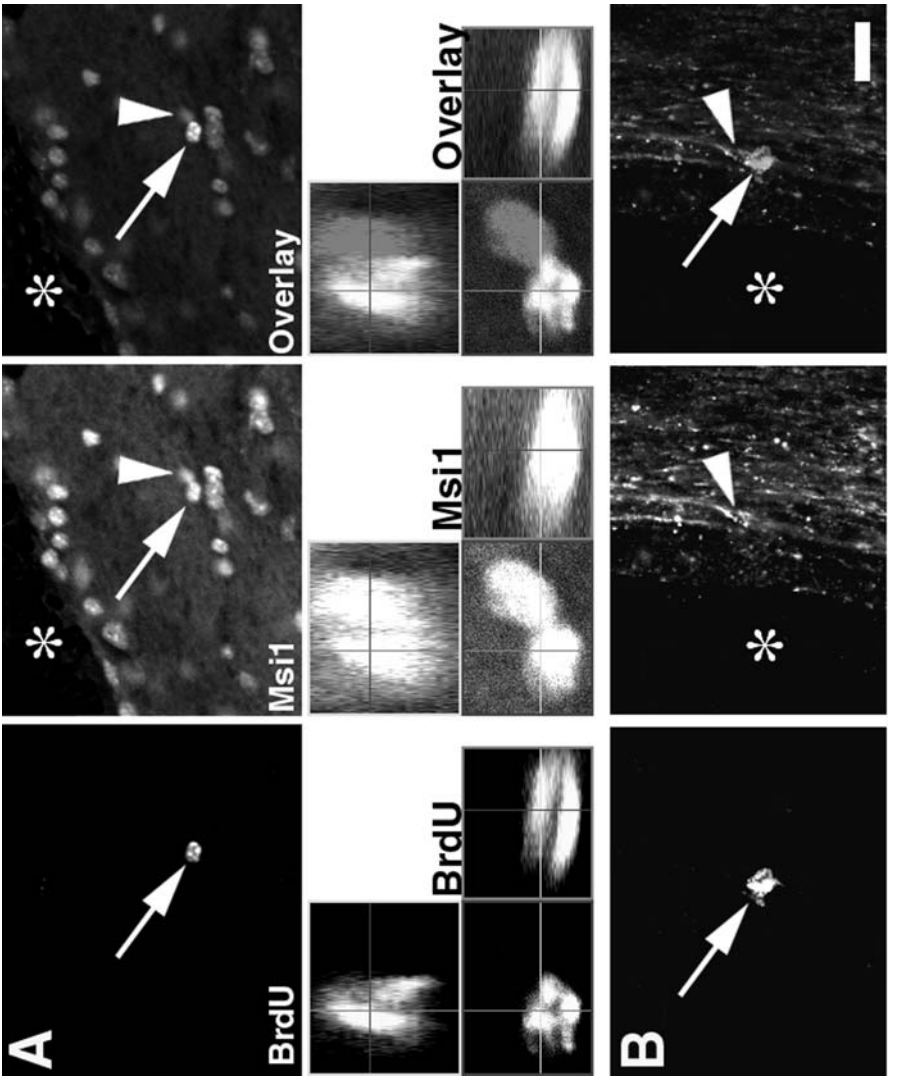

Fig. 27A, B Double-staining for BrdU and progenitor markers in SVZi of the long-term monkey group. **A** BrdU/Musashi1 double-staining (day 44) reveals a Musashi1$^+$ "doublet"; one of the cells is BrdU$^+$/Musashi1$^+$ (*arrows*), while the other is BrdU$^-$/Musashi1$^+$ (*arrowheads*). A high-magnification view of the "doublet" with channel separation and orthogonal projections is shown in the *lower panel*. **B** Double-staining for BrdU and Doublecortin (day 44) shows that a BrdU$^+$ cell (*arrows*) is adjacent but distinct from a Doublecortin$^+$ cell (*arrowheads*). *Asterisk*, lumen of inferior horn of the lateral ventricle. *Scale bar* = 20 μm

The percentages of $BrdU^+$ cells coexpressing Musashi1 or Nestin was 20%–40% at different time-points with no significant difference between control and postischemic animals (Table 6). In the long-term survival group, the $BrdU^+$ cells remaining in SVZi expressed neural progenitor markers such as Musashi1 (Fig. 27A, Table 6). Double-labeling with neuronal progenitor markers was not observed (Fig. 27B, Table 6), which is similar to the situation in adjacent CA.

3.3 Temporal Lobe

Two major subdivisions of the temporal lobe were investigated: PHR and the temporal neocortex (including IT and STG).

3.3.1 Parahippocampal Region

We investigated $BrdU^+$ cell distribution profiles in control and postischemic monkey PHR. The $BrdU^+$ nuclei were randomly scattered throughout the cortical layers and their density did not seem to change after ischemia. $BrdU^+$ clusters were not observed, and only rarely $BrdU^+$ "doublets" were seen, as most $BrdU^+$ cells were single cells. Statistical analysis confirmed the impression that ischemia had not altered the density of $BrdU^+$ cells—these had a density of about 15 cells/mm^2 in the short-term group and about 20 cells/mm^2 in the long-term group, without statistically significant changes between control and ischemic brains (Fig. 28). The only exception was the postischemic day-79 PHR showing a significant decrease of $BrdU^+$ cells compared to earlier time-points (Fig. 28).

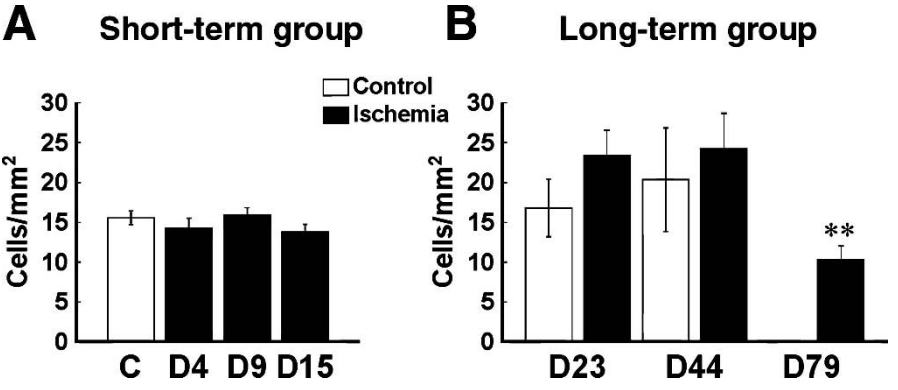

Fig. 28A, B Statistical analysis of the density of $BrdU^+$ cells in PHR. **A** In the short-term survival group after BrdU the density remains without significant changes. **B** In the long-term monkey group no change was observed between postischemic and control monkeys on days 23 and 44. However, the density on day 79 was significantly lower compared to days 23 and 44. $^{**}p < 0.001$, one-way ANOVA followed by Tukey–Kramer *post hoc*

The dramatic difference between the density of $BrdU^+$ cells in postischemic PHR and the density in neighboring regions such as CA1 or IT was evident when low-magnification micrographs were evaluated in control and postischemic monkeys. A dense band of positive cells in postischemic CA1 contrasted the dispersed single

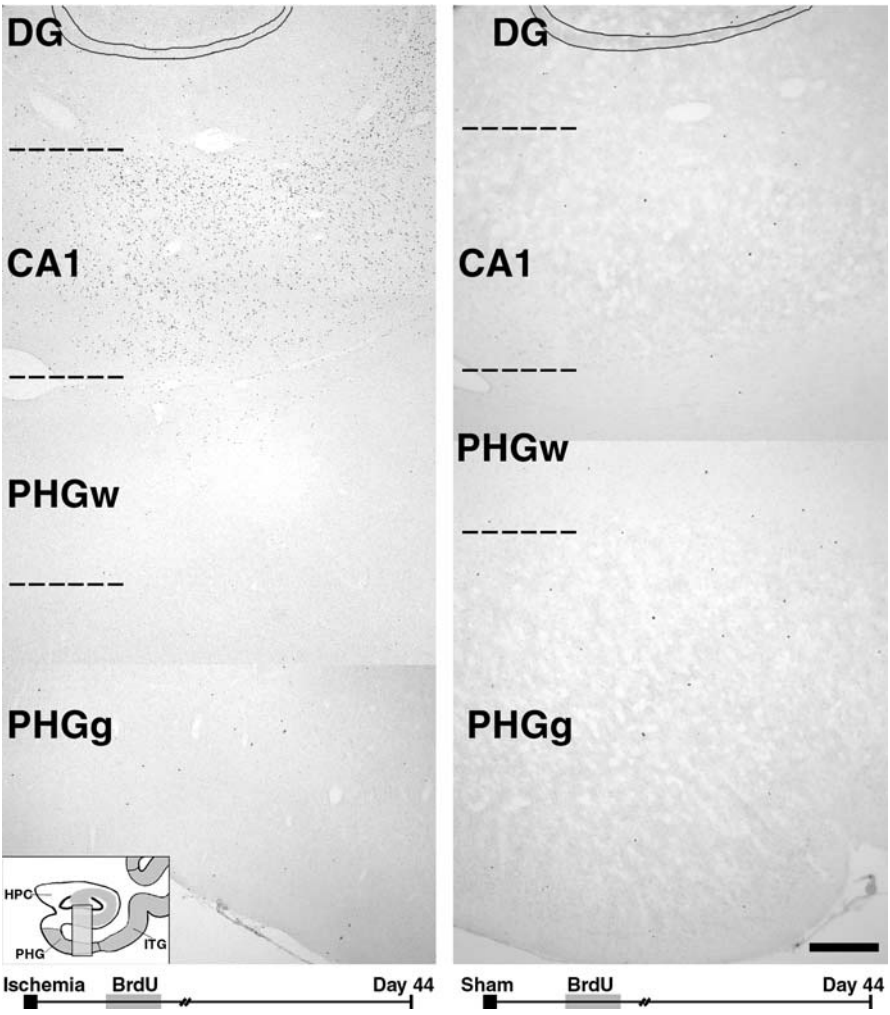

Fig. 29 Composite micrographs of BrdU immunostaining in the temporal lobe, including the hippocampal formation (HPC) and PHR (parahippocampal gyrus, PHG). Postischemic (*left*) and sham-operated (*right*) day-44 monkey brains are depicted. Note the greater density of positive cells in postischemic CA1 as compared to either postischemic PHR or control CA1. The frame on the map in the *inset* depicts the position of the visual field within the temporal lobe. The BrdU labeling protocol for each of the monkey groups is shown *below* the respective image. The contours of DGL are *outlined*; *PHGg*, *PHGw*, gray or white matter of PHG. *Scale bar* = 200 μm

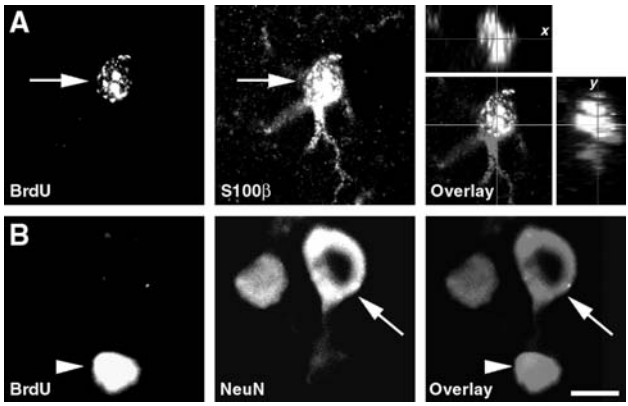

Fig. 30A, B Phenotype of BrdU$^+$ cells in PHR. **A** BrdU-labeled astroglial cell on postischemic day 23 (*arrows*). **B** NeuN$^+$ neurons (*arrows*) are negative for BrdU (*arrowheads*) (postischemic day 44). *Scale bar* = 10 μm

cells in PHR, while in control brains the BrdU$^+$ cells were few and single in all regions (Fig. 29). A similar sharp contrast was observed when comparing the lateral bank of the PHG (part of PHR) with the adjacent inferior bank of the inferior temporal gyrus (a component of IT). The occipitotemporal sulcus representing the boundary between the PHR and IT divided the zone with marked postischemic proliferation (IT) from the zone with unchanged proliferation after ischemia (PHR).

Investigating the phenotype of BrdU$^+$ in PHR we did not observe differences between control and postischemic brains. A proportion of BrdU$^+$ cells (up to 15%) expressed the phenotype of either microglia or astroglia (Fig. 30A), and some vascular cells incorporated BrdU as well. BrdU$^+$ oligodendrocytes or cells with a neuronal phenotype were not observed (Fig. 30B). Thus, over 75% of the BrdU$^+$ cells in the PHR were of an unknown phenotype.

3.3.2 Temporal Neocortex

Two main subdivisions of the temporal neocortex were investigated—the visual area IT and the auditory area STG. We did not observe important differences between IT and STG with regard to the distribution and phenotype of BrdU$^+$ cells, and therefore these regions are presented in a common section.

In IT the pattern of BrdU$^+$ cell distribution in control and postischemic brains followed that in the hippocampal formation. The quantity of the BrdU$^+$ on postischemic day 4 did not show differences compared to the control. However, from postischemic day 9, numerous BrdU$^+$ cells were observed in both gray and white matter of IT (Fig. 31). Statistical analysis confirmed the significant increase of BrdU$^+$ cells in the second postischemic week in both gray and white matter of IT

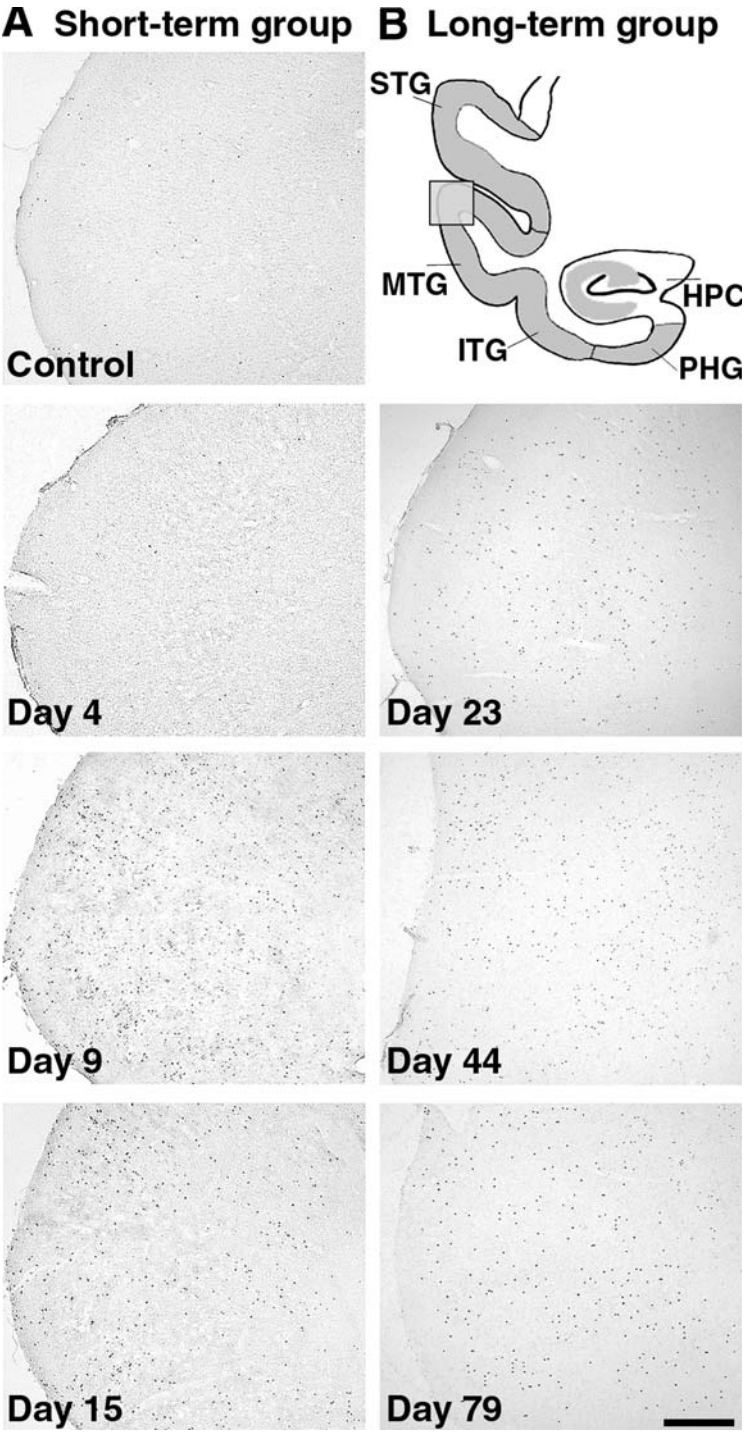
A Short-term group
B Long-term group
STG
MTG
HPC
ITG
PHG
Control
Day 4
Day 23
Day 9
Day 44
Day 15
Day 79

Fig. 31 Staining for BrdU in IT of short-term (**A**) and long-term (**B**) monkey groups. Note the increase of positive cells after ischemia. The position of the visual field within the temporal lobe is schematically depicted as a *frame* in the map (*upper right*). *STG*, *MTG*, and *ITG*, superior, middle and inferior temporal gyrus; *PHG*, parahippocampal gyrus; *HPC*, hippocampal formation. *Scale bar* = 500 μm

of the short-term survival group (Fig. 32A). In the long-term survival group, the postischemic monkeys had significantly more $BrdU^+$ cells than respective controls (Fig. 32B). The density of $BrdU^+$ cells in the long-term postischemic group was not statistically different from the short-term group (day 9), thus suggesting a sustained existence of newly generated cells in postischemic monkey IT.

In STG, ischemia increased the $BrdU^+$ cells in the second postischemic week (days 9 and 15; Fig. 33A), in a similar way to IT. The upregulated $BrdU^+$ cells sustained their presence and density in STG of the log-term survival monkey group with postischemic monkeys exhibiting significantly more $BrdU^+$ cells than controls (Fig. 33B). In both IT and STG, the $BrdU^+$ cells were more numerous in the gray matter than in the white matter. This was particularly evident in IT, where the density of $BrdU^+$ cells in gray matter was approximately three times higher than the density in white matter (Fig. 32A).

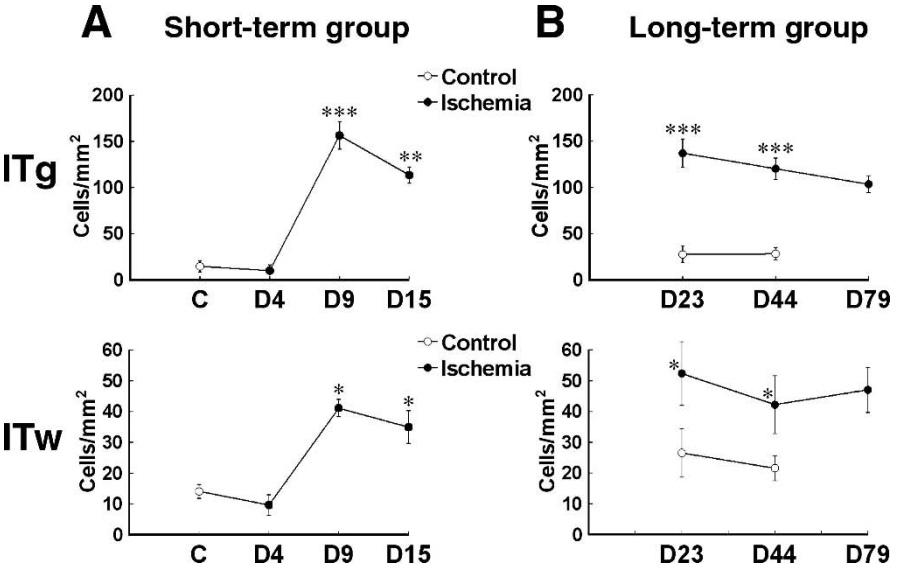

Fig. 32A, B Statistical analysis of the density of $BrdU^+$ cells in gray matter (*ITg*) and white matter (*ITw*) of IT. **A** In the short-term survival group after BrdU the density was increased in the second postischemic week. **B** In the long-term monkey group the postischemic monkeys on days 23 and 44 had more $BrdU^+$ cells compared to respective controls. $^{***}p < 0.001$, $^{**}p < 0.01$, $^{*}p < 0.05$ versus controls, *t* test or one-way ANOVA followed by Tukey–Kramer *post hoc*

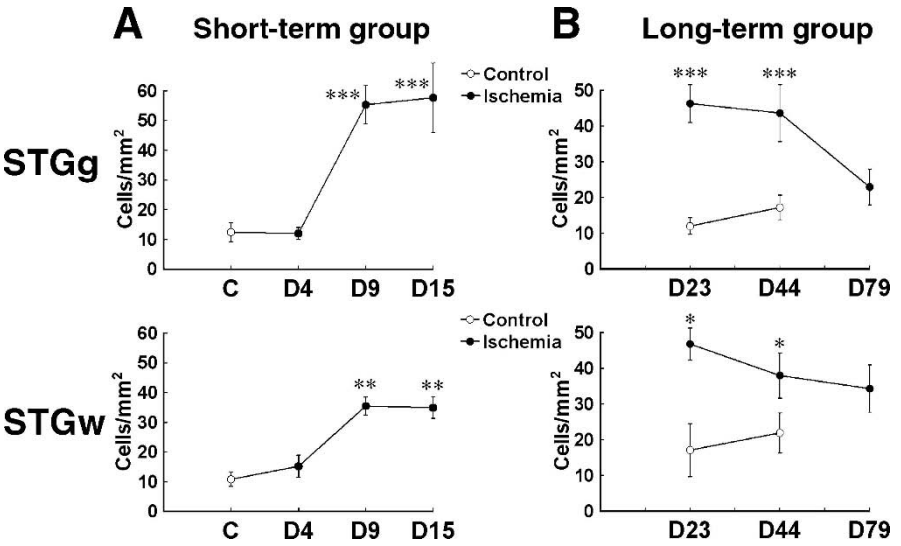

Fig. 33A, B Statistical analysis of the density of $BrdU^+$ cells in gray matter (*STGg*) and white matter (*STGw*) of STG. **A** In the short-term survival group after BrdU the density was increased in the second postischemic week. **B** In long-term monkey group the postischemic monkeys on days 23 and 44 had more $BrdU^+$ cells compared to respective controls. $^{***}p < 0.001$, $^{**}p < 0.01$, $^{*}p < 0.05$ versus controls, *t* test or one-way ANOVA followed by Tukey–Kramer *post hoc*

Table 7 Percentages of colabeling of BrdU with neuronal markers in SVZi/temporal white matter (Doublecortin, βIII-tubulin, TUC4, Hu) or gray matter (Hu, NeuN). $BrdU^+$ cells were sampled for colabeling as described in the text

	Day 9		Day 23		Day 44		Day 79	
	Control	Ischemia	Control	Ischemia	Control	Ischemia	Control	Ischemia
Doublecortin	0	2±0.5*	4±1	6±2	7±5	9±4	NA	8±3
βIII-Tubulin	0	3±0.5*	5±1	6±1	7±3	11±6	NA	5±2
TUC4	0	2±0.5*	3±2	8±4	6±3	7±3	NA	6±3
Hu	0	2±0.5*	0	4±2**	0.5±0.5	3±1**	NA	2±1
NeuN	0	1±0.2*	0	1±0.5*	0.5±0.5	2±0.5*	NA	1±0.5*

NA, not available $^{*}p < 0.05$, $^{**}p < 0.01$ versus respective controls, Kruskal–Wallis or Mann–Whitney tests

Fig. 34A–C Double-staining for BrdU and neuronal progenitor markers in superior rim of SVZi and temporal white matter. **A** $BrdU^+$/$Doublecortin^+$ cell (day 9; *arrow*). A $BrdU^+$/$Doublecortin^-$ cell is depicted by an *arrowhead*. **B** $BrdU^+$/βIII-$tubulin^+$ cell (day 9; *arrow*). **C** $BrdU^+$/$TUC4^+$ cell (day 15; *arrow*). Note that all these cells extend processes (*arrowheads*) in SVZ and adjacent white matter. *Asterisk*, inferior horn of lateral ventricle. *Scale bar* = 10 μm

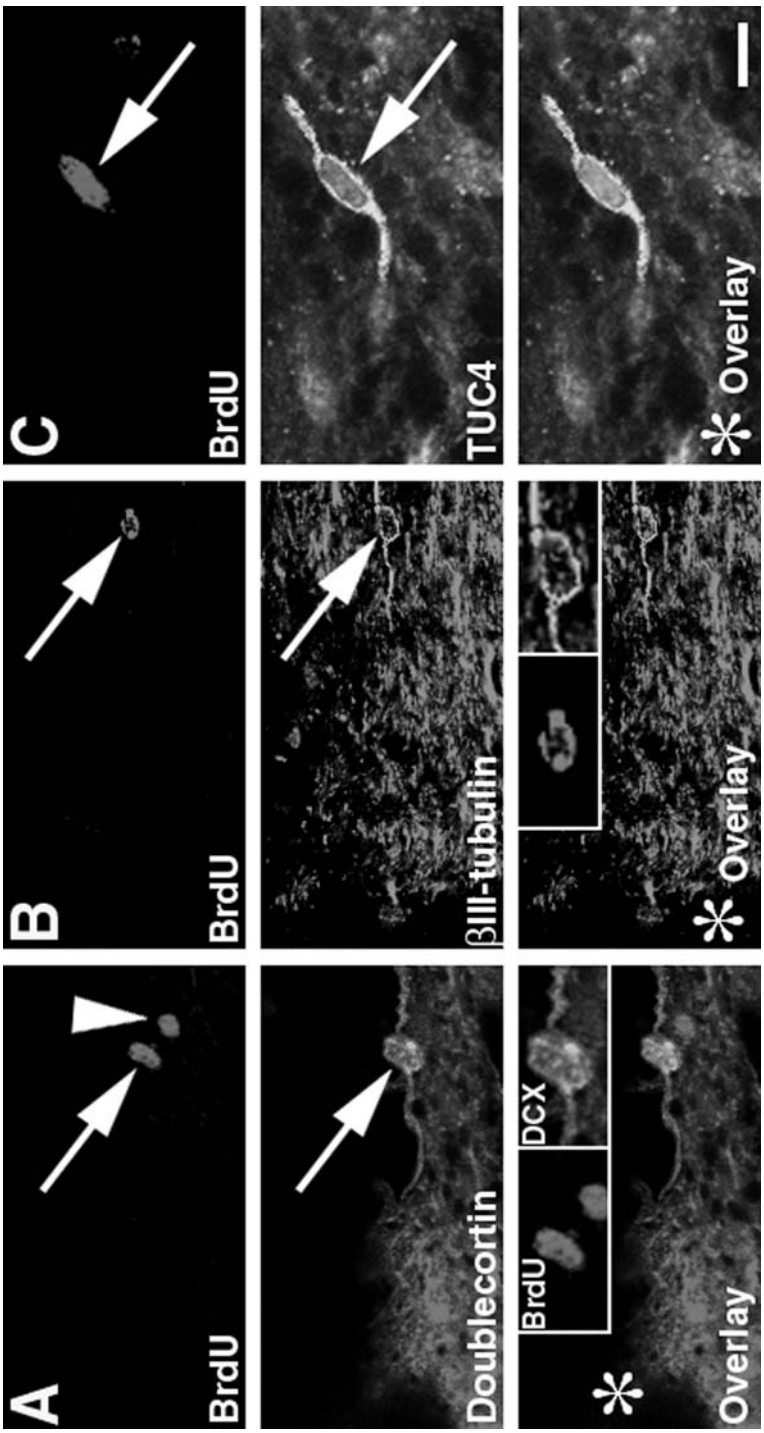
A
BrdU
Doublecortin
BrdU
DCX
Overlay
B
BrdU
βIII-tubulin
Overlay
C
BrdU
TUC4
Overlay

In the superior rim of SVZi adjacent to the temporal white matter as well as in the white matter itself, we observed cells positive for the neuronal markers βIII-tubulin, Doublecortin, TUC4, and Hu, while in the gray matter, cells were positive for Hu and NeuN. Some of these cells incorporated BrdU (Fig. 34). The $BrdU^+/\beta III\text{-tubulin}^+$ cells, $BrdU^+$/Doublecortin$^+$ cells, or BrdU/$TUC4^+$ cells were typically located near SVZi (Fig. 34; asterisks). In contrast, the $BrdU^+/Hu^+$ cells were located in deep white matter or gray matter (Tonchev et al. 2003a). $BrdU^+/NeuN^+$ cells were observed only in gray matter (Fig. 35A, B). Within the short-term survival group, BrdU co-

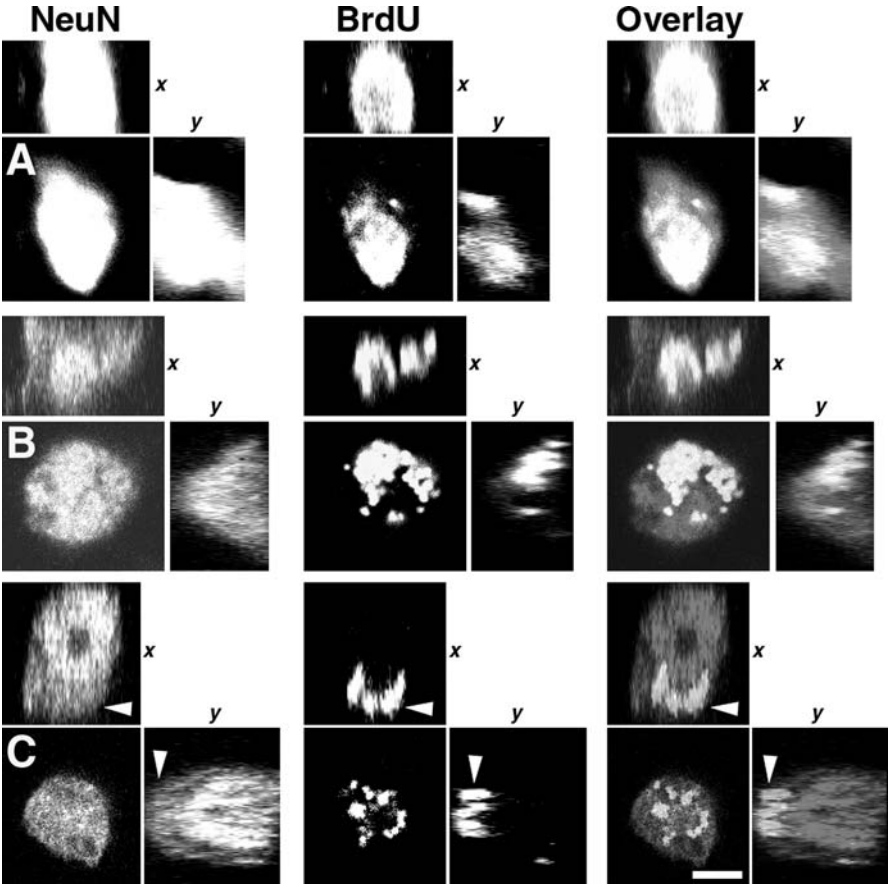

Fig. 35A–C Double-staining for BrdU and NeuN in temporal neocortex. Digital reconstructions of the cells in the *x* and *y* axes were generated to confirm colocalization of signals. **A** Double-labeled cell in postischemic day-15 IT. **B** Double-labeled cell in postischemic day-44 STG. Note the complete colocalization of the BrdU signals within the NeuN channels. **C** The $BrdU^+$ cell appears to be double-labeled when observed in the *z* axis. However, reconstructions in *x* and *y* axes revealed that the BrdU signal (*arrowheads*) is cytoplasmic, and this cell was not considered double-labeled. *Scale bar* = 5 μm

stained with any of the neuronal markers only in postischemic monkeys (Table 7). In the long-term survival group, BrdU$^+$/βIII-tubulin$^+$ cells, BrdU$^+$/Doublecortin$^+$ cells, or BrdU$^+$/TUC4$^+$ cells were seen also in the controls (Table 7). However, BrdU$^+$/NeuN$^+$, or BrdU$^+$/Hu$^+$ cells were found only in the postischemic monkeys, with the exception with single double-labeled cells in a sham-operated (day 44) monkey (Table 7). Thus, unambiguous evidence for neuronal differentiation of BrdU$^+$ cells in monkey temporal neocortex was evident only in postischemic monkeys. Some BrdU$^-$/NeuN$^+$ cells, in which the BrdU signal had perikaryal (not nuclear) localization, optically appeared as double-labeled. However, careful evaluation of a stack of serial optical planes acquired by laser confocal microscopy demonstrated the extranuclear localization of the BrdU signal (Fig. 35C), and such cells were excluded from our calculations of BrdU/NeuN double-stained cells.

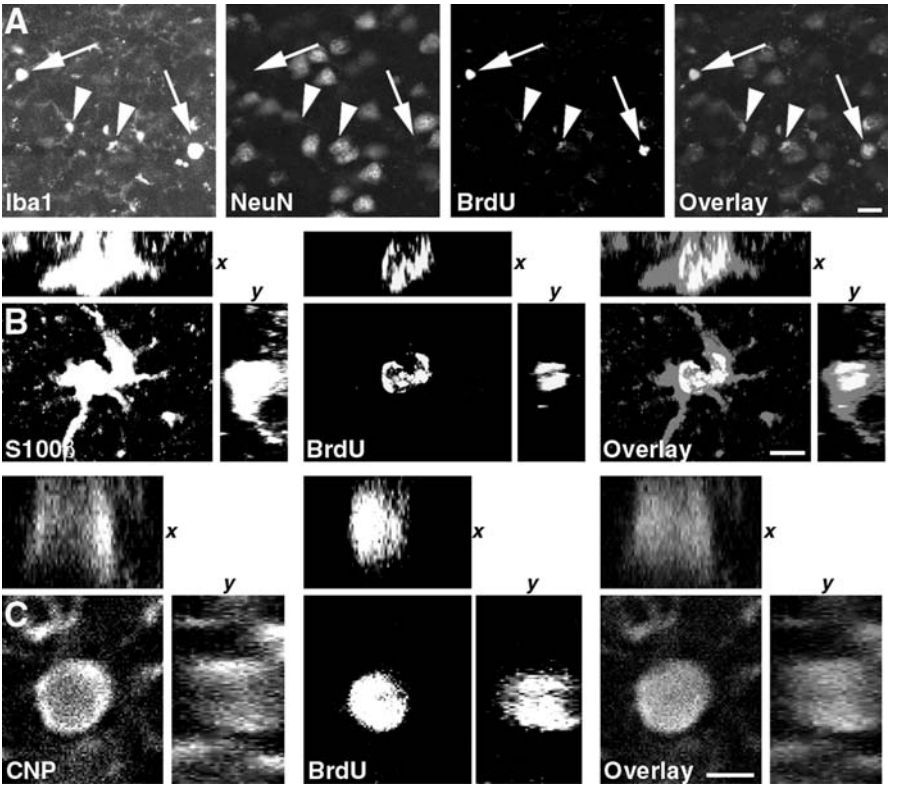

Fig. 36A–C Glial proliferation in temporal neocortex after ischemia. **A** Triple-staining for Iba1, NeuN, and BrdU in postischemic day-15 STG. Note Iba1/BrdU double-labeled clusters (*arrows*) or single cells in the vicinity of NeuN$^+$ neurons (*arrowheads*). **B** Double-staining for S100β and BrdU in postischemic day-23 IT. Note an S100β^+/BrdU$^+$ "doublet." **C** A CNP$^+$ oligodendrocyte colabeled for BrdU in the postischemic day-79 IT. *Scale bars* = 20 μm (**A**); 10 μm (**B**); 5 μm (**C**)

Table 8 Percentages of colabeling of BrdU with glial markers in temporal neocortex. $BrdU^+$ cells were sampled for colabeling with Iba1, S100β, or CNP as described in the text

	Day 9		Day 23		Day 44		Day 79	
	Control	Ischemia	Control	Ischemia	Control	Ischemia	Control	Ischemia
Iba1	8±3	77±17***	7±3	81±21***	10±6	79±24***	NA	73±12
S100β	0	13±6***	3±1	14±6***	3±1	12±5***	NA	10±5
CNP	0	2±0.5*	0,5	3±1*	0.5	4±2*	NA	3±2*

NA, not available ***$p < 0.001$, *$p < 0.05$ versus respective controls, Kruskal–Wallis or Mann–Whitney tests

As with CA, the majority proliferating cells in monkey temporal neocortex were of the glial phenotype. Microglial cells were the most numerous cell type, particularly in the postischemic monkeys, in which they constituted over 70% of the $BrdU^+$ cells (Fig. 36A; Table 8). Activated microglia/macrophages expressed the protein Ham56 (Tonchev et al. 2003b), frequently formed clusters (Fig. 36A; arrows), or were observed in the vicinity of neurons (Fig. 36A; arrowheads). Astrocytes were the second most common cell type with 10%–15% of the $BrdU^+$ cells adopting an astroglial phenotype (Table 8). BrdU-labeled astrocytes were either single cells or "doublets" (Fig. 36B). A few BrdU-labeled oligodendrocytes were seen, mostly in the white matter (Fig. 36C; Table 8). For all of the glial cell markers, the percentages of $BrdU^+$ cells coexpressing them were significantly higher in postischemic monkeys versus the respective controls (Table 8).

3.4 Subventricular Zone of the Anterior Horn of the Lateral Ventricle

We investigated the de novo generated cells in five representative locations within the SVZa (Fig. 3B, C): (1) dorsal SVZa at the roof of the ventricle capping the striatum; (2) septal SVZa along the medial wall of the lateral ventricle; (3) caudate SVZa along the lateral wall adjacent to the head of the caudate nucleus; (4) ventral SVZa at the floor of the ventricle; and (5) anterior SVZa at the rostral tip of the anterior horn of the lateral ventricle.

In dorsal SVZa, ischemia led to a visible increase of $BrdU^+$ cells, particularly on postischemic day 9 (Fig. 37). $BrdU^+$ cells were observed along a pathway located at the boundary between the frontal white matter and the striatal parenchyma that corresponds to RMS toward the olfactory bulb (Fig. 37; arrows). In the white matter, $BrdU^+$ cells were single (Fig. 37; arrowheads), and chains were not observed. Statistical evaluation of the density of $BrdU^+$ cells in dorsal SVZa revealed a significantly increased density on postischemic days 9 and 15 compared to short-term group control (Fig. 38A). In the long-term survival group after BrdU, the postischemic monkeys on days 23 and 44 exhibited significantly higher density of $BrdU^+$ cells compared to respective controls (Fig. 38B). We further analyzed the aggregation of $BrdU^+$ cells into small (composed of 2–4 cells) or large (composed of 5 or more

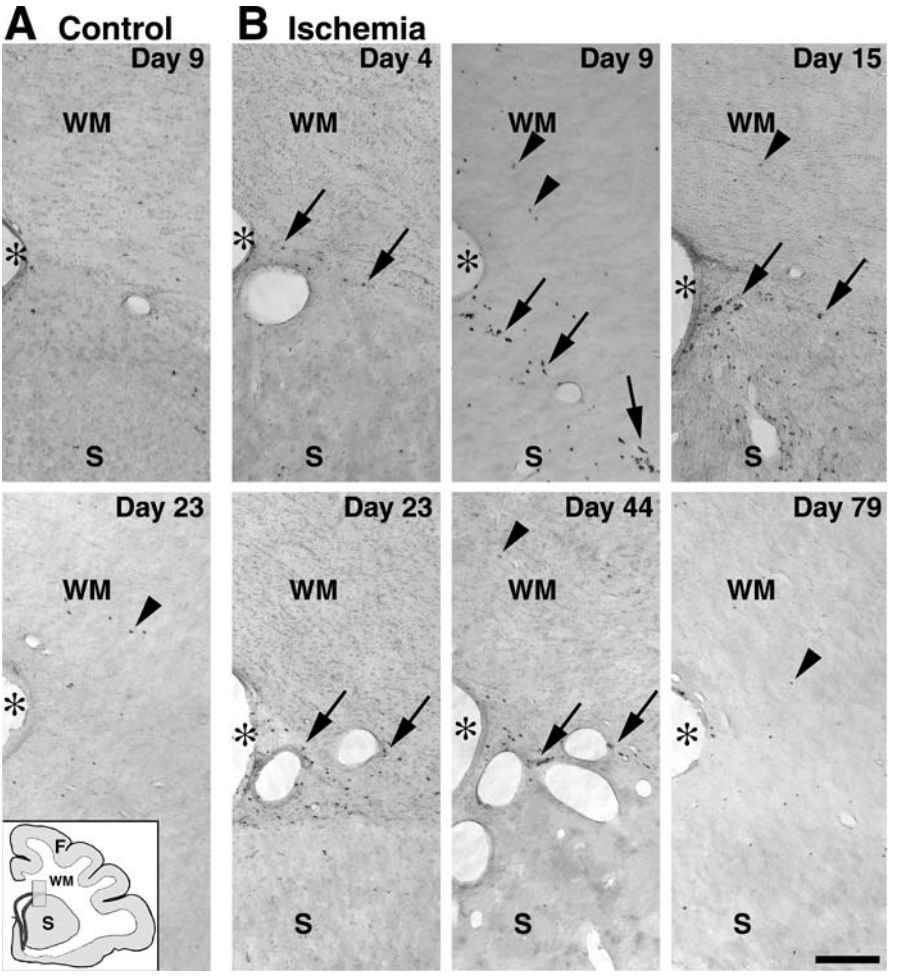

Fig. 37A, B Staining for BrdU in dorsal SVZa. **A** Control monkeys on days 9 and 23 after sham operation. **B** Postischemic monkeys on various time-points after ischemia. Note the increase of positive cells after ischemia. The position of the visual field within the frontal lobe is schematically depicted as a *frame* in the map (*lower left*). *F*, frontal cortex; *WM*, white matter; *S*, striatum. *Asterisk*, anterior horn of lateral ventricle. *Scale bar* = 200 μm

cells) clusters. The density of both the small and large clusters was significantly increased on postischemic days 9 and 15 compared to short-term group control (Fig. 38A). In the long-term survival group, however, small clusters were more numerous in the postischemic monkeys, while large cluster showed no differences to controls (Fig. 38B).

In septal SVZa, ischemia did not induce changes in the quantity of $BrdU^+$ cells (Fig. 39). Moreover, $BrdU^+$ cell clusters were absent, as all $BrdU^+$ cells were single cells.

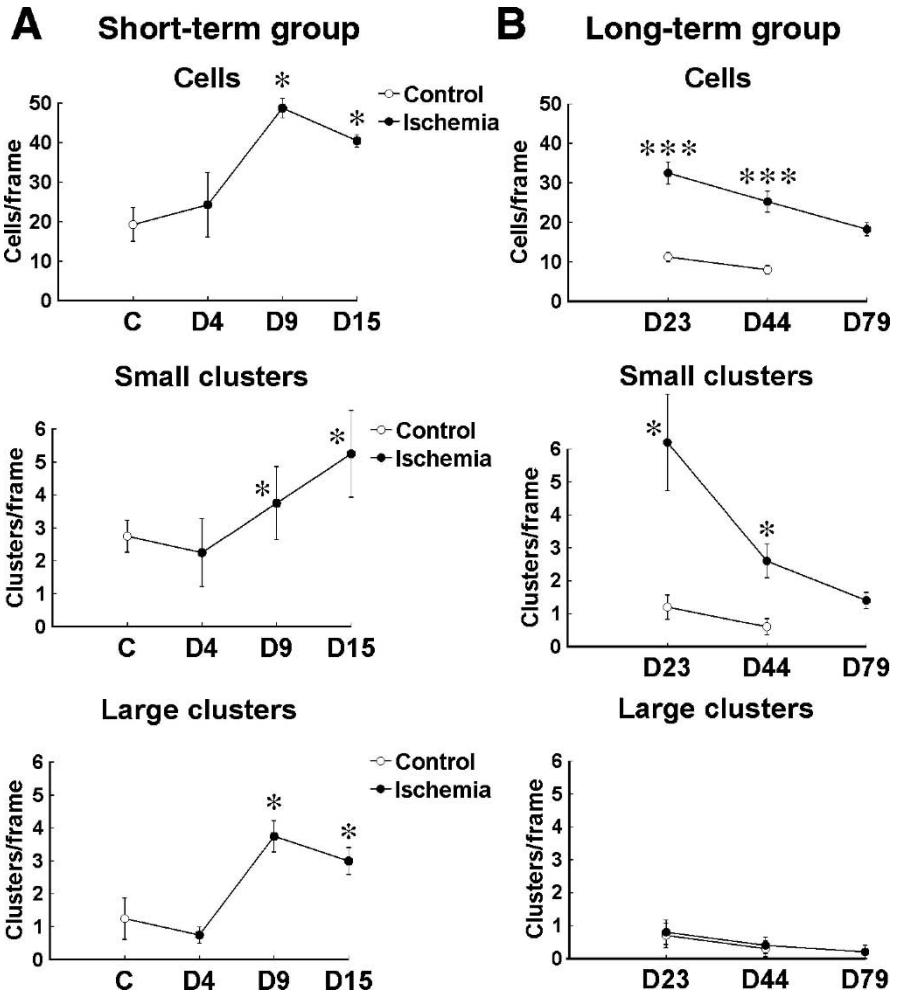

Fig. 38A, B Statistical analysis of the density of BrdU$^+$ cells in dorsal SVZa. **A** In the short-term survival group after BrdU, the BrdU$^+$ cells, small clusters, and large clusters experienced density increases in the second postischemic week. **B** In long-term monkey group the postischemic monkeys on days 23 and 44 had more BrdU$^+$ cells and more small clusters compared to respective controls, but the large clusters did not show differences. ***$p < 0.001$, *$p < 0.05$ versus control; *t* test or one-way ANOVA followed by Tukey–Kramer *post hoc*

In caudate SVZa, the BrdU$^+$ cells visibly increased after ischemia, and were grouped in large BrdU$^+$ cell clusters (Fig. 39; arrows). Statistical analysis showed that both cells and large clusters significantly increased density on postischemic days 9 and 15 compared to controls (Fig. 40A). In the long-term survival group, however, all of the BrdU$^+$ cells, small clusters, and large clusters exhibited a significantly higher density in the postischemic monkeys compared to controls (Fig. 40B).

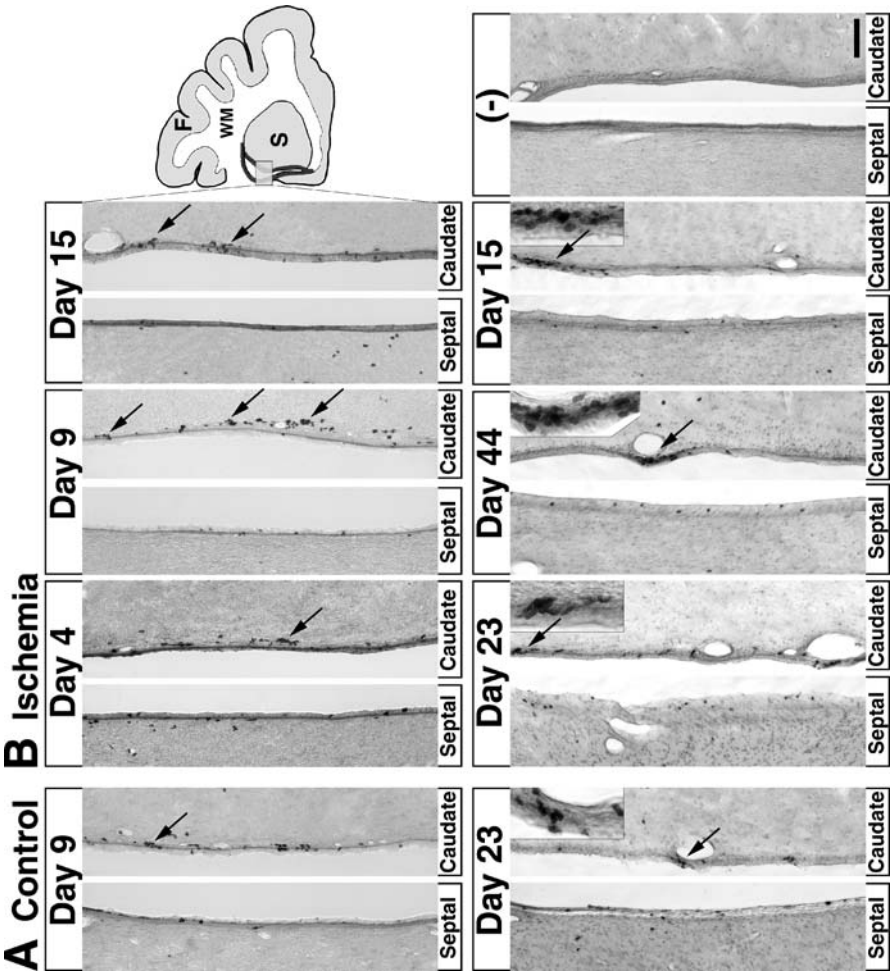

Fig. 39A, B Staining for BrdU in septal and caudate SVZa. **A** Control monkeys on days 9 and 23 after sham operation. **B** Postischemic monkeys on various time-points after ischemia. Note the increase of positive cells after ischemia. Clusters depicted by *arrows* are magnified in *insets*. The position of the visual field within the frontal lobe is schematically depicted as a *frame* on the map (*upper right*). (−), negative control showing no staining for BrdU; *F*, frontal cortex; *WM*, white matter; *S*, striatum. *Asterisk*, anterior horn of lateral ventricle. *Scale bar* = 100 μm

In ventral SVZa of the short-term survival monkeys, the $BrdU^+$ cells appeared as a single homogeneous aggregate (Fig. 41; arrows) initiating a chain of cells in RMS (Fig. 41; arrowheads). Therefore, in this group we were unable to discern between small and large clusters. In the long-term survival group, however, $BrdU^+$ chains were almost absent, and there were visibly fewer $BrdU^+$ cells than in the short-term survival group. Statistical analysis showed that the density of $BrdU^+$

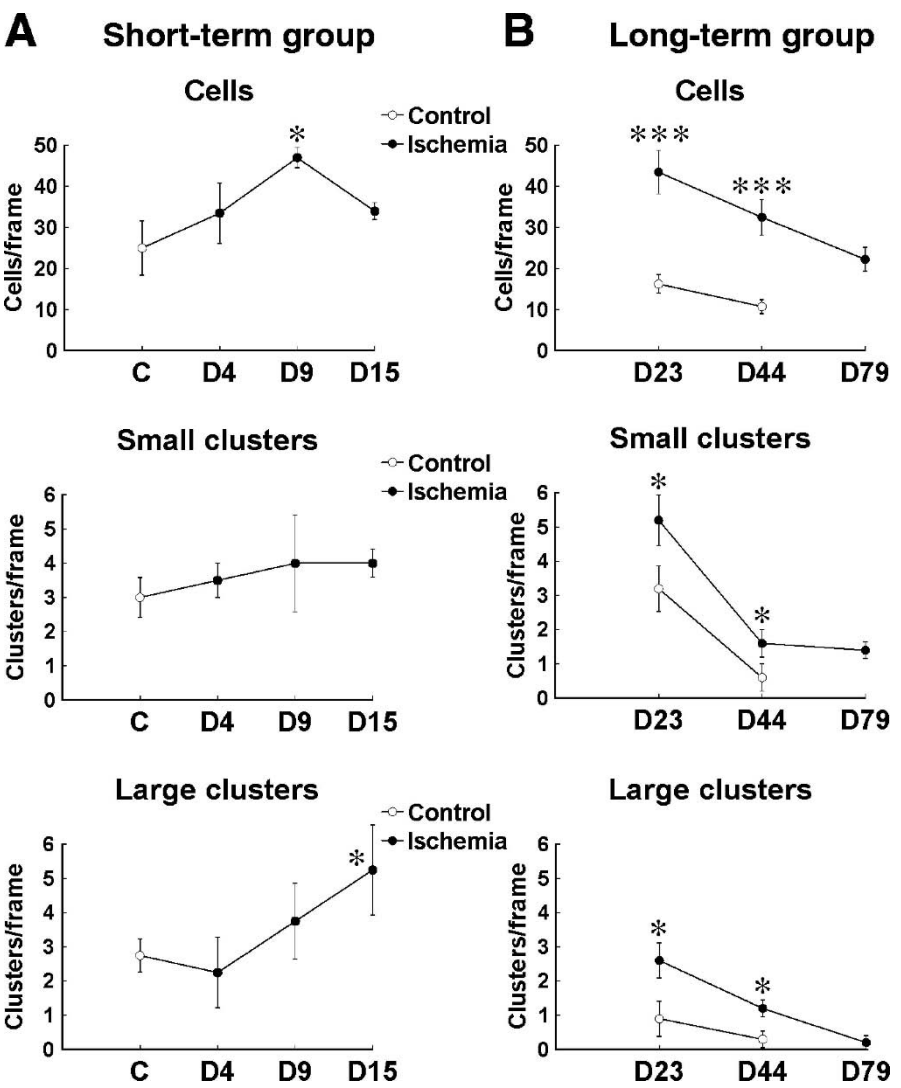

Fig. 40A, B Statistical analysis of the density of $BrdU^+$ cells in caudate SVZa. **A** In the short-term survival group, after BrdU the densities of $BrdU^+$ cells and large clusters increased in the second postischemic week, while the small clusters remained unchanged. **B** In the long-term monkey group the postischemic monkeys on days 23 and 44 had more $BrdU^+$ cells or more cell clusters (whether large or small) compared to the respective controls. ***$p < 0.001$, *$p < 0.05$ versus control; *t* test or one-way ANOVA followed by Tukey–Kramer *post hoc*

was significantly increased on postischemic days 9 (Fig. 42A). In the long-term survival group, none of the $BrdU^+$ cells or small or large clusters was significantly different in postischemic monkeys compared to controls (Fig. 42B). However, we calculated a statistically significant decrease of $BrdU^+$ cells over time, i.e.,

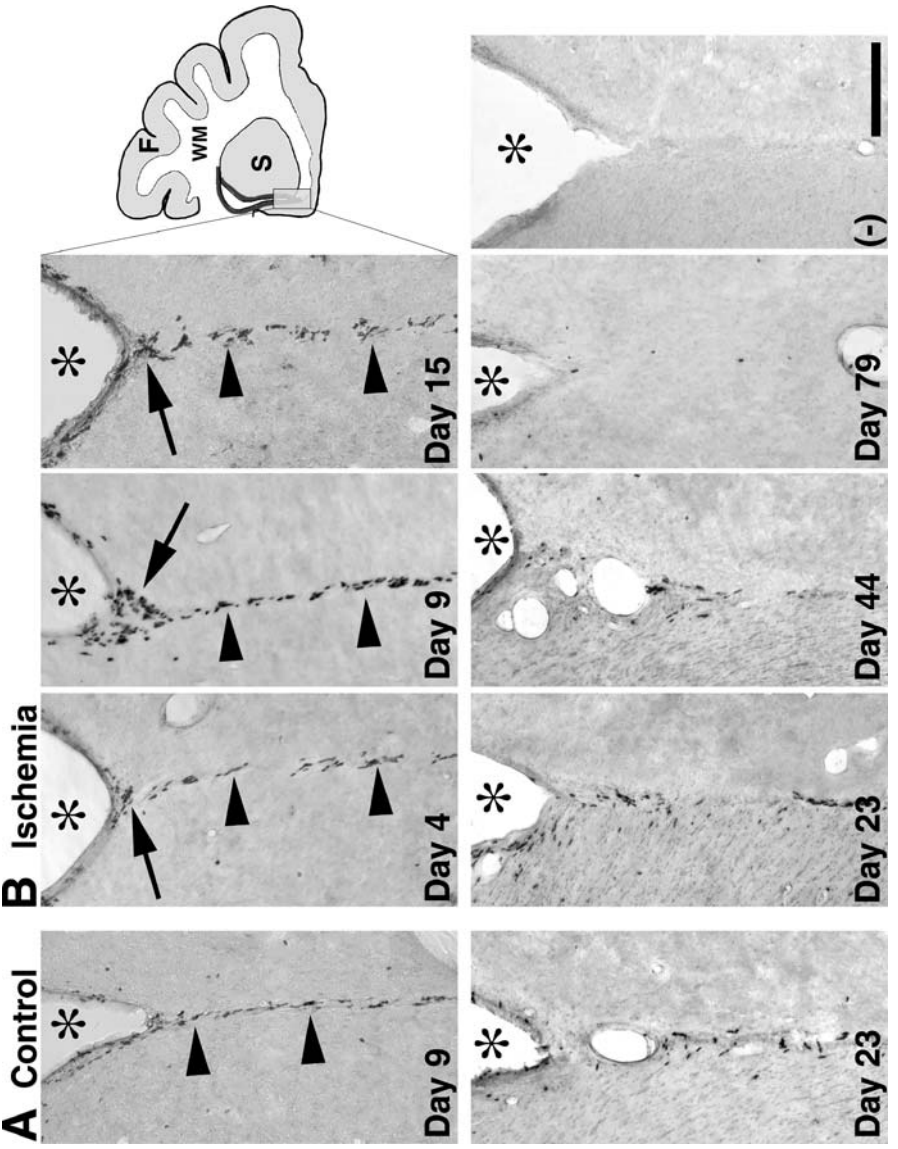

Fig. 41A, B Staining for BrdU in ventral SVZa. **A** Control monkeys on days 9 and 23 after the sham operation. Note the formation of a single common large aggregation of $BrdU^+$ cells in SVZa (*arrows*) and an almost continuous chain of cells ventrally from SVZa in RMS (*arrowheads*). **B** Postischemic monkeys on various time-points after ischemia. Note the gradual decrease of $BrdU^+$ cells compared to the short-term group and the lack of a continuous chain of $BrdU^+$ cells. The position of the visual field within the frontal lobe is schematically depicted as a *frame* on the map (*upper right*). (−), negative control showing no staining for BrdU; *F*, frontal cortex; *WM*, white matter; *S*, striatum. *Asterisk*, anterior horn of lateral ventricle. *Scale bar* = 200 μm

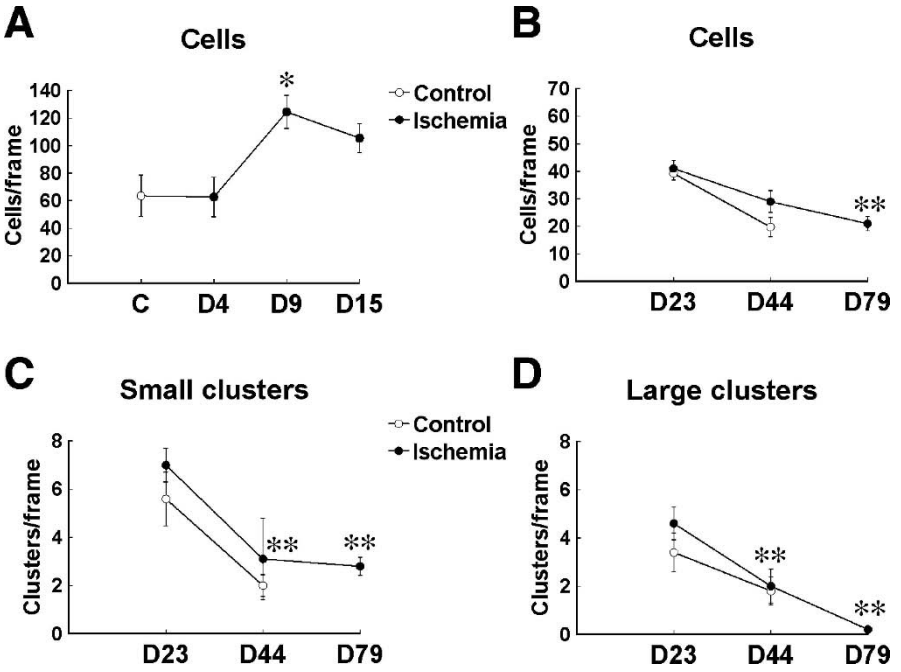

Fig. 42A–D Statistical analysis of the density of $BrdU^+$ cells in caudate SVZa. **A** In the short-term survival group after BrdU the density of $BrdU^+$ cells increased in the second postischemic week. $*p < 0.05$ versus control; one-way ANOVA followed by Tukey–Kramer *post hoc*. **B–D** In the long-term monkey group the postischemic animals did not show differences to controls in respect to the densities of cells, small clusters, or large clusters. However, differences were present within the postischemic group in respect to density of cells and cluster size. $**p < 0.01$ versus day 23; one-way ANOVA followed by Tukey–Kramer *post hoc*

monkeys surviving longer after ischemia had fewer $BrdU^+$ cells in ventral SVZa than monkeys surviving shorter after ischemia (Fig. 42B).

In anterior SVZa the $BrdU^+$ cells visibly increased after ischemia, and were grouped in either large or small $BrdU^+$ cell clusters (Fig. 43). $BrdU^+$ cells were also observed along a pathway located anteriorly to SVZa, at the boundary between the frontal white matter and the striatal parenchyma corresponding to RMS (Fig. 43; arrows). In the white matter, $BrdU^+$ cells were single, and chains were not observed. Statistical evaluation showed that both cells and large clusters significantly increased density on postischemic days 9 and 15 compared to controls (Fig. 44A). In the long-term survival group, all of the $BrdU^+$ cells and clusters exhibited a significantly higher density in the postischemic monkeys compared to respective controls (Fig. 44B).

Comparison of the density of $BrdU^+$ cells on postischemic day 9 (showing peak proliferation) revealed that the highest density was present in ventral SVZa (125 cells/frame), followed by anterior SVZa (75 cells/frame), while caudate and dor-

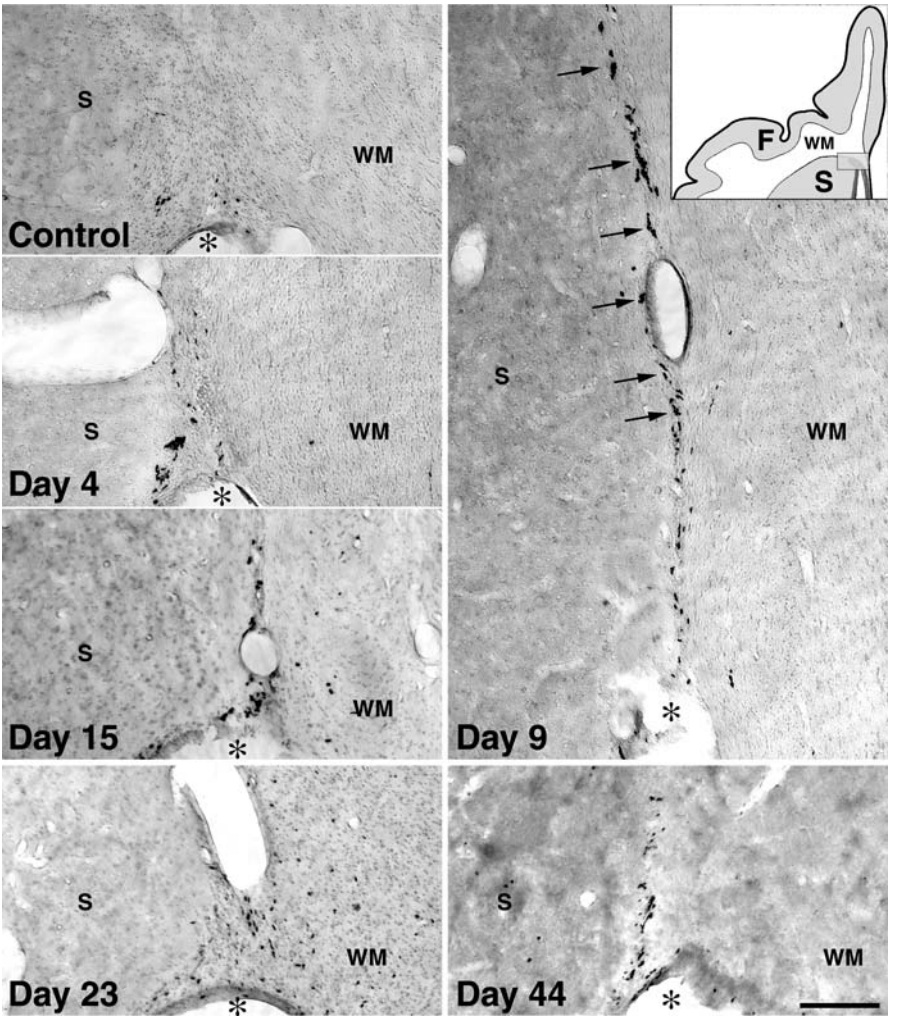

Fig. 43 Staining for BrdU in anterior SVZa of control monkeys or postischemic monkeys on days 4, 9, 15, 23, 44, or 79. Note the increase of positive cells after ischemia. *Arrows* depict $BrdU^+$ cells in RMS anteriorly to SVZa. The position of the visual field within the frontal lobe is schematically depicted as a *frame* on the map (*upper right*). *F*, frontal cortex; *WM*, white matter; *S*, striatum. *Asterisk*, anterior horn of lateral ventricle. *Scale bar* = 200 μm

sal SVZa exhibited similar densities of about 50 cells/frame (Fig. 45A). We also evaluated of the percentage of $BrdU^+$ cells sustaining their localization in SVZa on day 44 by comparing the density on postischemic day 44 versus day 9 with the density on day 44 after sham surgery versus day 9 after sham. Analysis showed significantly higher proportions of retained cells in the postischemic dorsal, caudate, and anterior SVZa, but not in ventral SVZa (Fig. 45B).

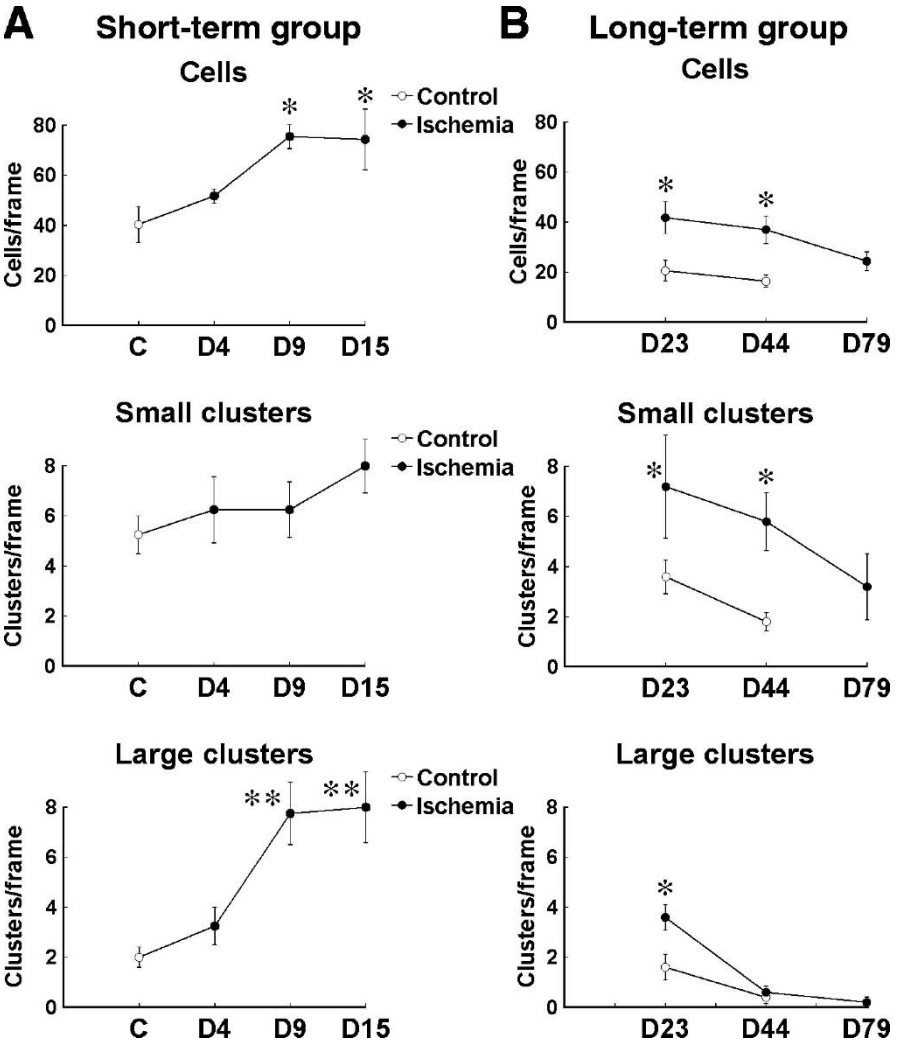

Fig. 44A, B Statistical analysis of the density of $BrdU^+$ cells in anterior SVZa. **A** In the short-term survival group after BrdU the density of $BrdU^+$ cells or large clusters increased in the second postischemic week, while small clusters remained unchanged. **B** In the long-term monkey group the postischemic monkeys had more $BrdU^+$ cells, or more small or large clusters compared to controls. $^{**}p < 0.01$, $^{*}p < 0.05$ versus control; *t* test or one-way ANOVA followed by Tukey–Kramer *post hoc*

As with other brain regions, upon determining the quantity and distribution of $BrdU^+$ cells, we performed colabeling for BrdU and two independent proliferation markers, Ki67 and phosphohistone H3. Triple-labeling of these three markers in the short-term survival monkey group demonstrated almost complete BrdU/Ki67 colabeling, while a lower percentage of $BrdU^+$ cells coexpressed phosphohistone H3

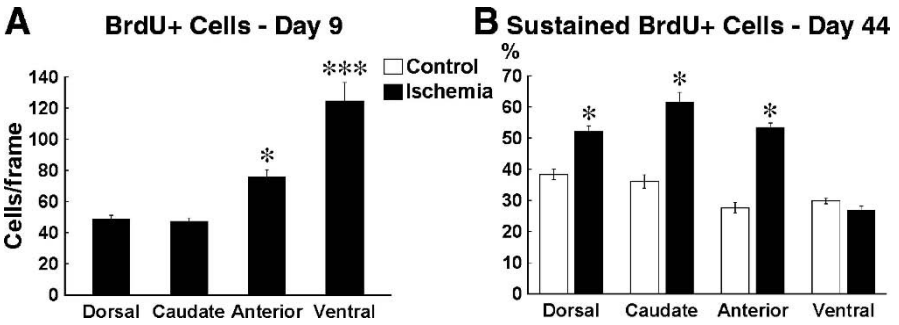

Fig. 45 A Statistical analysis of the density of $BrdU^+$ cells in SVZa on postischemic day 9. $^{***}p < 0.001$ versus anterior, caudate, and dorsal SVZa; $^{*}p < 0.05$ versus caudate and dorsal SVZa; one-way ANOVA followed by Tukey–Kramer post hoc. **B** Proportions of $BrdU^+$ cells retaining presence in SVZa. Densities of $BrdU^+$ cells on day 44 after sham/ischemia were calculated as a percentage of the densities of day 9 after sham/ischemia. $^{*}p < 0.05$ versus respective sham-operated control; Kruskal–Wallis or Mann–Whitney tests

(Fig. 46A). In the long-term survival group most $BrdU^+$ cells (Fig. 46B; arrowheads) did not coexpress Ki67 and only a few $BrdU^+$ cells were double-labeled (Fig. 46B; arrows). Thus, the percentage of $BrdU^+$ cells co-stained for Ki67 significantly decreased on day 44 compared to day 9 (Fig. 46C). Double-staining for BrdU and TUNEL or active caspase-3 showed that the $BrdU^+$ cells were not colabeled by these assays, and therefore were not dying cells (Tonchev et al. 2005).

As with SGZ, in SVZa many $BrdU^+$ cell clusters in the short-term survival monkey group were positive for the neural progenitor marker Musashi1 (Fig. 47A; arrowheads) and at the same time were ensheathed by, but negative themselves for, the astrocyte marker GFAP (Fig. 47A; frame). The $BrdU^+$/Musashi1$^+$ clusters coexpressed Nestin, another marker of neural progenitors (Fig. 47B; arrows). In the long-term survival group, the few $BrdU^+$/$Ki67^+$ cells present (Fig. 46B) coexpressed Musashi1 (Fig. 47C), but not βIII-tubulin, a neuronal progenitor marker. However, many of the $BrdU^+$/$Ki67^-$ cells were positive for βIII-tubulin, particularly in the long-term survival monkey group. Such $BrdU^+$/βIII-tubulin$^+$ cells were arranged

Table 9 Percentages of colabeling of BrdU with various cell markers in SVZa. $BrdU^+$ cells were sampled for colabeling with either Musashi1 or Nestin as described in the text

	Day 9		Day 23		Day 44		Day 79	
	Control	Ischemia	Control	Ischemia	Control	Ischemia	Control	Ischemia
Musashi1	75±13	72±19	13±5	11±5	12±5	12±6	NA	10±5
βIII-Tubulin	8±3	10±5	71±21	69±20	73±17	75±22	NA	80±21
Iba1	2±1	4±1*	2±1	5±2*	4±2	6±3	NA	5±3

NA, not available $^{*}p < 0.05$ versus respective controls, Kruskal–Wallis or Mann–Whitney tests

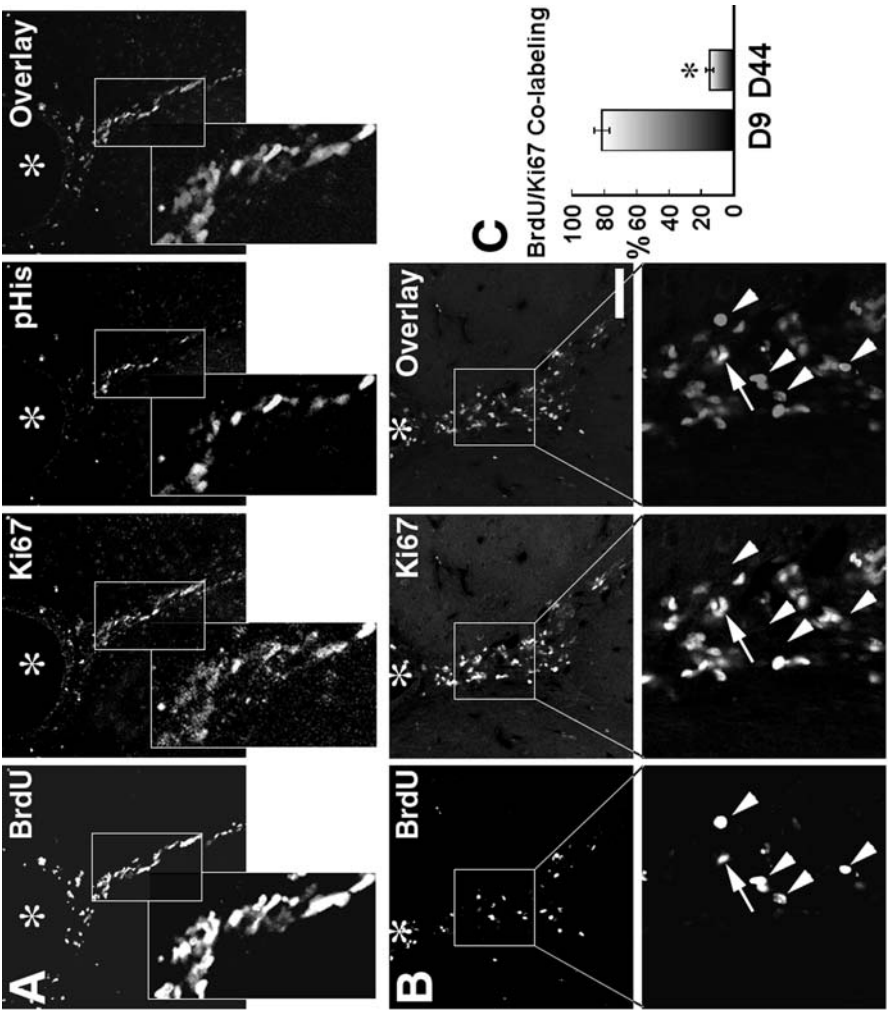

Fig. 46A–C Colabeling of BrdU with other proliferation markers in SVZa. **A** Triple-staining for BrdU, Ki67, and phosphohistone H3 on postischemic day 9. Almost all $BrdU^+$ cells were colabeled by Ki67, while fewer $BrdU^+$ cells were also stained for phosphohistone H3 (*pHis*). *Framed area* is magnified in the *insets*. **B** Double-labeling for BrdU and Ki67 on postischemic day 44. *Framed area* is magnified in the *insets*. Note a single $BrdU^+$ cell co-stained for Ki67 (*arrow*), while the other $BrdU^+$ cells (*arrowheads*) are negative for Ki67. *Scale bar* = 100 µm. **C** Percentages of $BrdU^+$ cells co-stained for Ki67 on postischemic days 9 or 44. $*p < 0.05$ versus day 9; Kruskal–Wallis or Mann–Whitney tests

in chains in the ventral extension of SVZa (Fig. 48A) or formed clusters in anterior, dorsal, or caudate SVZa (Fig. 48B). A high percentage of BrdU/Musashi1 colabeling was present in the short-term group (~75%), while in the long-term survival group most of the $BrdU^+$ cells were positive for βIII-tubulin (~80%) (Table 9).

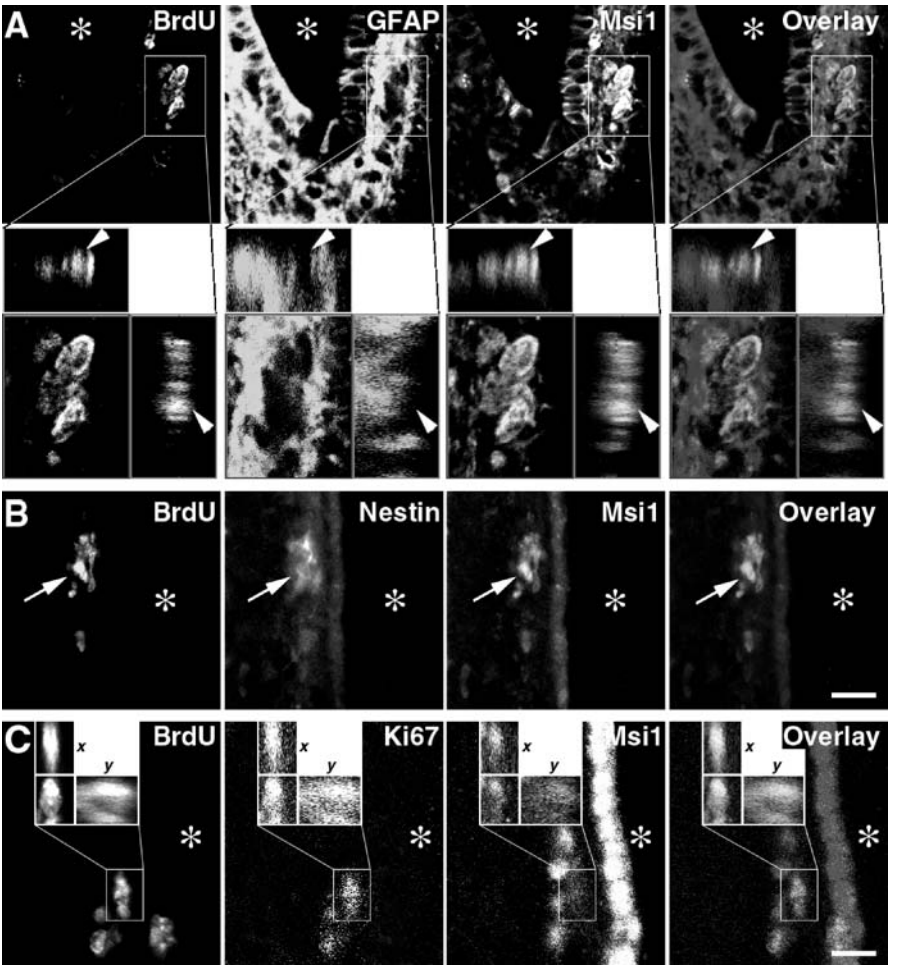

Fig. 47A–C Neural progenitor cell proliferation in SVZa. **A** Triple-staining for BrdU, Musashi1 (*Msi1*) and GFAP in postischemic day-9 ventral SVZa. A $BrdU^+$/$Musashi1^+$ cell cluster is wrapped by $GFAP^+$ fibers (*frame*). Generation of digital 3D reconstructions shows that the $BrdU^+$/$Musashi1^+$ nuclei are not surrounded by GFAP immunoreactivity on all sides (*arrows*) and thus are not colabeled by GFAP. **B** Triple-staining for BrdU, Musashi1, and Nestin in postischemic day-9 caudate SVZa. Musashi1 and Nestin stain the same $BrdU^+$ cluster (*arrows*). **C** Triple-staining for BrdU, Musashi1, and Ki67 in postischemic day-79 caudate SVZa. Note that $BrdU^+$/$Ki67^+$ cells coexpress Musashi1. The cell in the *frame* is magnified in the *inset* with 3D reconstructions on the *x* and *y* axes. *Asterisk*, anterior horn of lateral ventricle. *Scale bars* = 20 μm (**B**); 10 μm (**C**)

A few microglial cells incorporated BrdU (~5%), particularly in the postischemic monkeys (Fig. 48C; Table 9).

PSA-NCAM, an alternative progenitor cell marker, also colabeled with BrdU in SVZa (Fig. 49A; arrows). Double-staining for PSA-NCAM and βIII-tubulin in SVZa

Fig. 48A–C Neuronal progenitor and microglial cell proliferation in SVZa. **A** Double-staining for BrdU and βIII-tubulin in postischemic day-23 ventral SVZa. The *framed* section is magnified in the *lower panel*. Most $BrdU^+$ nuclei colabel with βIII-$tubulin^+$ chains of cells (*arrows*). **B** Double-staining for BrdU and βIII-tubulin in postischemic day-44 caudate SVZa. Some of the cells within a βIII-$tubulin^+$ cluster express BrdU (*arrows*). Note the perivascular position of the cluster (*bv*, blood vessel). **C** Double-staining for BrdU and Iba1 in postischemic day-44 caudate SVZa. A $BrdU^+$/$Iba1^+$ cell (*arrows*) and a $BrdU^-$/$Iba1^+$ cell (*arrowheads*) are depicted. *Asterisk*, anterior horn of lateral ventricle. *Scale bars* = 50 μm (**A**); 20 μm (**B**); 10 μm (**C**)

Fig. 49A–C (on page 70) Phenotype of PSA-$NCAM^+$ cells in SVZa. **A** Double-staining for BrdU and PSA-NCAM in postischemic day-4 anterior SVZa. A large $BrdU^+$ cluster is negative for PSA-NCAM (*arrowheads*). Nevertheless, some of the cells of an adjacent PSA-$NCAM^+$ aggregate express BrdU (*arrows*; the *framed area* is magnified in the *lower panel*). **B** Double-staining for PSA-NCAM and βIII-tubulin in postischemic day-23 anterior SVZa. Note almost complete colabeling. **C** Double-staining for PSA-NCAM and Nestin in postischemic day-9 caudate SVZa. Double-labeled cells are depicted by *arrows*. *Asterisk*, anterior horn of lateral ventricle. *Scale bars* = 100 μm (**A, B**); 50 μm (**C**)

revealed that the two markers largely co-stained (Fig. 49B). Furthermore, PSA-NCAM but not βIII-tubulin exhibited coexpression with the neural progenitor cell marker Nestin (Fig. 49C). Thus, a sequential change of expression of progenitor cell markers appears to exist in SVZa that is similar to SGZ, with PSA-NCAM providing a phenotypical "link" between cells of the neural progenitor (Nestin$^+$) phenotype and cells of the neuronal (βIII-$tubulin^+$) phenotype.

3.5 Rostral Migratory Stream and Olfactory Bulb

RMS is a pathway from SVZa to the olfactory bulb along which SVZa travel tangentially, and upon arrival in the olfactory bulb some of these cells become granule or periglomerular neurons (Luskin 1993; Lois et al. 1996; Doetsch and Alvarez-Buylla 1996; Pencea et al. 2001b; Carleton et al. 2003; Kohwi et al. 2005).

As reported in the previous section, on sections single-stained for BrdU, chains of positive cells were seen in RMS, while outside of the stream (e.g., in subcortical white matter) only single dispersed $BrdU^+$ cells were evident (Fig. 37; arrowheads). After staining for BrdU/βIII-tubulin in RMS, double-positive cells were arranged in a chain-like manner in RMS, while the few scattered $BrdU^+$ cells outside of these chains did not colabel with βIII-tubulin (Tonchev et al. 2005). Consistent with the increase of $BrdU^+$ cells in SVZa of the short-term survival monkey group, we found an increased number of $BrdU^+$ cells along the postischemic RMS of the long-term survival group (postischemic day 23, Fig. 50), compared to respective sham-operated controls.

Immunostaining for BrdU and markers for immature migrating neurons (PSA-NCAM, βIII-tubulin or Doublecortin) in frontal white matter did not reveal chains

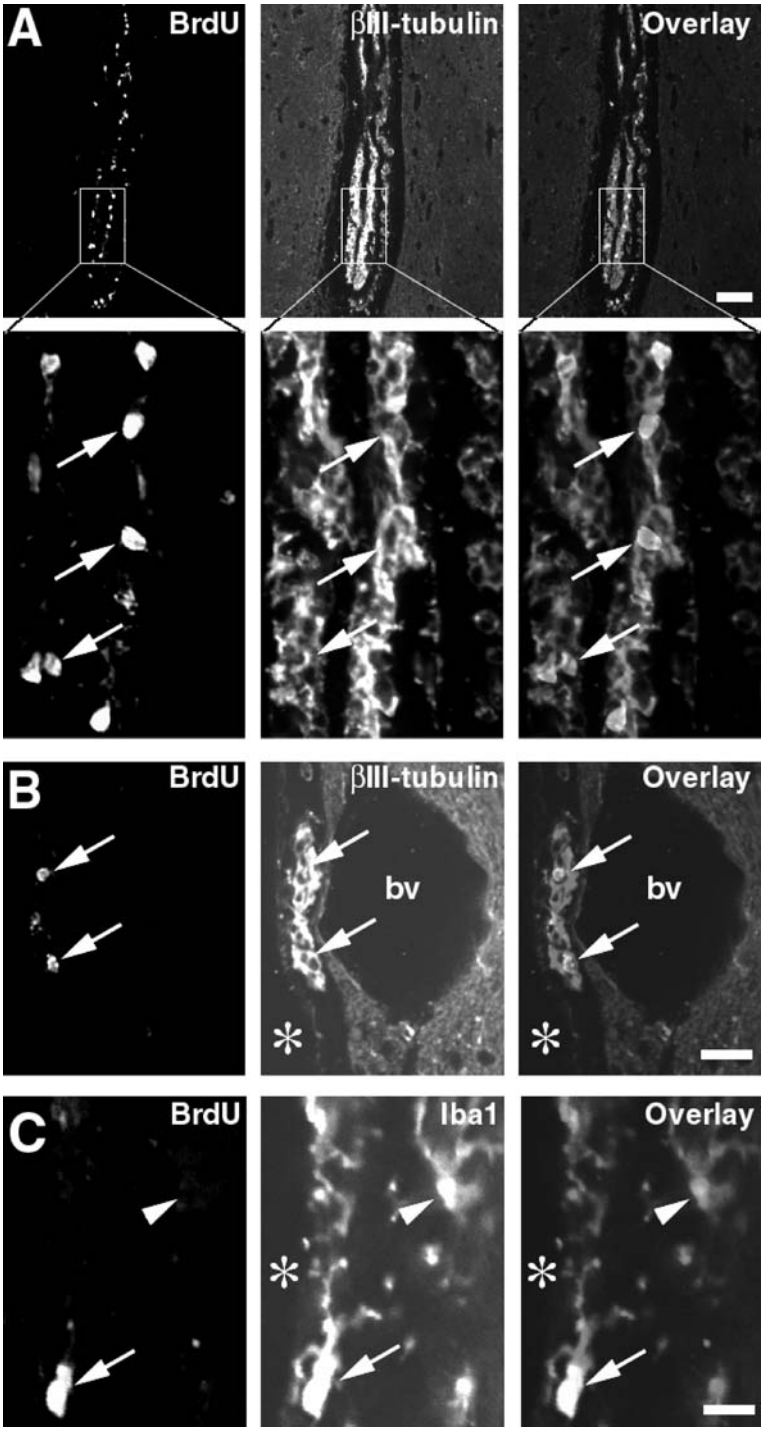
A
BrdU
βIII-tubulin
Overlay
B
BrdU
βIII-tubulin
Overlay
bv
bv
C
BrdU
Iba1
Overlay

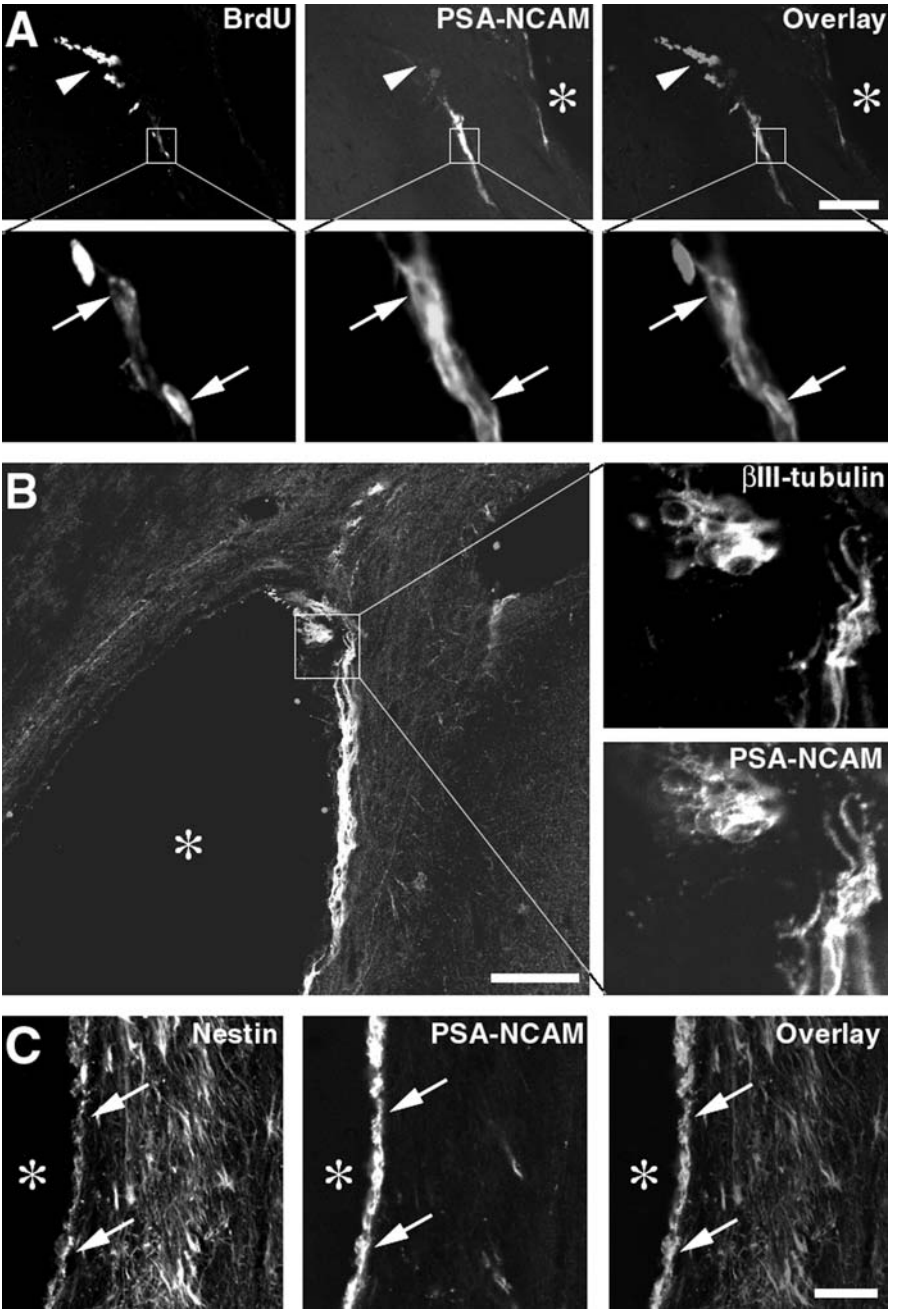
A
BrdU
PSA-NCAM
Overlay
B
βIII-tubulin
PSA-NCAM
C
Nestin
PSA-NCAM
Overlay

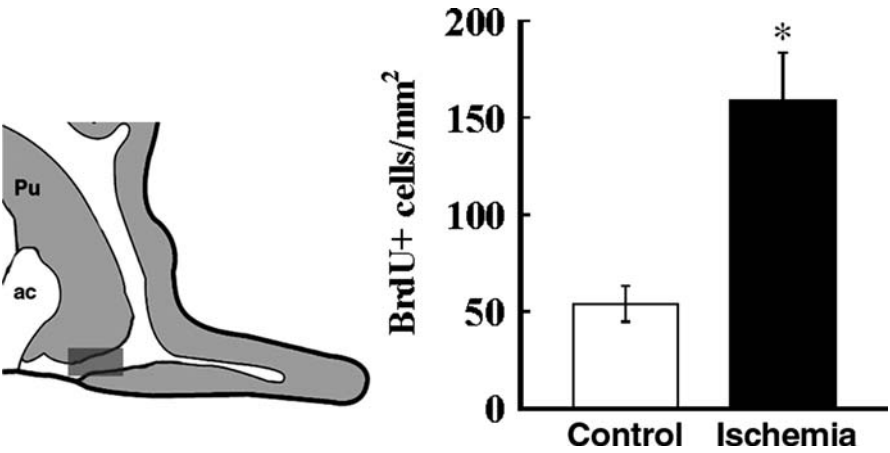

Fig. 50 A schematic map of a horizontal frontal lobe section showing the location where double-labeling for βIII-tubulin and BrdU in postischemic day-23 monkey RMS was investigated. *Pu*, putamen; *ac*, anterior commissure. This statistical analysis of the density of $BrdU^+$ cells in RMS involves postischemic day 23. $^*p < 0.05$ versus control; paired *t* test

of cells positive for any of these markers in the adult monkeys (either postischemic or control). In contrast, in a postnatal (P14) monkey, we observed numerous positive aggregates up to several millimeters away from SVZa in subcortical white matter (Fig. 51, left column; arrows). In the adult monkeys the $BrdU^+$ cells on anatomically comparable sections were restricted to the vicinity of SVZa (Fig. 51, right column; arrows). These data indicated that the negative findings in adult white matter had not resulted by an insufficiency of our staining protocol, as sections from adult and postnatal monkeys were processed simultaneously.

The most distal portion of RMS is the olfactory peduncle, which is continuous with the white matter of the olfactory bulb core (Alonso et al. 1998; Kornack and Rakic 2001a). In the short-term survival group, $BrdU^+$ cells were observed predominantly in the core white matter as opposed to the adjacent granule cell layer (Fig. 52A), and were frequently in clusters. No obvious increase of $BrdU^+$ cells was observed within this monkey group, and statistical analysis showed an average cell density of 20 cells/mm^2 without significant differences among the monkeys in the group (Tonchev et al. 2003b).

In the long-term survival monkey group, however, we found differences between control and ischemic brains. These were observed in the olfactory parenchyma, as postischemic monkeys on day 44 exhibited higher density of $BrdU^+$ cells than the respective controls (Fig. 52B). Statistical analysis revealed that the differences were significant (59.5±8.8 versus 33.1±2.4 $BrdU^+$ cells/mm^2; $p < 0.05$, paired *t* test).

We analyzed the phenotype of $BrdU^+$ cells in core white matter and olfactory parenchyma. Many of the $BrdU^+$ cells, particularly in clusters, in the olfactory peduncle and core white matter were positive for the progenitor marker Musashi1 (Fig. 53A; arrows). The same cell type was also positive for the marker Nestin

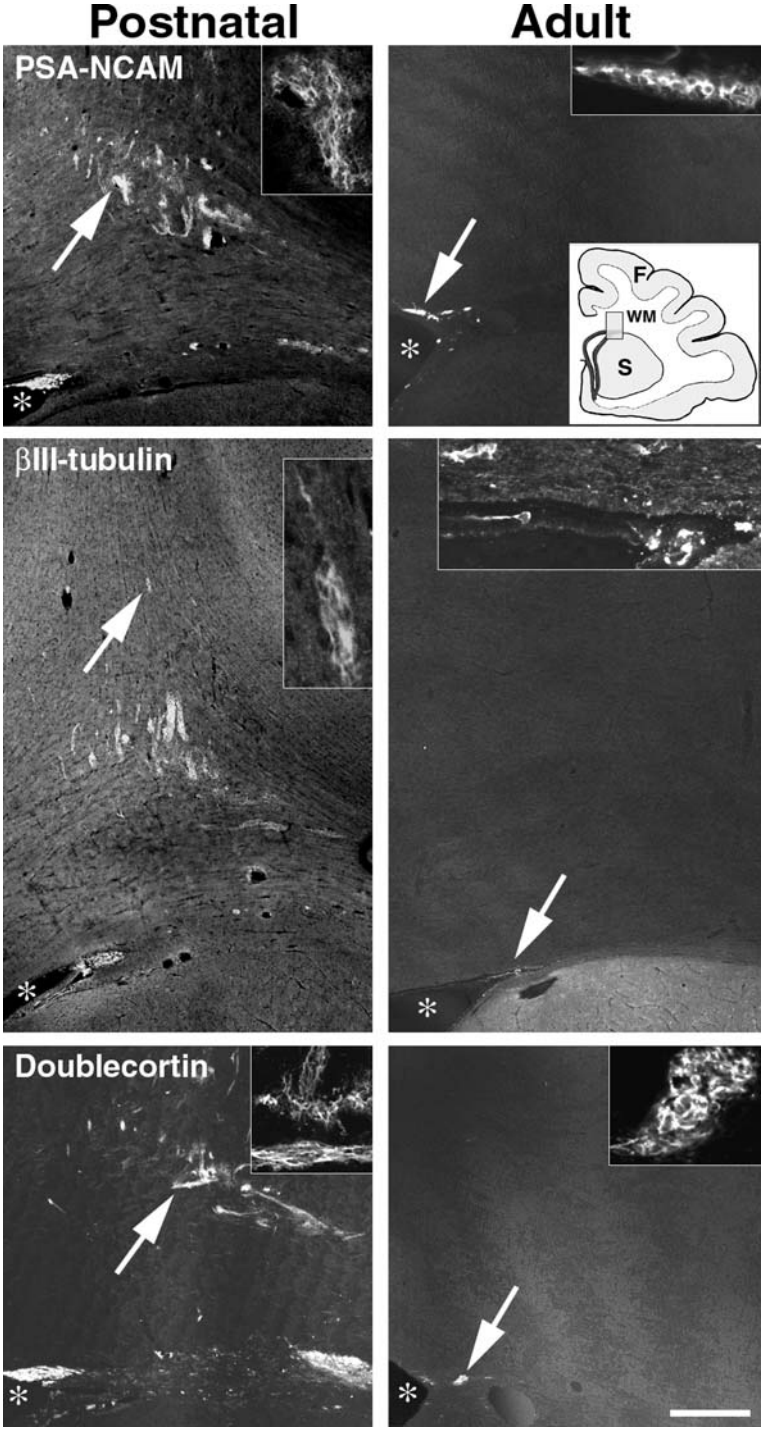
Postnatal
Adult
PSA-NCAM
βIII-tubulin
Doublecortin
F
WM
S

Fig. 51 Staining for PSA-NCAM, βIII-tubulin, or Doublecortin in the subcortical white matter of postnatal (P14) or adult postischemic day-23 monkey brains. Note the lack of positive cells in the adult monkey white matter contrasting with the numerous positive clusters (*left column*; *arrows*) in the postnatal brain. In adult brain, positive clusters were invariably in the vicinity of SVZa (*right column*; *arrows*). Clusters depicted by *arrows* are magnified in the *insets*. The position of the visual field corresponds to the *frame* on the schematic map. *F*, frontal cortex; *WM*, white matter; *S*, striatum. *Asterisk*, anterior horn of lateral ventricle. *Scale bar* = 400 μm

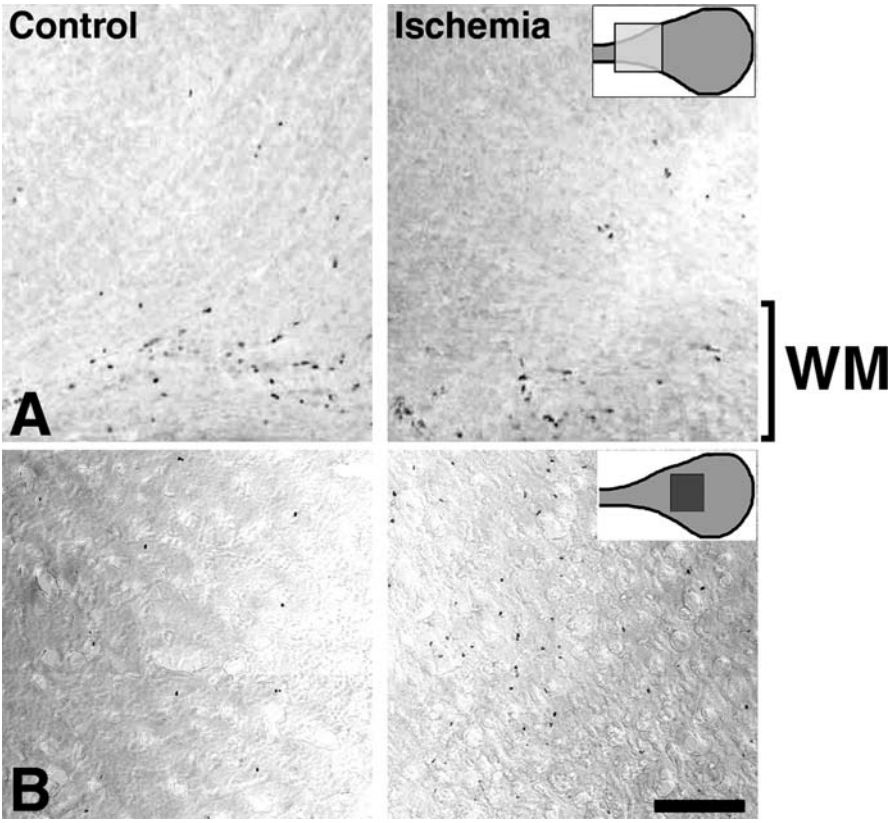

Fig. 52A, B Representative micrographs of BrdU immunostaining in the olfactory bulb in control and ischemic subjects. **A** In the core white matter (*WM*) and adjacent portions of the granule cell layer the density and distribution of positive cells in either control or ischemic (example given with day 4) brains remained unchanged in the short-term survival monkey group. **B** In the long-term survival monkeys, however, the number of $BrdU^+$ cells in the postischemic bulb parenchyma was increased (example given with day 44). The position of the visual field is depicted as a *frame* on the schematic maps; *upper right*. *Scale bar* = 200 μm

(Fig. 53B; arrows). The BrdU$^+$/Musashi1$^+$/Nestin$^+$ cells constituted 75% of the BrdU$^+$ cells in olfactory core. In addition, BrdU$^+$ cells colabeled for βIII-tubulin were observed, forming mesh-like aggregates (Fig. 53C; arrows). These cells constituted 15% of the BrdU$^+$ cells in the olfactory core. Within BrdU$^+$/Musashi1$^+$ clusters, most of the cells were negative for βIII-tubulin, but were tightly associated with βIII-tubulin$^+$ fibers (Fig. 53D; arrowheads). Single BrdU$^+$/Musashi1$^+$ cells

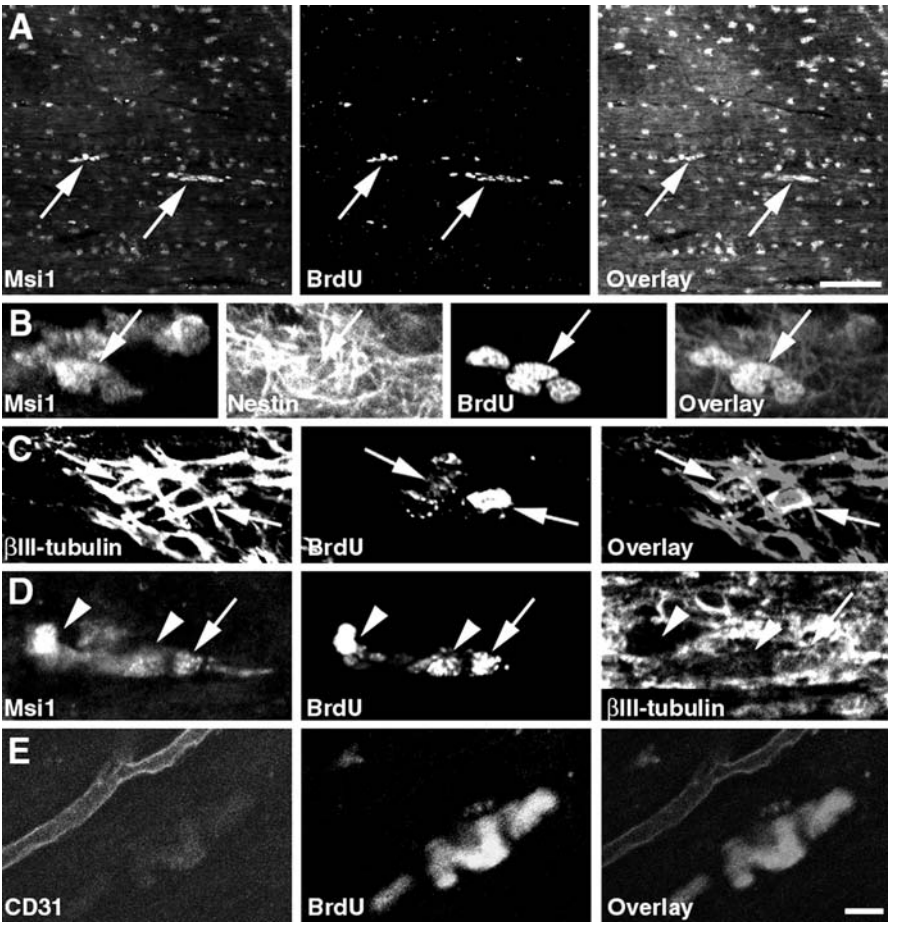

Fig. 53A–E Phenotype of BrdU$^+$ cells in olfactory peduncle and core white matter. **A** BrdU$^+$ cell clusters coexpress Musashi1 (*arrows*); control monkey. **B** Example of a BrdU$^+$/Musashi1$^+$ cluster triple-labeled for Nestin (*arrows*); day 4 after ischemia. **C** BrdU$^+$ cells coexpress βIII-tubulin (*arrows*) on postischemic day 9. **D** Triple-staining for BrdU, Musashi1, and βIII-tubulin (day 9). A BrdU$^+$ cluster is depicted, most of the cells in which are BrdU$^+$/Musashi1$^+$/βIII-tubulin$^-$ (*arrowheads*). A single cell is triple-labeled (*arrows*). **E** Double-staining for endothelial cell marker CD31 and BrdU demonstrates the perivascular localization of a BrdU$^+$ cluster. *Scale bars* = 100 μm (**A**); 10 μm (**E**)

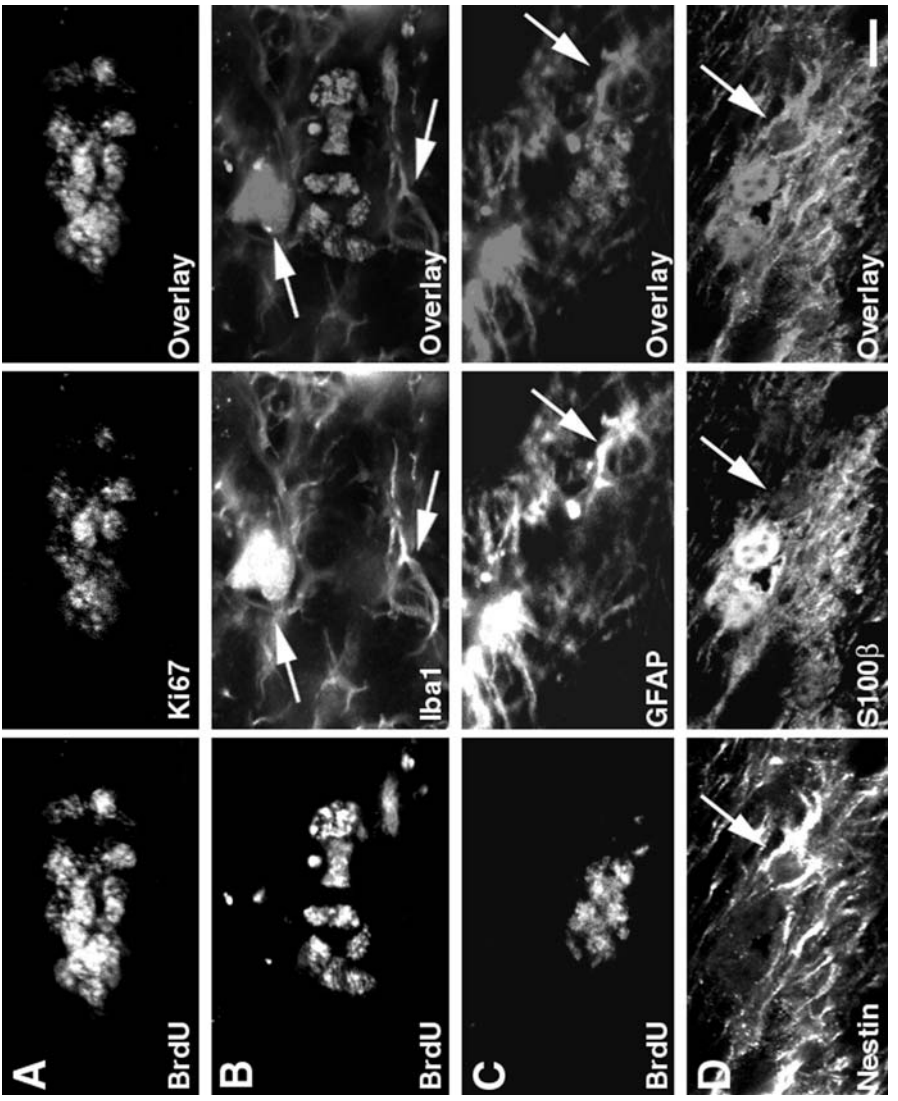

Fig. 54A–D Phenotype of $BrdU^+$ cells in olfactory peduncle and core white matter. **A** BrdU/Ki67 colabeling showing that most of the cells in a $BrdU^+$ cluster are Ki67 co-positive (day 9). **B** BrdU/Iba1 double-staining (day 15) showing a $BrdU^+$ cluster in the vicinity of $Iba1^+$ cells (*arrows*), but distinct from them. **C** BrdU/GFAP double-staining (day 9) showing a $BrdU^+$ cluster adjacent to a $GFAP^+$ astrocyte (*arrows*) and processes of other astrocytes, but distinct from them. **D** Nestin/S100β double-staining (day 4) showing a $Nestin^+/S100\beta^-$ cell (*arrows*) adjacent to an aggregate of $S100\beta^+$ astrocytes. *Scale bar* = 10 μm

within the cluster, however, were triple-labeled for βIII-tubulin (Fig. 53D; arrows), indicating a phenotypical link between BrdU$^+$/Musashi1$^+$ cells and BrdU$^+$/βIII-tubulin$^+$ cells. The BrdU$^+$ clusters were frequently perivascular, as demonstrated by colabeling with CD31 (Fig. 53E).

Co-staining of BrdU$^+$ clusters with Ki67 showed that most of the BrdU$^+$ cells were double-labeled by Ki67 (Fig. 54A). Furthermore, we observed BrdU$^+$/$^+$Nestin cells exhibiting mitotic figures as well as Musashi1$^+$ cells colabeled for the mitotic marker phosphohistone H3 (Tonchev et al. 2003b), altogether indicating that the BrdU$^+$/Musahsi1$^+$/Nestin$^+$ cellsNestin were actively dividing in olfactory core white matter. Colabeling of the clusters with microglial marker Iba1 revealed that while the BrdU$^+$ cells were adjacent to microglial cell bodies and processes, they were not microglial cells (Fig. 54B). Similarly, double-staining for BrdU and the astroglial marker GFAP demonstrated BrdU$^+$ clusters ensheathed by GFAP$^+$ processes but distinct from the GFAP$^+$ cell nucleus (Fig. 54C; arrows). In accordance with the latter data, double-labeling for NestinNestin and the astrocyte marker S100β showed that some Nestin$^+$ cells were negative for S100β (Fig. 54D; arrows).

In olfactory parenchyma of the long-term survival monkey group, we searched for evidence of neuronal generation. Double-staining for BrdU and NeuN showed the presence of double-positive cells. Such cells were located in the granule cell layer (Fig. 55A; arrows) or in the glomerular cell layer (Fig. 55B; arrows) of both control and ischemic monkeys. The BrdU$^+$/NeuN$^+$ cells were similar in size and shape to adjacent BrdU$^-$/NeuN$^+$ neurons, supporting the conclusion these cells represented adult-generated neurons. The BrdU$^+$/NeuN$^+$ cells constituted 15%–20% of the BrdU$^+$ cells on day 44 after sham/ischemia.

Proliferating microglia were also observed in olfactory parenchyma as demonstrated by BrdU/Iba1 co-staining (Fig. 55C). The double-positive cells constituted 6%–8% of the BrdU$^+$ cells in control monkeys, while in the postischemic monkeys the percentage was considerably higher (15%–20%), a difference which proved to be significant ($^*p < 0.05$, Kruskal–Wallis or Mann–Whitney tests). A few astrocytes and oligodendrocytes also incorporated BrdU (up to 10% of the BrdU$^+$ cells).

3.6
Frontal Cortex and Striatum

Ischemia enhanced proliferation in the frontal cortex (Fig. 56), the BrdU$^+$ cells being homogeneously dispersed among the neocortical layers. Statistical analysis revealed that the density of BrdU$^+$ cells in the monkeys of the short-term group was significantly increased on postischemic days 9 and 15. In the monkeys of the long-term survival group, the BrdU$^+$ cells in postischemic frontal cortex significantly outnumbered those in the control monkeys at both 2 and 5 weeks after BrdU treatment, i.e., on days 23 and 44 after surgery (Fig. 57A).

In the striatum, postischemic proliferation was also increased. As in the frontal cortex, the BrdU$^+$ cells were either single cells or "doublets," but were not in clusters. Statistical analysis revealed that the density of BrdU$^+$ cells in the monkeys

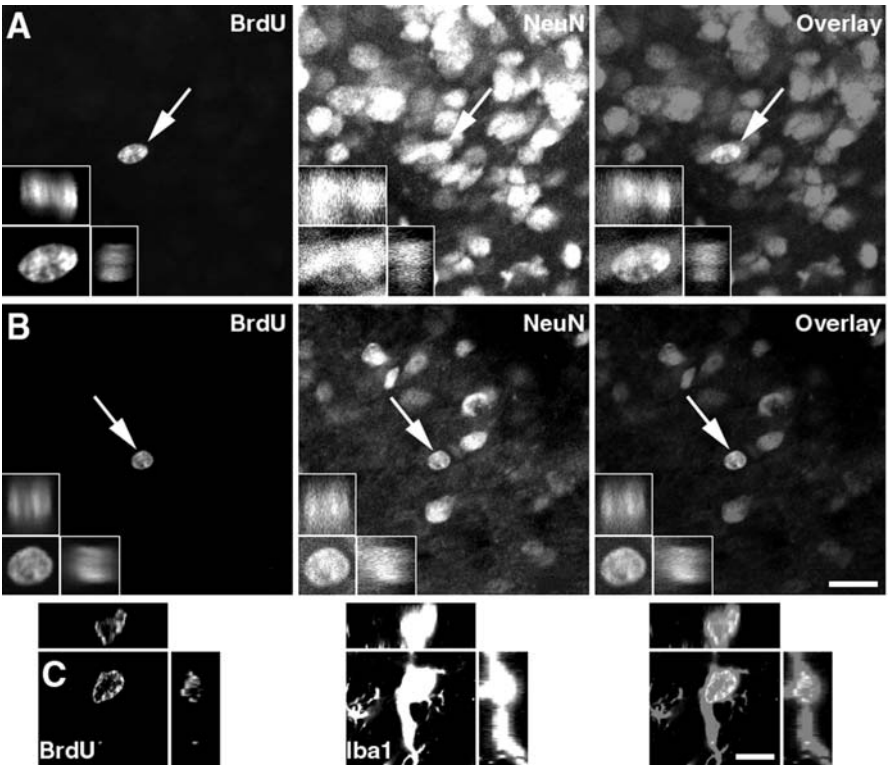

Fig. 55A–C Phenotype of $BrdU^+$ cells in olfactory parenchyma (day 44 after ischemia). **A** BrdU/NeuN double-staining in granule cell layer depicting a $BrdU^+/NeuN^+$ cell (*arrows*) identical in morphology to neighboring $BrdU^-/NeuN^+$ cells. The cell is magnified with channel separation and orthogonal projections in the *insets*. **B** BrdU/NeuN double-staining in the glomerular layer, depicting a $BrdU^+/NeuN^+$ cell (*arrows*) identical in morphology to neighboring $BrdU^-/NeuN^+$ cells. The cell is magnified with channel separation and orthogonal projections in the *insets*. **C** BrdU/Iba1 double-staining in the glomerular layer showing $BrdU^+/Iba1^+$ cells with orthogonal projections. *Scale bars* = 20 μm (**B**); 10 μm (**C**)

of the short-term group was significantly increased on postischemic days 9 and 15. In the monkeys of the long-term survival group, the $BrdU^+$ cells in postischemic striatum significantly outnumbered those in the control monkeys at both 2 and 5 weeks after BrdU treatment, i.e., on days 23 and 44 after surgery (Fig. 57B).

The majority of $BrdU^+$ cells in postischemic monkey striatum and frontal cortex expressed the microglial marker Iba1 (Fig. 58A; arrowheads) or the astroglial marker S100β (Fig. 58A; arrows). In total, proliferating glia accounted for nearly 90% of the $BrdU^+$ cells in these two regions after ischemia (Table 10). Microglial cells were much more numerous than astrocytes, by a relation of approximately 8:1 (Table 10). Astroglia were frequently found in proliferating "doublets" (Fig. 58B; arrows), as seen in the postischemic monkey hippocampus and temporal neo-

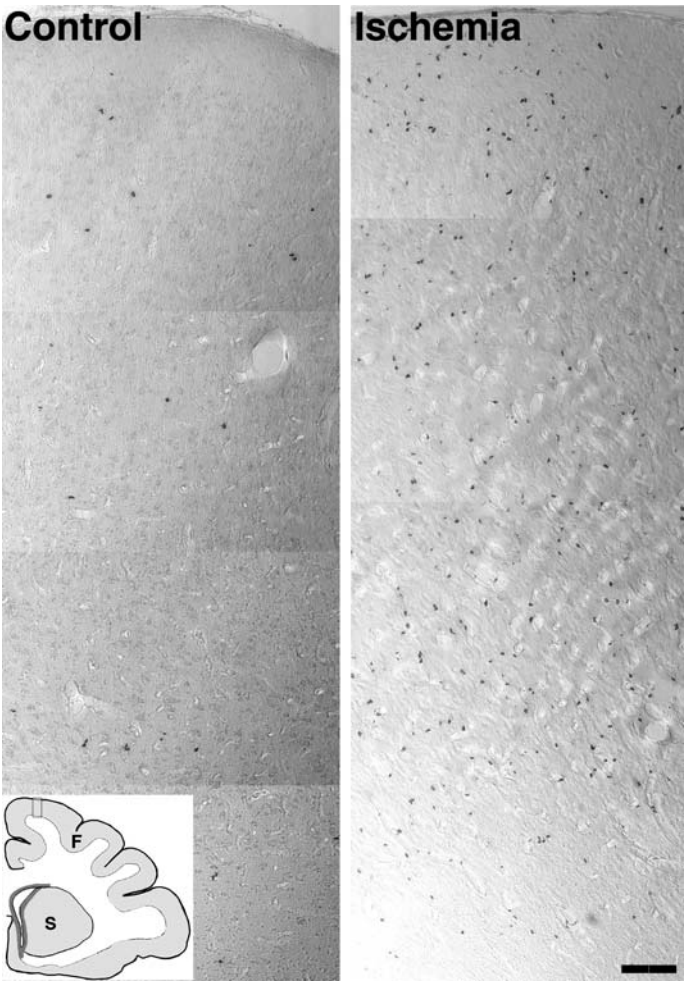

Fig. 56 Representative composite micrographs of BrdU immunostaining spanning all neocortical layers of the frontal cortex of control and postischemic day-9 monkeys. The position of the visual field is depicted as a *frame* on the schematic map (*upper right*). Note the increased number of positive cells after ischemia. *F*, frontal cortex; *S*, striatum. *Scale bar* = 200 μm

cortex. A few $BrdU^+$ cells expressing the oligodendrocyte marker CNP were also found (Fig. 58C).

Previous studies have reported the generation of neurons in frontal cortex and striatum of normal adult monkeys (Gould et al. 2001; Bedard et al. 2002). We therefore searched for evidence of de novo generation of cells with a neuronal immunophenotype in the striatum and frontal cortex of postischemic monkeys. We first performed double-staining for BrdU and the mature neuronal marker

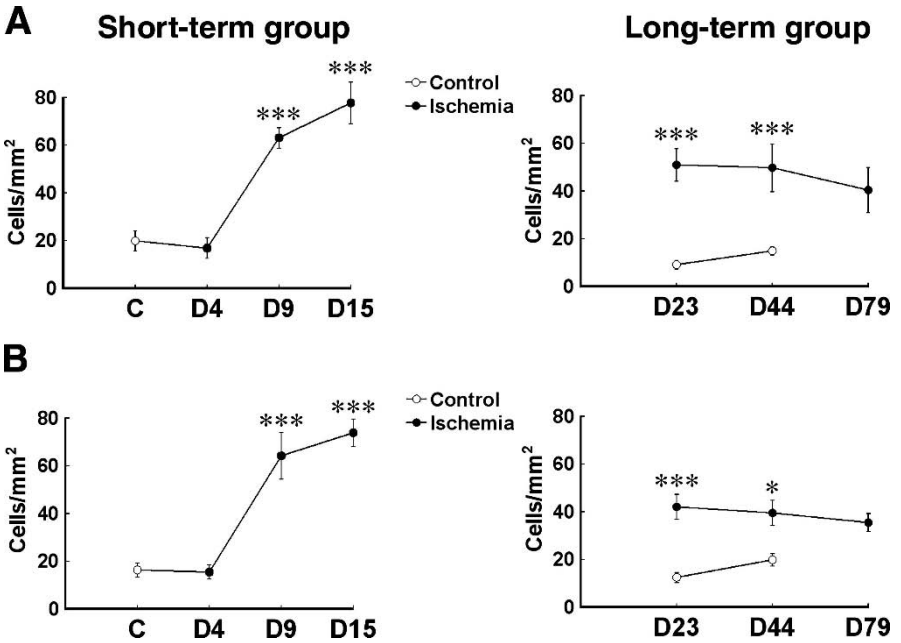

Fig. 57A, B Quantitative analysis of $BrdU^+$ cells in frontal cortex and striatum. **A** Frontal cortex. **B** Striatum. $^{***}p < 0.001$ versus controls; *t* test or one-way ANOVA followed by Tukey–Kramer *post hoc*

NeuN (Eriksson et al. 1998; Gould et al. 1999b, 2001; Kornack and Rakic 1999, 2001b; Arvidsson et al. 2002; Parent et al. 2002) in an attempt to identify double-labeled cells whose size and morphology were similar to the surrounding $NeuN^+$ neurons. We indeed found such cells, typically located in layers II–IV of the neocortex (Fig. 59) or lateral putamen in striatum (Fig. 60). Morphologically, $BrdU^+/NeuN^+$ cells (Fig. 59, 60; arrows) were similar in size and shape to adjacent $BrdU^-/NeuN^+$ neurons (Fig. 59, 60; arrowheads). Confocal analysis revealed that the $NeuN^+/BrdU^+$ constituted about 1% of the $BrdU^+$ cells in either frontal neocortex or striatum (Table 10).

We provided additional confirmation for the neuronal phenotype of the $NeuN^+/BrdU^+$ cells. We found that the $NeuN^+/BrdU^+$ cells coexpressed GAD, a marker of GABAergic neurons as well as region-specific neuronal transcription factors (Tonchev et al. 2005). In the sham-operated monkeys, rare $BrdU^+/NeuN^+$ cells were observed only in striatum and neocortex of the day-44 brains (Table 10).

In addition to cells with a glial or neuronal phenotype, another proliferating cell population with immunophenotypically distinct features was present in striatal and cortical parenchyma. We identified $BrdU^+$ cells that were positive for the neural progenitor cell marker Musashi1 but at the same time were negative for the astrocytic marker GFAP (Fig. 61B; frame). This immunophenotype resembled that of the progenitor cells in SGZ or SVZa. The $BrdU^+/Musashi1^+/GFAP^-$ cells were

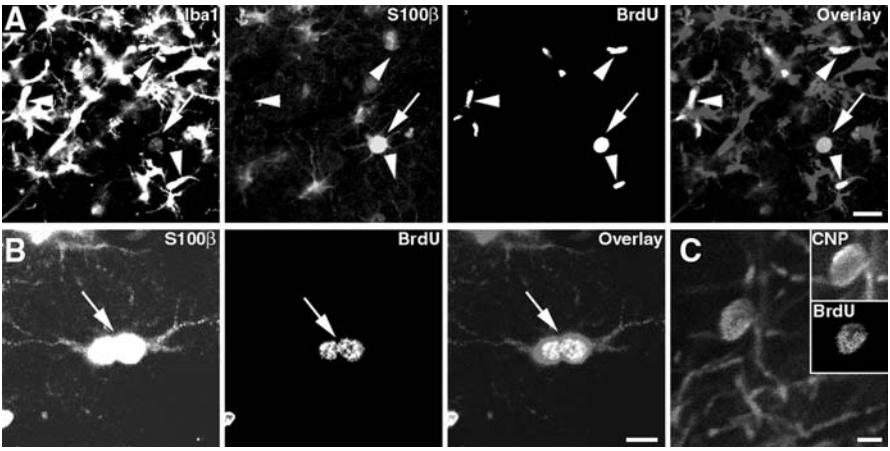

Fig. 58A–C Glial generation in postischemic striatum and frontal cortex. **A** Triple labeling for Iba1, S100β, and BrdU in the postischemic day-44 frontal cortex. Note that the Iba1$^+$/BrdU$^+$ cells (*arrowheads*) are much more numerous than the S100β^+/BrdU$^+$ cells (*arrows*). **B** Example of a BrdU$^+$/S100β^+ "doublet" in day-23 cortex (*arrows*). **C** BrdU$^+$ cells coexpress CNP in postischemic day-79 striatum. Channel separation is shown in *insets*. *Scale bars* = 20 μm (**A**); 10 μm (**B**); 5 μm (**C**)

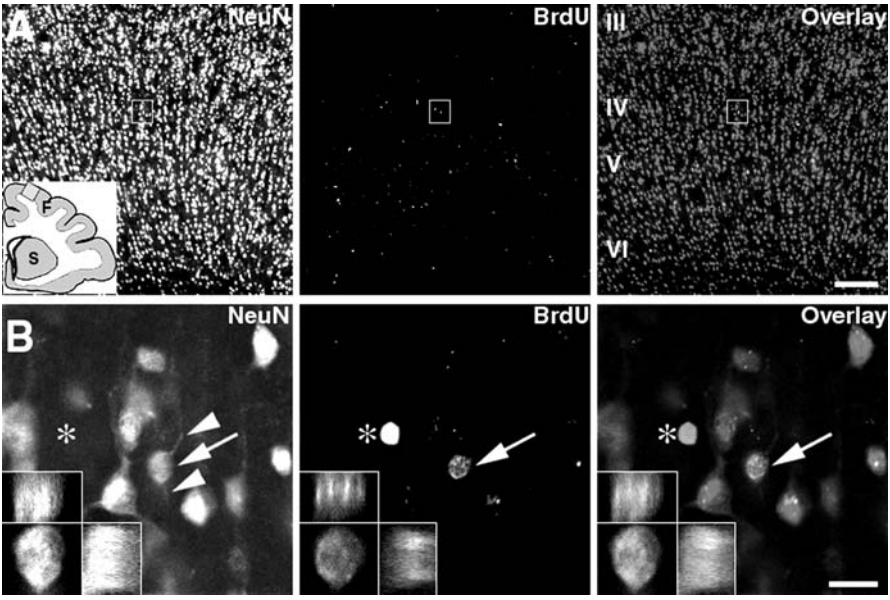

Fig. 59A, B Neuronal production in postischemic frontal cortex. **A** Double-staining for NeuN and BrdU on postischemic day 44. The depicted region corresponds to the *frame* on the schematic map (*lower left*). A *frame* in layer IV focuses on the region magnified in **B**. **B** Note that the BrdU$^+$/NeuN$^+$ cell (*arrows*), which is similar in size and shape to adjacent BrdU$^-$/NeuN$^+$ neurons, extends processes toward them (*arrowheads*). The BrdU$^+$/NeuN$^+$ cell is shown with channel separation and 3D reconstructions in *insets*. A BrdU$^+$/NeuN$^-$ cell is depicted by *arrowheads*. *F*, frontal cortex; *S*, striatum. *Scale bars* = 200 μm (**A**); 20 μm (**B**)

Table 10 Average percentages of colabeling of BrdU with various cell markers in parenchyma of frontal cortex and striatum. $BrdU^+$ cells were sampled for colabeling with either Musashi1 or Nestin as described in the text

	Day 9		Day 23		Day 44		Day 79	
	Control	Ischemia	Control	Ischemia	Control	Ischemia	Control	Ischemia
Iba1	7±3	79±19*	6±3	81±15*	6±3	80±26*	NA	78±21
S100β	0	12±6*	4±2	11±6*	4±3	10±5*	NA	11±5
CNP	0	3±1*	0,5	2±1*	0,5	2±1*	NA	2±1
NeuN	0	0.5	0	1.3±0.4*	0,5	1.5±0.5*	NA	1±0.5
Musashi1[§]	5±3	6±1	4±1	5±2	4±2	5±3	NA	5±3

NA, not available $*p < 0.05$ versus respective controls, Kruskal–Wallis or Mann–Whitney tests; [§], $Musashi1^+/GFAP^-/S100\beta^-$ cells; note that most $BrdU^+/S100\beta^+$ or $BrdU^+/GFAP^+$ cells were also positive for Musashi1

slightly larger in size than the proliferating $BrdU^+/Musashi1^+/GFAP^+$ astrocytes (Fig. 61A; arrows). Furthermore, the $BrdU^+/Musashi1^+/GFAP^-$ cells were single cells, while the $BrdU^+/Musashi1^+/GFAP^+$ cells were typically in "doublets." We

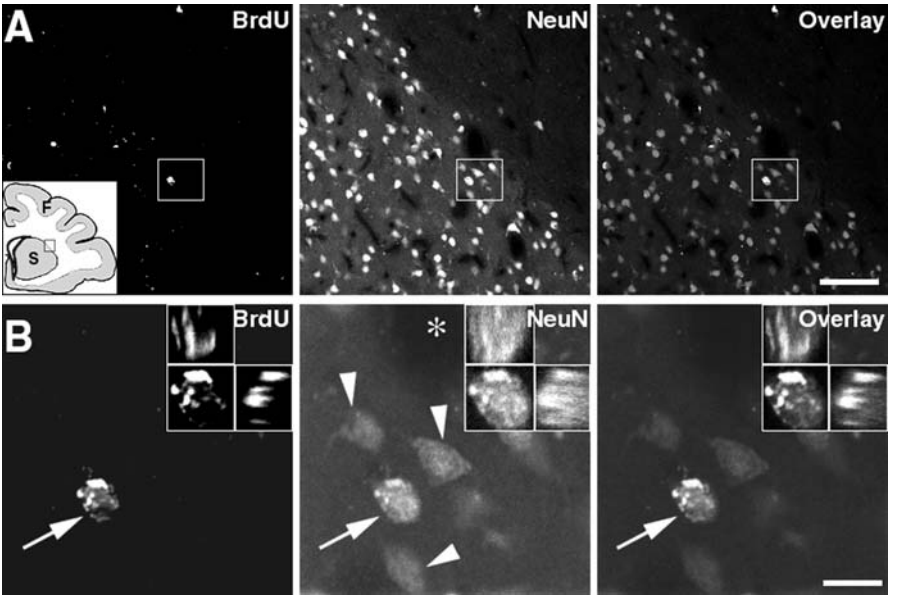

Fig. 60A, B Neuronal production in postischemic striatum. **A** Double-staining for NeuN and BrdU on postischemic day 44. The depicted region corresponds to the *frame* on the schematic map (*lower left*). A *frame* at the boundary between lateral putamen and white matter focuses on the region magnified in **B**. **B** Note the $BrdU^+/NeuN^+$ cell (*arrows*), which is similar in size and shape to the adjacent $BrdU^-/NeuN^+$ neurons (*arrowheads*). The $BrdU^+/NeuN^+$ cell is shown with channel separation and 3D reconstructions in *insets*. *F*, frontal cortex; *S*, striatum. *Scale bars* = 100 μm (**A**); 20 μm (**B**)

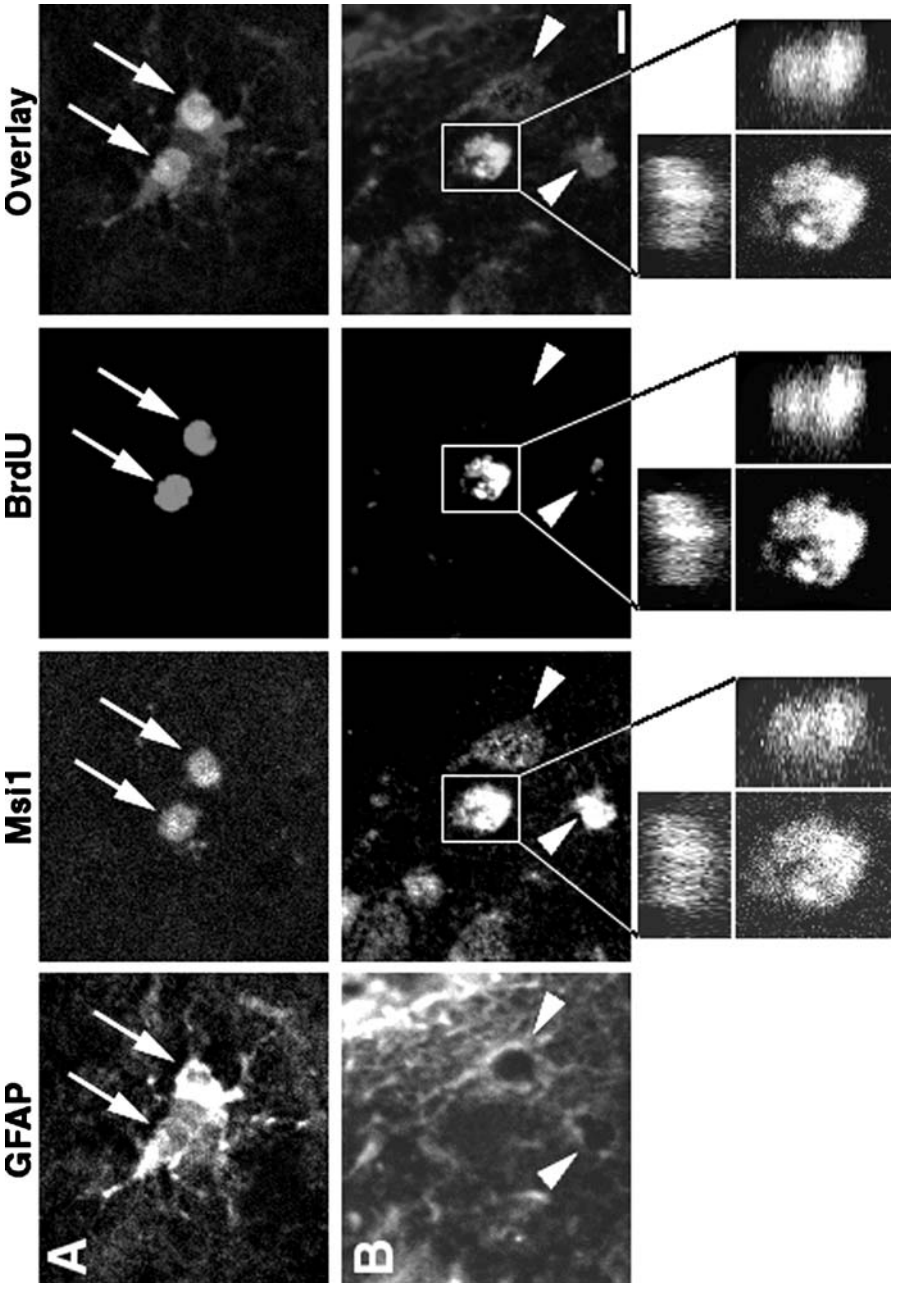

Fig. 61A, B Immunophenotype of $BrdU^+$/$Musashi1^+$ cells in frontal neocortex on postischemic day 44. **A** Two adjacent $BrdU^+$/$Musashi1^+$ cells are triple-labeled for GFAP (*arrows*). **B** A $BrdU^+$/$Musashi1^+$/$GFAP^-$ cell is depicted in *frames*, while adjacent $BrdU^-$/$Musashi1^+$/$GFAP^+$ cells are depicted by *arrowheads*. The cell in *frames* is presented with 3D orthogonal projections in the *bottom panel*. *Msi1*, Musashi1. *Scale bar* = 10 μm

estimated that the phenotype BrdU$^+$/Musashi1$^+$/GFAP$^-$ represented about 5% of the BrdU$^+$ cells in striatal or cortical parenchyma without significant differences between control and ischemia monkeys (Table 10). %STOP

4 Discussion

We present here the first comprehensive analysis of the distribution, quantity, and phenotype of de novo-generated cells in several regions of adult primate brain after transient global cerebral ischemia.

4.1 BrdU as a Proliferation Marker

Because BrdU is an indicator of DNA synthesis, not a direct mitotic marker, its incorporation into newly synthesized DNA can occur not only during the S-phase of the cell cycle preceding cell division, but also during the repair of damaged DNA (Nowakowski and Hayes 2001; Rakic 2002a, b). Brain ischemia followed by reperfusion is a known factor elevating DNA damage (Liu et al. 2001a), thus increasing the possibility that BrdU is taken up by cells during the repair of this damage. Therefore, we specifically addressed the issue of whether BrdU is a selective proliferation marker, i.e., whether BrdU labels only the adult-generated cells without being incorporated into nondividing cells undergoing some kind of abortive DNA synthesis.

The following lines of evidence demonstrate that for our monkey model and under the current BrdU labeling protocol, BrdU selectively stains dividing cells. First, BrdU$^+$ cells were colabeled by independent proliferation markers: Ki67 (Scholzen and Gerdes 2000; Kee et al. 2002) and phosphohistone H3 (Hendzel et al. 1997; Strahl and Allis 2000). Furthermore, we independently performed single staining for Ki67 and phosphohistone H3 that also revealed an increase of positive cells. In the short-term survival monkey group, the BrdU$^+$ cells slightly outnumbered the Ki67$^+$ cells, because the latter represent only the fraction of cells proliferating at the time of animal sacrifice, while BrdU was incorporated within a period of 96 h. The fraction of BrdU$^+$ cells colabeled by phosphohistone H3 was even lower (~20%) because phosphohistone H3 is expressed only during the M phase. Thus, the presence of BrdU$^+$ cells that were negative for Ki67 and/or phosphohistone H3 indicated the BrdU$^+$ cells had exited the cell cycle, i.e., were postmitotic. This is typical of the long-term survival monkey group. The use of Ki67 and phosphohistone H3 (endogenous to the cells proteins) also excluded the possibility that the elevated BrdU reaction after ischemia results from postischemic increase of blood–brain barrier permeability.

Second, BrdU was not detected in cells exhibiting features of DNA damage, repair, or programmed cell death. DNA damage was detected using the TUNEL assay. As expected, ischemia increased the number of TUNEL$^+$ cells in several

estimated that the phenotype BrdU$^+$/Musashi1$^+$/GFAP$^-$ represented about 5% of the BrdU$^+$ cells in striatal or cortical parenchyma without significant differences between control and ischemia monkeys (Table 10). %STOP

4 Discussion

We present here the first comprehensive analysis of the distribution, quantity, and phenotype of de novo-generated cells in several regions of adult primate brain after transient global cerebral ischemia.

4.1 BrdU as a Proliferation Marker

Because BrdU is an indicator of DNA synthesis, not a direct mitotic marker, its incorporation into newly synthesized DNA can occur not only during the S-phase of the cell cycle preceding cell division, but also during the repair of damaged DNA (Nowakowski and Hayes 2001; Rakic 2002a, b). Brain ischemia followed by reperfusion is a known factor elevating DNA damage (Liu et al. 2001a), thus increasing the possibility that BrdU is taken up by cells during the repair of this damage. Therefore, we specifically addressed the issue of whether BrdU is a selective proliferation marker, i.e., whether BrdU labels only the adult-generated cells without being incorporated into nondividing cells undergoing some kind of abortive DNA synthesis.

The following lines of evidence demonstrate that for our monkey model and under the current BrdU labeling protocol, BrdU selectively stains dividing cells. First, BrdU$^+$ cells were colabeled by independent proliferation markers: Ki67 (Scholzen and Gerdes 2000; Kee et al. 2002) and phosphohistone H3 (Hendzel et al. 1997; Strahl and Allis 2000). Furthermore, we independently performed single staining for Ki67 and phosphohistone H3 that also revealed an increase of positive cells. In the short-term survival monkey group, the BrdU$^+$ cells slightly outnumbered the Ki67$^+$ cells, because the latter represent only the fraction of cells proliferating at the time of animal sacrifice, while BrdU was incorporated within a period of 96 h. The fraction of BrdU$^+$ cells colabeled by phosphohistone H3 was even lower (~20%) because phosphohistone H3 is expressed only during the M phase. Thus, the presence of BrdU$^+$ cells that were negative for Ki67 and/or phosphohistone H3 indicated the BrdU$^+$ cells had exited the cell cycle, i.e., were postmitotic. This is typical of the long-term survival monkey group. The use of Ki67 and phosphohistone H3 (endogenous to the cells proteins) also excluded the possibility that the elevated BrdU reaction after ischemia results from postischemic increase of blood–brain barrier permeability.

Second, BrdU was not detected in cells exhibiting features of DNA damage, repair, or programmed cell death. DNA damage was detected using the TUNEL assay. As expected, ischemia increased the number of TUNEL$^+$ cells in several

brain regions, including the hippocampus, neocortex, and striatum. Double-staining of TUNEL with the neuronal marker NeuN revealed that most $TUNEL^+$ cells were neurons. At the same time, TUNEL/BrdU double-staining did not identify double-labeled cells. To unequivocally exclude the possibility that some rare cases of $TUNEL^+/NeuN^+$ cells could have incorporated BrdU, we performed BrdU/TUNEL/NeuN triple-labeling, which demonstrated that the $BrdU^+/NeuN^+$ cells were $TUNEL^-$ and, conversely, that the $TUNEL^+/NeuN^+$ cells were $BrdU^-$ (Tonchev et al. 2003a, 2005). The lack of BrdU/TUNEL colabeling in our study demonstrates either or both of the following: (1) The BrdU dose we have applied (500 mg/kg per monkey totally) is insufficient for incorporation into cells undergoing abortive DNA synthesis within our ischemic model. In fact, such an abortive incorporation has been shown to depend on the injury model (Kuan et al. 2004). (2) Our BrdU immunohistochemistry protocol cannot detect the small amounts (if any) of BrdU possibly incorporated in some neurons during DNA damage/repair/apoptosis. Furthermore, we demonstrated that BrdU did not co-stain with a marker of DNA repair, Gadd45. After ischemia, the Gadd45 immunoreactivity translocated from the cytoplasm into the nucleus of neurons, consistent with increased DNA repair activity in these cells. However, none of the $Gadd45^+$ cells incorporated BrdU (Tonchev et al. 2003b). Finally, we showed a lack of co-staining of BrdU with the apoptotic cell marker active caspase-3 (Tonchev et al. 2005).

Third, we showed the sequential coexpression of BrdU with various markers for neuronal development at multiple time-points after ischemia. In the monkeys of the short-term survival group, most nonglial cells positive for BrdU exhibited features of neural progenitors ($Musashi1^+/Nestin^+$), while in the long-term survival group the proportions of cells with neuronal progenitor (βIII-$tubulin^+/Doublecortin^+/TUC4^+$) or neuronal ($NeuN^+/GAD^+$) phenotypes increased. Such results argue strongly for a gradual development of $BrdU^+$ cells into neurons and are in disagreement with the notion that BrdU had been incorporated into neuronal cells undergoing DNA repair or programmed cell death (Cooper-Kuhn and Kuhn 2002).

Altogether, we conclude that for the current model/BrdU protocol, BrdU can be safely interpreted as a selective marker for adult-generated cells and their progeny.

4.2 Effects of Ischemia on Cell Proliferation and Differentiation

In most of the studied regions, we found that ischemia did increase the generation of new brain cells (Figs. 62 and 63). These regions included the hippocampal formation, SVZi, SVZa, neocortical and striatal regions studied, and the olfactory bulb (in the long-term survival monkey group). Ischemia did not change the quantity or phenotype of proliferating cells in PHR, and the olfactory bulb of the short-term survival monkey group. Importantly, in postischemic brains the increased $BrdU^+$ cells sustained their presence, contrasting their transient existence in normal macaque brain (Gould et al. 2001).

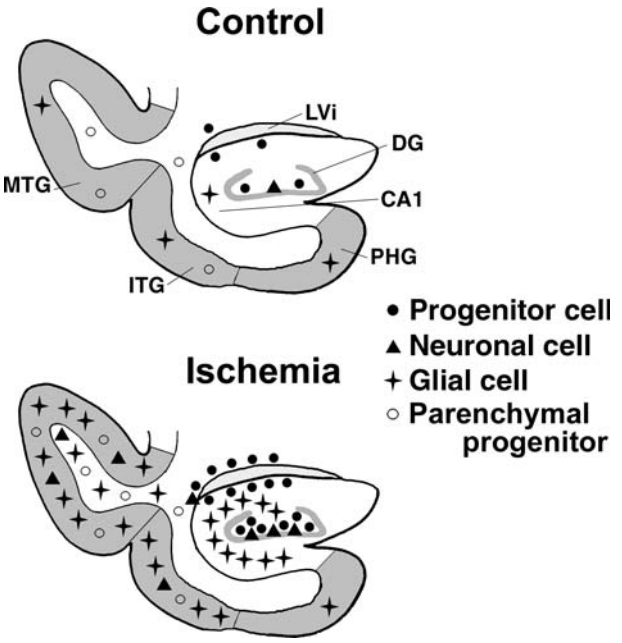

Fig. 62 Schematic presentation of the effects of ischemia on cell proliferation and differentiation in the temporal lobe. A coronal section through the temporal lobe at the level of the hippocampal body is shown (see Fig. 2A). The distribution of various cell types is depicted, including progenitors (Musashi1$^+$/Nestin$^+$), neuronal cells (including immature and mature neurons), glial cells (including microglia, astroglia, and oligodendroglia), and putative parenchymal progenitors (see text for details). Note the postischemic increase of all cell types in the regions of interest, with the exception of PHG. Also note the purely glial phenotype of proliferating cells in CA1. *LVi*, inferior horn of the lateral ventricle; *ITG* and *MTG*, inferior and middle temporal gyri; *PHG*, parahippocampal gyrus

In SGZ, numerous BrdU$^+$ cells expressed Musashi1 or Nestin, markers of neural progenitors (Lendahl et al. 1990; Sakakibara et al. 1996; Kaneko et al. 2000). At the same time, these markers are also expressed by astrocytes (Sakakibara and Okano 1997; Duggal et al. 1997). We therefore performed triple-staining for BrdU, Musashi1 (or Nestin), and the astrocyte marker GFAP, which demonstrated that the BrdU$^+$/Musashi1$^+$ or BrdU$^+$/Nestin$^+$ cells were negative for GFAP. The BrdU$^+$/Musashi1$^+$/GFAP$^-$ or BrdU$^+$/Nestin$^+$/GFAP$^-$ cells most probably represent multipotent neural progenitors in adult monkey DG (Tonchev et al. 2003a). The percentage of BrdU$^+$ cells that were colabeled with either Musashi1 or Nestin did not vary significantly among the experimental groups. However, as the total number of BrdU$^+$ cells was significantly increased after ischemia, postischemic DG contained significantly more proliferating neural progenitors than control DG. In rodent SGZ, the putative progenitors of DGL neurons were GFAP$^+$ cells, and accordingly such GFAP$^+$ cells were the earliest BrdU-incorporating cells in mouse

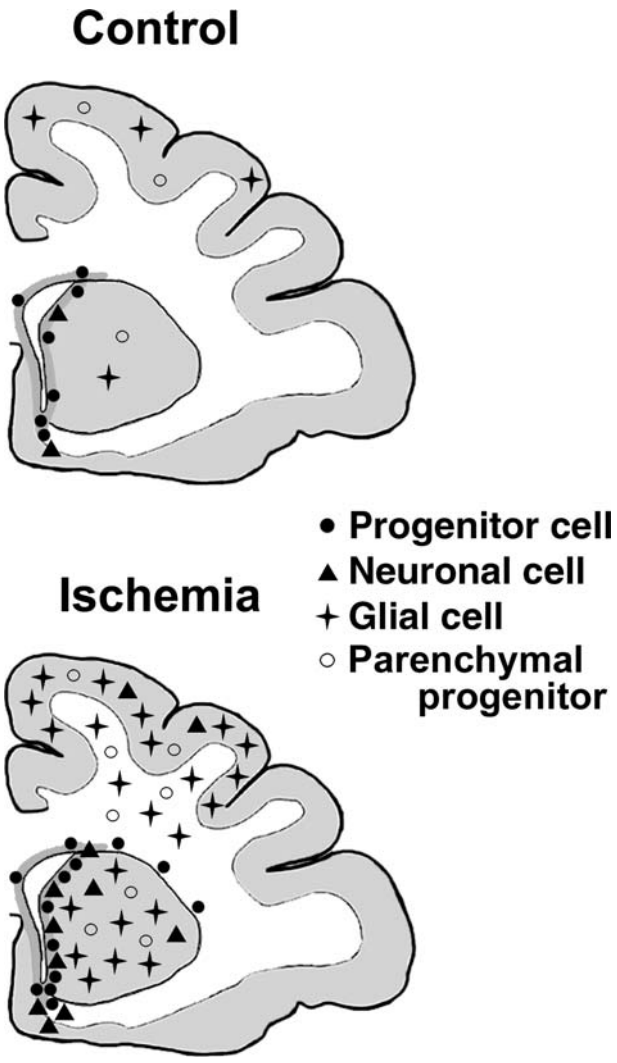

Fig. 63 Schematic presentation of the effects of ischemia on cell proliferation and differentiation in the frontal lobe. A coronal section through the frontal lobe is shown (see Fig. 2B). The distribution of various cell types is depicted, including progenitors (Musashi1$^+$/Nestin$^+$), neuronal cells (including immature and mature neurons), glial cells (including microglia, astroglia, and oligodendroglia), and putative parenchymal progenitors (see text for details). Note the postischemic increase of all cell types in the regions of interest

SGZ (Seri et al. 2001). Our findings appear to differ from these results, and the reason could be that species variations may exist between monkeys and rodents with regard to the molecular identity of SGZ progenitors.

A distinct proportion of newly generated cells in DG expressed neuronal features—colabeling with immature markers such as Doublecortin, Hu, TUC4, or PSA-NCAM, or with immature/adult markers such as βIII-tubulin, NeuN, or GAD. While in the short-term survival group these cells constituted only 2%–3% of the $BrdU^+$ cells, in the long-term group they were 15%–20% of the $BrdU^+$ cells (Table 11). The proliferating cells expressing neuronal phenotype were localized in either SGZ adjacent to DGL (for Doublecortin, Hu, TUC4, PSA-NCAM, or βIII-tubulin) or in inner layers of DGL (for NeuN, GAD). In the short-term survival monkeys, immature neurons extended processes parallel to DGL, while in the long-term group a single process was extended perpendicularly to DGL (Fig. 64). Furthermore, adult-generated neurons appeared to establish morphological contacts with neighboring neuronal cells and expressed a GABAergic transmitter phenotype characteristic for dentate granule neurons (Jongen-Relo et al. 1999). Altogether, these represent data of the maturation of putative new DG neurons.

In contrast to DG, no signs of neuronal production were detected in postischemic CA1, where despite the marked cell loss followed by a striking increase of proliferating cells, the latter were invariably of a glial phenotype. Most $BrdU^+$ cells in monkey CA1 were microglia, as with the rodent brain (Liu et al. 2001b);

Table 11 Approximate proportions of various de novo-generated cell phenotypes in several regions of adult monkey forebrain after ischemia (long-term survival animals). Note that outside the germinative centers DG and SVZa, the most common proliferating cells were microglial cells followed by astrocytes. *$BrdU^+$/$Musashi1^+$/$GFAP^-$ cells in parenchyma were considered putative local progenitors (see text for details). Note that such cells were absent in *cornu Ammonis*

Region	Phenotype of $BrdU^+$ cells
Dentate gyrus	45%—Neural progenitors
	30%—Microglia
	12%—Neuronal progenitors
	8%—Neurons
	5%—Other
Cornu Ammonis	80%—Microglia
	15%—Astrocytes
	3%—Oligodendrocytes
	2%—Other
SVZa	75%—Neuronal progenitors
	10%—Neural progenitors
	5%—Microglia
	10%—Other
Neocortex/striatum	80%—Microglia
	10%—Astrocytes
	5%—Parenchymal progenitors*
	3%—Oligodendrocytes
	1%—Neurons
	1%—Other

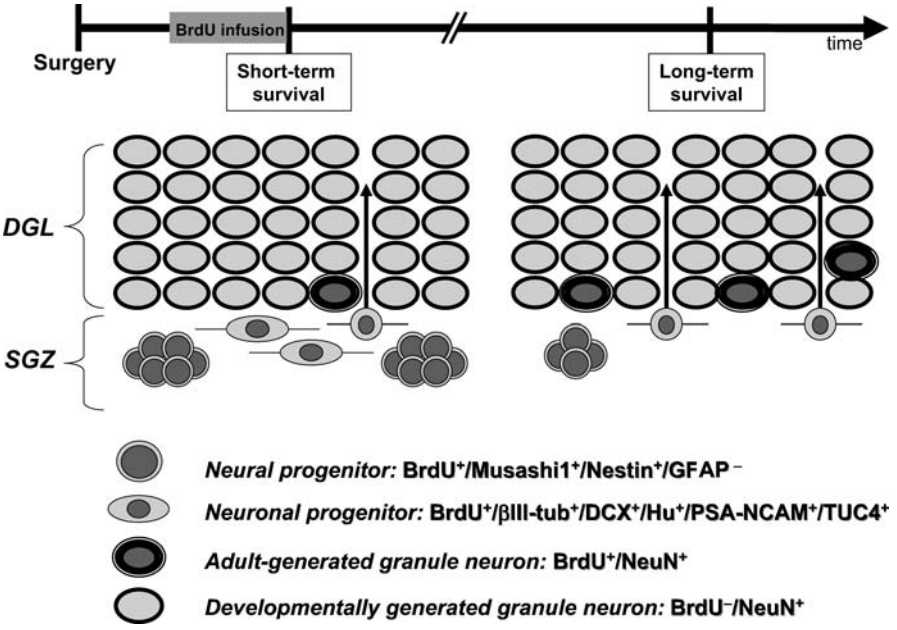

Fig. 64 Distribution and phenotype of adult-generated cells in postischemic monkey DG at short-term and long-term survival time periods after surgery. Note the numerous progenitor cells forming clusters in SGZ at short-term survival; some of these cells were preserved at long-term survival. Typical for the early periods after ischemia were neuronal progenitors extending processes parallel to DGL, while at long-term survival the processes were spanning DGL. The quantity of newly generated cells with a mature neuronal phenotype increased over time

astrocytes were the second most common cell type; only a few adult-generated oligodendrocytes were seen (Table 11). A more detailed discussion of the various glial markers expressed in postischemic monkey CA1 and their significance is presented elsewhere (Tonchev et al. 2003b). The lack of neuronal replacement in CA1 is noteworthy as CA1 is the most vulnerable to global ischemia brain region. In rodent global ischemic models, progenitor cell activation adjacent to the CA1 periventricular region resulted in neuronal replacement after insult (Nakatomi et al. 2002; Schmidt and Reymann 2002). In the monkey brain, the periventricular area adjacent to CA1 is the zone along the inferior horn of the lateral ventricle: SVZi. Like SGZ, SVZi also contained $BrdU^+/Musashi1^+/GFAP^-$ or $BrdU^+/Nestin^+/GFAP^-$ cells whose proliferation was upregulated after ischemia. However, these progenitors did not show a stable existence over time, and more importantly, did not exhibit an ability to differentiate into neuronal cells. These data suggest that SGZ or SVZi progenitors may be regulated by differential molecular mechanisms responsible for their differential ability to produce neurons.

Compared to SGZ, SVZa, the other major germinative zone in adult brain, was a region with a similarly marked accumulation of proliferating cells. These cells

were frequently in clusters, located in dorsal, caudate, ventral, or anterior SVZa (see Fig. 63). In septal SVZa, clusters were almost never seen, and in this aspect of SVZa, cell proliferation was unaffected by ischemia. The phenotype and sequence of expression of both neural and neuronal progenitor cells in SVZa resembled that in SGZ—positivity for Musashi1/Nestin with negativity for GFAP for neural progenitors (abundant in the short-term survival monkey group), and positivity for Doublecortin, PSA-NCAM or βIII-tubulin for neuronal progenitors (abundant in the long-term survival group; Table 11). Noteworthy is the postischemic increase of precursors in SVZa (particularly its ventral aspect) on day 9 followed by an increase of progenitors migrating in RMS toward the olfactory bulb on day 23, and by $BrdU^+$ cell upregulation in olfactory bulb parenchyma on postischemic day 44. In contrast, progenitor cells residing in olfactory peduncle and core white matter remained unaffected by ischemia in the first two postischemic weeks. These data indicate that the increased quantity of $BrdU^+$ cells in olfactory bulb on day 44 was due to the increased progenitor cell generation in SVZa and subsequent migration in RMS rather than to the local progenitor cell population in the olfactory peduncle/core.

In contrast to the chain migration of progenitors in monkey RMS toward the olfactory bulb, no such chains of cells were seen toward the frontal cortex or striatum. The $BrdU^+$ cells in subcortical white matter remained dispersed single cells, and immunostaining for Doublecortin, PSA-NCAM, or βIII-tubulin also failed to stain chains of cells. However, in a P14 monkey we observed numerous $BrdU^+/\beta$III-$tubulin^+$, $BrdU^+$/PSA-$NCAM^+$, or $BrdU^+$/$Doublecortin^+$ subcortical clusters, indicating that dividing neuronal progenitors continue to migrate from SVZa toward neocortex in early postnatal life. These data dismiss the possibility that the lack of subcortical progenitor clusters in adult monkey brains could be an artifact. Altogether they suggest that migration from SVZa to neocortex in the monkey stops during postnatal life and cannot be reactivated by a global ischemic insult per se. Our results are at variance with studies in rodent focal ischemic models that have shown that SVZa appears the main source of precursor cells for neuronal replacement in striatum and cortex (Zhang et al. 2001, 2004; Arvidsson et al. 2002; Parent et al. 2002; Jin et al. 2003). However, our model of transient global ischemia caused a less pronounced injury than the large focal injury induced in the rat stroke models. Thus, the differences in progenitor cell migration might be related to the strength of the insult—a milder ischemic insult might be unable to trigger progenitor cell migration toward postischemic neocortex or striatum. Application of a monkey focal ischemic model in future studies would be important to define more precisely the ability of primate progenitors to respond to stroke.

Despite the lack of evidence for migration from SVZa to frontal neocortex or striatum, ischemia led to a marked increase of proliferating cells in these regions. Similar results were observed in temporal neocortex. As in CA1, the most abundant proliferating cell types were microglia followed by astrocytes, while just a few oligodendrocytes were produced (Table 11). Importantly, 1% of the $BrdU^+$ cells expressed features of GABAergic interneurons—positivity for the neuronal marker NeuN, region-specific transcription factors, and the GABAergic marker GAD. The

GABAergic transmitter phenotype is consistent with the preferential localization of these cells in neocortical layers II–IV. The newly generated neurons were morphologically identical to neighboring developmentally generated neurons; they survived for up to 79 days after ischemia and remained a stable proportion of the $BrdU^+$ cells in neocortex and striatum. In contrast, newly generated neurons in normal monkey neocortex were reported to have a transient existence (Gould et al. 2001). Our view that we have indeed identified new neurons in adult brains was strengthened by the fact that we did not rely on a single marker to label these cells. Rather, we used a combination of markers. Thus, putative adult-generated neurons were not identified solely as $BrdU^+/NeuN^+$ cells, but were triple-labeled for independent neuron-specific proteins such as GAD and neuron-specific transcription factors. The colabeling of various signals was confirmed by 3D confocal microscopy to exclude the possibility that $BrdU^+$ satellite glial cells superimposed on neurons could be falsely interpreted as de novo generated neurons (Rakic 2002b).

The lack of evidence for progenitor cell migration from SVZ to neocortex or striatum contrasts the evidence for neuronal and glial production in these regions, and thus raises the issue of the origin of the progenitor cells that had generated the putative new neurons. Following the strategy adopted from our investigations in SGZ and SVZ to label precursor cells by BrdU/Musashi1/GFAP triple-staining, we identified that about 5% of the $BrdU^+$ cells in neocortical or striatal parenchyma were of the phenotype $BrdU^+/Musashi1^+/GFAP^-$ (Table 11), which was identical to the phenotype of progenitor cells in SGZ and SVZ. The $BrdU^+/Musashi1^+/GFAP^-$ cells were dispersed within brain parenchyma and were therefore spatially close to the adult-generated neurons or glia (astrocytes or oligodendrocytes) for which they might be precursors (Fig. 63). This spatial proximity could explain the findings of cells with a glial or neuronal phenotype a long distance away from SVZa in the short-term survival group (i.e., within 96 h after the onset of BrdU incorporation). It is unlikely that precursor cells originating in SVZa can reach the neocortex or striatum within this short period of time, given the dimensions of the monkey brain. Other groups have previously reported findings in primates, which are in accordance with a conclusion that newly generated neocortical and striatal neurons might arise from parenchymal progenitors. Progenitor cells were isolated in vitro of from adult human gray and white matter (Arsenijevic et al. 2001; Nunes et al. 2003). Furthermore, a small fraction of neural stem cells migrating from SVZa toward developing monkey neocortex remained in brain parenchyma in an undifferentiated state (Ourednik et al. 2001), and thus could in theory sustain their existence into adulthood until activated by injury. In adult rodent neocortex, supportive evidence that GABAergic interneurons might be generated by a local pool of precursors was also provided (Dayer et al. 2005).

Our data indicate that progenitor cells from various monkey brain regions were activated by ischemia. This paradigm had only a few exceptions. $BrdU^+/Musashi1^+/GFAP^-$ or $BrdU^+/Nestin^+/GFAP^-$ cells in olfactory peduncle and core white matter did not respond to ischemia with changes in cell proliferation (in the short-term monkey group), despite the fact that, as intracranial structures,

olfactory bulbs were subjected to the same insult as the rest of the brain. In PHR, a region in which we did not observe clear evidence of progenitor existence, cell proliferation was also unchanged after ischemia. PHR is a component of the medial temporal lobe system involved in the formation of declarative memory (Squire and Zola-Morgan 1991). Ischemic injury to structures within the medial temporal lobe is thought to cause memory impairment (reviewed by Squire and Zola 1996). However, in our model we did not detect cell loss in PHR, and neither did we detected it in the olfactory bulb. This might explain the lack of postischemic $BrdU^+$ cell increase we observed in these two regions. Nevertheless, whatever the cause of the differential postischemic response in cell proliferation, it is most probably defined by differential molecular signaling. Identifying the molecular switches underlying the diversity of the postischemic reaction in monkeys may lead to the development of novel sources for repair of the human brain.

4.3 Sustained Progenitor Cell Existence in Germinative Zones

Evaluation of proliferating cells in the long-term survival monkeys revealed a phenomenon common to SGZ and SVZa. In both germinative zones, a significant proportion of $BrdU^+$ cells sustained an immature phenotype over time without exhibiting features of differentiation.

In DG, some 15% of the $BrdU^+$ cells expressed the neuronal phenotype in DGL, but many (about 50%) of the adult-generated cells in monkeys surviving long-term after ischemia were located in SGZ, rather than in DGL (Fig. 64). Such a distribution is typical for early postischemic time-points, while at time-points of 4 weeks or longer after ischemia, most $BrdU^+$ cells in rodent DG were found in DGL where they become neurons (Liu et al. 1998; Kee et al. 2001; Yagita et al. 2001; Nakatomi et al. 2002). The preservation of immaturity of these sustained $BrdU^+$ cells was supported by their clustering and expression of Musashi1. The lack of migration to DGL and/or differentiation of a large proportion of $BrdU^+$ cells raises the issue of which are the molecular signals responsible for this phenomenon. These could be extrinsic signals from the environment surrounding the progenitor cells (e.g., growth factors and/or cytokines) or intrinsic molecular switches such as transcription factors. Their identification will help to manipulate more efficiently adult primate brain progenitor cells.

In SVZa, we found that a proportion of $BrdU^+$ cells in both control and ischemic brains sustain their presence in SVZa, consistent with previous findings in normal monkeys (Kornack and Rakic 2001a). However, we calculated that postischemic SVZa retained a significantly higher proportion of the $BrdU^+$ cells in its caudate, dorsal, and anterior aspects. Notably, about 15% of these long-term BrdU-retaining cells co-stained for Musashi1 and Ki67, indicating they were neural progenitors in the active phases of their cell cycle. In ventral SVZa, differences between postischemic and control monkeys were not observed, consistent with the view that the $BrdU^+$ cells in this SVZa aspect migrate in RMS away from SVZa.

Several possibilities may explain the existence of long-term BrdU-retaining cells in germinative zones. First, the high dose of BrdU (about 10 times larger than used in most studies) may diminish the possibility for a BrdU label dilution by cell division below immunohistochemically detectable levels. A high BrdU dose may ensure BrdU detection throughout long-term survival periods, especially given the fact that the turnover of some adult-generated cells in the monkey brain is not rapid (Kornack and Rakic 2001a; Gould et al. 2001). Second, stem/progenitor cells in monkey brain may have the ability to exit and then re-enter the cell cycle in a similar way to what was shown in rodents (Maslov et al. 2004). Thus, the long-term BrdU label-retaining cells in the SVZa that were colabeled by Ki67 represent good candidates for precursor cells or their progeny reentering the cell cycle. Third, the retention of SVZa progenitors might result from the lack of migration and/or differentiation signals or, alternatively, to an enhanced signal maintaining the stem/progenitor phenotype. The molecular nature of such putative signals in the primate is currently being elucidated in our laboratories. Fourth, the sustained $BrdU^+$ cells might be abnormal cells. In our view this is the least probable explanation, as these cells remained negative for markers of DNA damage and apoptosis.

Our results are related to the findings in a recent study performing transplantation of human neural stem cells in lateral ventricles of monkeys during their embryonic period (Ourednik et al. 2001). The authors observed that most of the implanted stem cells migrated toward neocortex or striatum where they adopted the fate of neurons or glia. Interestingly, a subpopulation the stem cells retained their location in SVZa 4 weeks after implantation, exhibiting features of undifferentiated progenitors (Ourednik et al. 2001). Our results extend these findings by demonstrating that long-term retention of an immature phenotype and preserved localization in the niche is a characteristic not only of embryonic, but also of adult primate progenitors, and that this characteristic is enhanced by injury. Performing BrdU/Ki67 double-staining in SVZa of long-term-survival monkeys, we identified three distinct cellular phenotypes: $BrdU^+/Ki67^+$, $BrdU^+/Ki67^-$, and $BrdU^-/Ki67^+$ cells (Fig. 65). The $BrdU^+/Ki67^-$ cells were positive for βIII-tubulin and thus were considered neuronal progenitors (immature neurons) that have exited the cell cycle. The $BrdU^+/Ki67^+$ cells represented the sustained neural progenitors in the active cell cycle discussed in Sect. 3.4. The $BrdU^-/Ki67^+$ cells were most probably mitotic progenitors that were generated after the stop of BrdU infusion (day 9), i.e., recently with respect to the time of euthanasia (days 23, 44, or 79). The spatial coexistence of $BrdU^+/Ki67^+$ and $BrdU^-/Ki67^+$ cells suggests that sustained and recently generated precursors were located in the same niche (Fig. 65), and thus might interact with each other. Revealing the mechanisms of this potential interaction may have implications in more effectively modulating progenitor cells in situ for therapeutic purposes.

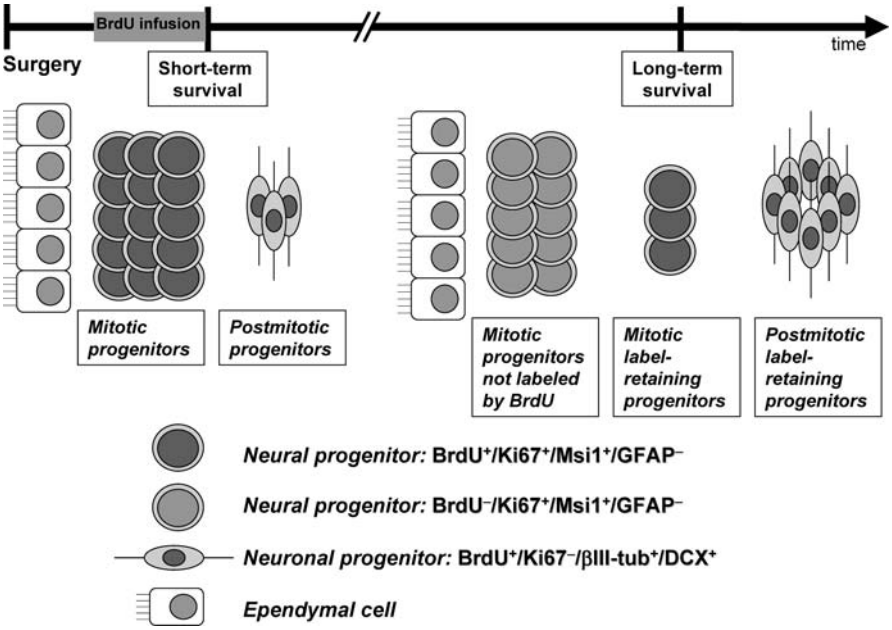

Fig. 65 Distribution and phenotype of adult-generated cells in postischemic monkey SVZa at short-term and long-term survival time periods after surgery. Early after ischemia nearly all progenitors were positive for BrdU, Ki67, and Musashi1, while only a few have exited the cell cycle (Ki67$^-$) and were positive for βIII-tubulin. The latter cell type predominated at long-term survival time periods, while the neural progenitor immunophenotypes became more complex based on their expression of BrdU and Ki67. The long-term BrdU-retaining neural (Musashi1$^+$) progenitors exhibited features of mitotic (Ki67$^+$) cells. On the other hand, numerous BrdU$^-$/Ki67$^+$ cells were observed, which most probably represent progenitors generated after the stop of BrdU infusion

4.4 Implications of Monkey Findings for Therapies in Humans

Currently, two major therapeutic approaches for brain repair by stem/progenitor cells have emerged (reviewed by Hallbergson et al. 2003). First, endogenous progenitors might be recruited to sites of injury (reviewed by Picard-Riera et al. 2004). Second, in vitro-expanded stem/progenitor cells might be transplanted in sites of injury, after appropriate "priming" procedures directing these cells toward the desired neuronal lineages (Hallbergson et al. 2003).

In cases of endogenous progenitor activation, the apparent sites of origin of such cells seem to be the germinative centers. Indeed, SVZa progenitor cells targeted to the olfactory bulb have been redirected to postischemic striatum or cortex (Arvidsson et al. 2002; Parent et al. 2003; Jin et al. 2003; Zhang et al. 2004). The possibility of endogenous brain progenitor cell activation has been addressed mainly using rodent models. Therefore, studies in monkey disease models were

indicated, as monkeys are phylogenetically closer to humans than are rodents. Significant variability exists between primates and lower mammals in respect to certain proliferation parameters, such as the timing and number of cell divisions during cortical development, resulting in interspecies variability in cortical size and organization (Kornack 2000). Furthermore, in normal adult monkey DG, the fraction of newly generated neurons was smaller than the calculated fraction for the adult mouse DG by one order of a magnitude (Kornack and Rakic 1999).

Our monkey model of global brain ischemia provided additional evidence for the existence of differences between monkeys and rodents with respect to neurogenesis. The postischemic monkey DG exhibited a lower quantity of progenitors per square millimeter than the gerbil (Liu et al. 1998). Importantly, the proportion of progenitors adopting neuronal phenotype was minimal in the monkey versus the rat (Kee et al. 2001). In CA1, the differences between monkey and rodent were even more striking—no sign of neuronal replacement was evident in monkey CA1, while as much as 40% of lost CA1 neurons were regenerated in rat CA1 (Bendel et al. 2005), an effect that was greatly augmented by growth factor treatment (Nakatomi et al. 2002). As we observed a few progenitor cells in SVZi that failed to become neurons, we speculate that signals from the environment or intrinsic to the progenitor cells signals (or both) were responsible for the nonneurogenic monkey response. This implies that the identification of pro-neural signals is of crucial importance in the attempt to instruct the differentiation of primate hippocampal precursor cells toward neuronal fate.

In monkey SVZa, a significant proportion of progenitors sustained their presence in the niche, particularly after ischemia. Assuming that a similar sustained progenitor existence is present in the adult human brain after ischemia, our data indicate a window of opportunity for progenitor cell sampling from SVZa within the second postischemic week, when the quantity of SVZa progenitors is maximal. Sampling of precursors could be readily achieved by resecting approximately 1-mm-thick subependymal tissue at the bottom of the anterior horn of the lateral ventricle through a ventricular drainage tube with the aid of neurosurgical endoscopy or microscopy. After ex vivo manipulations, the progenitor cells might become a valuable source of autologous grafting and gene delivery to the injured human brain following stroke.

Another opportunity for therapeutic implications is suggested by our results showing that adult brain parenchyma, including neocortex and striatum, may harbor local progenitor cells. The well-known germinative centers are distant from many brain regions, particularly in the large primate brain, and the possibility of directing migration from these centers to distant sites of injury remains restricted. However, endogenous parenchymal precursors within or adjacent to the injured region do not need to overcome long distances to reach their target areas. Therefore, manipulation of these cells may provide an opportunity for neuronal production in situ.

By advancing our knowledge of how the fate of monkey endogenous progenitor cells is controlled, we shall more efficiently construct strategies for repair of the

human brain. Such strategies should also take into account the age-related changes in the capacity of the brain to generate and support stem/progenitor cells, as it is known that stroke is much more common in older patients. The identification of region-, species-, and age-dependent differences in the regulation of adult neurogenesis requires extensive fundamental research efforts. Our results strengthen the view that nonhuman primate models of disease represent an essential component of these efforts.

5 Summary

We performed transient global cerebral ischemia on adult macaque monkeys by reversibly stopping blood flow to the brain. We labeled de novo-generated cells in postischemic animals as well as in sham-operated controls by infusing the DNA synthesis indicator BrdU, and subsequently investigated the distribution and phenotype of BrdU-labeled cells in several telencephalic regions at various timepoints after ischemia.

The ischemic insult significantly increased the number of proliferating cells in the hippocampus, SVZ, neocortex, and striatum, but had no such effect in PHR. In the olfactory bulb, ischemia did not change the proliferating cell levels in the first two postischemic weeks, but did increase these levels at long-term survival time periods. The majority of newly generated cells outside the germinative centers were of a glial phenotype, while neurons constituted only 1% of these cells. Notably, no new neurons were observed in the hippocampal CA1 sector, the region exhibiting the highest vulnerability to ischemia. Within the germinative centers, most BrdU-labeled cells were of a progenitor phenotype and a large proportion of these precursors sustained their existence in the niche for months after ischemia. Furthermore, cells with a progenitor phenotype were identified in brain parenchyma, and these might be responsible for the limited parenchymal neurogenesis as well as for the oligodendrogliogenesis and astrogliogenesis in striatum and neocortex.

Our results show that ischemia differentially activates endogenous neural precursors residing in diverse locations of the adult primate CNS. A limited endogenous potential for postischemic neuronal repair exists in neocortex and striatum, but not in the hippocampus proper of the adult macaque monkey brain. The presence of putative parenchymal progenitors and of sustained progenitors in germinative centers opens novel possibilities for precursor cell recruitment to sites of injury. The molecular manipulation of this process may advance our ability to effectively apply brain progenitor cells in the treatment of human neurological diseases.

Acknowledgements Research was supported by Grants-in-Aid for Strategic Promotion System for Brain Science (SPSBS) and for Scientific Research (Kiban-Kennkyu (B) 15390432, 18390392) from the Japanese Ministry of Education, Culture, Sports, Science, and Technology, and by a grant from the National Science Fund of Bulgaria (L1311/03). We thank

human brain. Such strategies should also take into account the age-related changes in the capacity of the brain to generate and support stem/progenitor cells, as it is known that stroke is much more common in older patients. The identification of region-, species-, and age-dependent differences in the regulation of adult neurogenesis requires extensive fundamental research efforts. Our results strengthen the view that nonhuman primate models of disease represent an essential component of these efforts.

5 Summary

We performed transient global cerebral ischemia on adult macaque monkeys by reversibly stopping blood flow to the brain. We labeled de novo-generated cells in postischemic animals as well as in sham-operated controls by infusing the DNA synthesis indicator BrdU, and subsequently investigated the distribution and phenotype of BrdU-labeled cells in several telencephalic regions at various timepoints after ischemia.

The ischemic insult significantly increased the number of proliferating cells in the hippocampus, SVZ, neocortex, and striatum, but had no such effect in PHR. In the olfactory bulb, ischemia did not change the proliferating cell levels in the first two postischemic weeks, but did increase these levels at long-term survival time periods. The majority of newly generated cells outside the germinative centers were of a glial phenotype, while neurons constituted only 1% of these cells. Notably, no new neurons were observed in the hippocampal CA1 sector, the region exhibiting the highest vulnerability to ischemia. Within the germinative centers, most BrdU-labeled cells were of a progenitor phenotype and a large proportion of these precursors sustained their existence in the niche for months after ischemia. Furthermore, cells with a progenitor phenotype were identified in brain parenchyma, and these might be responsible for the limited parenchymal neurogenesis as well as for the oligodendrogliogenesis and astrogliogenesis in striatum and neocortex.

Our results show that ischemia differentially activates endogenous neural precursors residing in diverse locations of the adult primate CNS. A limited endogenous potential for postischemic neuronal repair exists in neocortex and striatum, but not in the hippocampus proper of the adult macaque monkey brain. The presence of putative parenchymal progenitors and of sustained progenitors in germinative centers opens novel possibilities for precursor cell recruitment to sites of injury. The molecular manipulation of this process may advance our ability to effectively apply brain progenitor cells in the treatment of human neurological diseases.

Acknowledgements Research was supported by Grants-in-Aid for Strategic Promotion System for Brain Science (SPSBS) and for Scientific Research (Kiban-Kennkyu (B) 15390432, 18390392) from the Japanese Ministry of Education, Culture, Sports, Science, and Technology, and by a grant from the National Science Fund of Bulgaria (L1311/03). We thank

the following colleagues for generous gifts of antibodies: Hideyuki Okano (Keio University, Tokyo, Japan) for the anti-Musashi1 antibody, Masaharu Ogawa and Takaki Miyata (Brain Science Institute, RIKEN, Saitama, Japan) for the anti-Nestin antibody, Masashi Mizuguchi (Jichi Medical School, Tochigi, Japan) for the anti-Doublecortin antibody, Yoshinori Imai (National Institute of Neuroscience, Tokyo, Japan) for the anti-Iba1 antibody, and Tatsunori Seki (Juntendo University, Tokyo, Japan) for the anti-PSA-NCAM antibody.

References

Abrahams JM, Gokhan S, Flamm ES, Mehler MF (2004) De novo neurogenesis and acute stroke: are exogenous stem cells really necessary? Neurosurgery 54:150–155

Allen E (1912) The cessation of mitosis in the central nervous system of the albino rat. J Comp Neurol 19:547–568

Alonso JR, Porteros A, Crespo C, Arevalo R, Brinon JG, Weruaga E, Aijon J (1998) Chemical anatomy of the macaque monkey olfactory bulb: NADPH-diaphorase/nitric oxide synthase activity. J Comp Neurol 402:419–434

Altman J (1962a) Autoradiographic study of degenerative and regenerative proliferation of neuroglia cells with tritiated thymidine. Exp Neurol 5:302–318

Altman J (1962b) Are new neurons formed in the brains of adult mammals? Science 135:1127–1128

Altman J (1963) Autoradiographic investigation of cell proliferation in the brains of rats and cats. Anat Rec 145:573–591

Altman J, Das GD (1965) Autoradiographic and histological evidence of postnatal hippocampal neurogenesis in rats. J Comp Neurol 124:319–335

Altman J, Das GD (1966) Autoradiographic and histological studies of postnatal neurogenesis. I. A longitudinal investigation of the kinetics, migration and transformation of cells incorporating tritiated thymidine in neonate rats, with special reference to postnatal neurogenesis in some brain regions. J Comp Neurol 126:337–389

Arsenijevic Y, Villemure JG, Brunet JF, Bloch JJ, Deglon N, Kostic C, Zurn A, Aebischer P (2001) Isolation of multipotent neural precursors residing in the cortex of the adult human brain. Exp Neurol 170:48–62

Arvidsson A, Kokaia Z, Lindvall O (2001) *N*-Methyl-D-aspartate receptor-mediated increase of neurogenesis in adult rat dentate gyrus following stroke. Eur J Neurosci 14:10–18

Arvidsson A, Collin T, Kirik D, Kokaia Z, Lindvall O (2002) Neuronal replacement from endogenous precursors in the adult brain after stroke. Nat Med 8:963–970

Bartley J, Soltau T, Wimborne H, Kim S, Martin-Studdard A, Hess D, Hill W, Waller J, Carroll J (2005) BrdU-positive cells in the neonatal mouse hippocampus following hypoxic-ischemic brain injury. BMC Neurosci 6:15

Bedard A, Levesque M, Bernier PJ, Parent A (2002a) The rostral migratory stream in adult squirrel monkeys: contribution of new neurons to the olfactory tubercle and involvement of the antiapoptotic protein Bcl-2. Eur J Neurosci 16:1917–1924

Bedard A, Cossette M, Levesque M, Parent A (2002b) Proliferating cells can differentiate into neurons in the striatum of normal adult monkey. Neurosci Lett 328:213–216

Bendel O, Bueters T, von Euler M, Ove Ogren S, Sandin J, von Euler G (2005) Reappearance of hippocampal CA1 neurons after ischemia is associated with recovery of learning and memory. J Cereb Blood Flow Metab 25:1586–1595

Benraiss A, Chmielnicki E, Lerner K, Roh D, Goldman SA (2001) Adenoviral brain-derived neurotrophic factor induces both neostriatal and olfactory neuronal recruitment from endogenous progenitor cells in the adult forebrain. J Neurosci 21:6718–6731

Bernier PJ, Bedard A, Vinet J, Levesque M, Parent A (2002) Newly generated neurons in the amygdala and adjoining cortex of adult primates. Proc Natl Acad Sci USA 99:11464–11469

Bondolfi L, Calhoun M, Ermini F, Kuhn HG, Wiederhold KH, Walker L, Staufenbiel M, Jucker M (2002) Amyloid-associated neuron loss and gliogenesis in the neocortex of amyloid precursor protein transgenic mice. J Neurosci 22:515–522

Boyes BE, Kim SU, Lee V, Sung SC (1986) Immunohistochemical co-localization of S-100b and the glial fibrillary acidic protein in rat brain. Neuroscience 17:857–865

Brierley JB, Brown AW, Excell BJ, Meldrum BS (1969) Brain damage in the rhesus monkey resulting from profound arterial hypotension. I. Its nature, distribution and general physiological correlates. Brain Res 13:68–100

Brodmann K (1905) Beitrage zur histologischen Lokalisation der Grosshirnrinde. Dritte Mitteilung: die Rindenfelder der niederen Affen. J Psychol Neurol 4:177–226

Butler TL, Kassed CA, Sanberg PR, Willing AE, Pennypacker KR (2002) Neurodegeneration in the rat hippocampus and striatum after middle cerebral artery occlusion. Brain Res 929:252–260

Carleton A, Petreanu LT, Lansford R, Alvarez-Buylla A, Lledo PM (2003) Becoming a new neuron in the adult olfactory bulb. Nat Neurosci 6:507–518

Cepko CL, Ryder E, Austin C, Golden J, Fields-Berry S, Lin J (1998) Lineage analysis using retroviral vectors. Methods 14:393–406

Cooper-Kuhn CM, Kuhn HG (2002) Is it all DNA repair? Methodological considerations for detecting neurogenesis in the adult brain. Brain Res Dev Brain Res 134:13–21

Darsalia V, Heldmann U, Lindvall O, Kokaia Z (2005) Stroke-induced neurogenesis in aged brain. Stroke 36:1790–1795

Daval JL, Pourie G, Grojean S, Lievre V, Strazielle C, Blaise S, Vert P (2004) Neonatal hypoxia triggers transient apoptosis followed by neurogenesis in the rat CA1 hippocampus. Pediatr Res 55:561–567

Dayer AG, Cleaver KM, Abouantoun T, Cameron HA (2005) GABAergic interneurons in the adult neocortex and striatum are generated from different precursors. J Cell Biol 168:415–427

Dempsey RJ, Sailor KA, Bowen KK, Tureyen K, Vemuganti R (2003) Stroke-induced progenitor cell proliferation in adult spontaneously hypertensive rat brain: effect of exogenous IGF-1 and GDNF. J Neurochem 87:586–597

Doetsch F, Alvarez-Buylla A (1996) Network of tangential pathways for neuronal migration in adult mammalian brain. Proc Natl Acad Sci USA 93:14895–14900

Du Bois M, Bowman PD, Goldstein GW (1985) Cell proliferation after ischemic infarction in gerbil brain. Brain Res 347:245–252

Duggal N, Schmidt-Kastner R, Hakim AM (1997) Nestin expression in reactive astrocytes following focal cerebral ischemia in rats. Brain Res 768:1–9

Eckenhoff MF, Rakic P (1988) Nature and fate of proliferative cells in the hippocampal dentate gyrus during the life span of the rhesus monkey. J Neurosci 8:2729–2747

Eriksson PS, Perfilieva E, Bjork-Eriksson T, Alborn AM, Nordborg C, Peterson DA, Gage FH (1998) Neurogenesis in the adult human hippocampus. Nat Med 4:1313–1317

Fagel DM, Ganat Y, Silbereis J, Ebbitt T, Stewart W, Zhang H, Ment LR, Vaccarino FM (2006) Cortical neurogenesis enhanced by chronic perinatal hypoxia. Exp Neurol 199:77–79

Felling RJ, Levison SW (2003) Enhanced neurogenesis following stroke. J Neurosci Res 73:277–283

Francis F, Koulakoff A, Boucher D, Chafey P, Schaar B, Vinet MC, Friocourt G, McDonnell N, Reiner O, Kahn A, McConnell SK, Berwald-Netter Y, Denoulet P, Chelly J (1999) Doublecortin is a developmentally regulated, microtubule-associated protein expressed in migrating and differentiating neurons. Neuron 23:247–256

Fujioka M, Nishio K, Miyamoto S, Hiramatsu KI, Sakaki T, Okuchi K, Taoka T, Fujioka S (2000) Hippocampal damage in the human brain after cardiac arrest. Cerebrovasc Dis 10:2–7

Gage FH (2000) Mammalian neural stem cells. Science 287:1433–1438

Gage FH, Kempermann G, Palmer TD, Peterson DA, Ray J (1998) Multipotent progenitor cells in the adult dentate gyrus. J Neurobiol 36:249–266

Garcia-Verdugo JM, Doetsch F, Wichterle H, Lim DA, Alvarez-Buylla A (1998) Architecture and cell types of the adult subventricular zone: in search of the stem cells. J Neurobiol 36:234–248

Gleeson JG, Lin PT, Flanagan LA, Walsh CA (1999) Doublecortin is a microtubule-associated protein and is expressed widely by migrating neurons. Neuron 23:257–271

Goldman SA, Nottebohm F (1983) Neuronal production, migration and differentiation in a vocal control nucleus of the adult female canary brain. Proc Natl Acad Sci USA 80:2390–2394

Gould E, Tanapat P, McEwen BS, Flugge G, Fuchs E (1998) Proliferation of granule cell precursors in the dentate gurus of adult monkeys is diminished by stress. Proc Natl Acad Sci USA 95:3168–3171

Gould E, Reeves AJ, Fallah M, Tanapat P, Gross CG, Fuchs E (1999a) Hippocampal neurogenesis in adult Old World primates. Proc Natl Acad Sci USA 96:5263–5267

Gould E, Reeves AJ, Graziano MS, Gross CG (1999b) Neurogenesis in the neocortex of adult primates. Science 286:548–552

Gould E, Vail N, Wagers M, Gross CG (2001) Adult-generated hippocampal and neocortical neurons in macaques have a transient existence. Proc Natl Acad Sci USA 98:10910–10917

Gown AM, Tsukada T, Ross R (1986) Human atherosclerosis. II. Immunocytochemical analysis of the cellular composition of human atherosclerotic lesions. Am J Pathol 125:191–207

Gross CG (1994) How inferior temporal cortex became a visual area. Cereb Cortex 4:455–469

Gross CG (2000) Neurogenesis in the adult brain: death of a dogma. Nat Rev Neurosci 1:67–73

Gustafsson E, Lindvall O, Kokaia Z (2003) Intraventricular infusion of TrkB-Fc fusion protein promotes ischemia-induced neurogenesis in adult rat dentate gyrus. Stroke 34:2710–2715

Hallbergson AF, Gnatenco C, Peterson DA (2003) Neurogenesis and brain injury: managing a renewable resource for repair. J Clin Invest 112:1128–1133

Hamilton A (1901) The division of differentiated cells in the central nervous system of the white rat. J Comp Neurol 11:297–320

Hendzel MJ, Wei Y, Mancini MA, Van Hooser A, Ranalli T, Brinkley BR, Bazett-Jones DP, Allis CD (1997) Mitosis-specific phosphorylation of histone H3 initiates primarily within pericentromeric heterochromatin during G2 and spreads in an ordered fashion coincident with mitotic chromosome condensation. Chromosoma 106:348–360

Hulette CM, Downey BT, Burger PC (1992) Macrophage markers in diagnostic neuropathology. Am J Surg Pathol 16:493–499

Imai Y, Ibata I, Ito D, Ohsawa K, Kohsaka S (1996) A novel gene iba1 in the major histocompatibility complex class III region encoding an EF hand protein expressed in a monocytic lineage. Biochem Biophys Res Commun 224:855–862

Imitola J, Raddassi K, Park KI, Mueller FJ, Nieto M, Teng YD, Frenkel D, Li J, Sidman RL, Walsh CA, Snyder EY, Khoury SJ (2004) Directed migration of neural stem cells to sites of CNS injury by the stromal cell-derived factor 1alpha/CXC chemokine receptor 4 pathway. Proc Natl Acad Sci USA 101:18117–18122

Ito D, Imai Y, Ohsawa K, Nakajima K, Fukuuchi Y, Kohsaka S (1998) Microglia-specific localization of a novel calcium binding protein, Iba1. Brain Res Mol Brain Res 57:1–9

Iwai M, Sato K, Omori N, Nagano I, Manabe Y, Shoji M, Abe K (2002) Three steps of neural stem cells development in gerbil dentate gyrus after transient ischemia. J Cereb Blood Flow Metab 22:411–419

Iwai M, Sato K, Kamada H, Omori N, Nagano I, Shoji M, Abe K (2003) Temporal profile of stem cell division, migration, and differentiation from subventricular zone to olfactory bulb after transient forebrain ischemia in gerbils. J Cereb Blood Flow Metab 23:331–341

Jiang W, Gu W, Brannstrom T, Rosqvist R, Wester P (2001) Cortical neurogenesis in adult rats after transient middle cerebral artery occlusion. Stroke 32:1201–1207

Jin K, Minami M, Lan JQ, Mao XO, Batteur S, Simon RP, Greenberg DA (2001) Neurogenesis in dentate subgranular zone and rostral subventricular zone after focal cerebral ischemia in the rat. Proc Natl Acad Sci USA 98:4710–4715

Jin K, Mao XO, Sun Y, Xie L, Jin L, Nishi E, Klagsbrun M, Greenberg DA (2002a) Heparin-binding epidermal growth factor-like growth factor: hypoxia-inducible expression in vitro and stimulation of neurogenesis in vitro and in vivo. J Neurosci 22:5365–5373

Jin K, Mao XO, Sun Y, Xie L, Greenberg DA (2002b) Stem cell factor stimulates neurogenesis in vitro and in vivo. J Clin Invest 110:311–319

Jin K, Sun Y, Xie L, Peel A, Mao XO, Batteur S, Greenberg DA (2003) Directed migration of neuronal precursors into the ischemic cerebral cortex and striatum. Mol Cell Neurosci 24:171–189

Jin K, Minami M, Xie L, Sun Y, Mao XO, Wang Y, Simon RP, Greenberg DA (2004) Ischemia-induced neurogenesis is preserved but reduced in the aged rodent brain. Aging Cell 3:373–377

Jongen-Relo AL, Pitkanen A, Amaral DG (1999) Distribution of GABAergic cells and fibers in the hippocampal formation of the macaque monkey: an immunohistochemical and in situ hybridization study. J Comp Neurol 408:237–271

Kageyama R, Hirata H, Hatakeyama J (2003) Retroviral vectors for gene delivery to neural precursor cells. Int Rev Neurobiol 55:123–147

Kaneko Y, Sakakibara S, Imai T, Suzuki A, Nakamura Y, Sawamoto K, Ogawa Y, Toyama Y, Miyata T, Okano H (2000) Musashi1: an evolutionally conserved marker for CNS progenitor cells including neural stem cells. Dev Neurosci 22:139–153

Kaplan MS (1981) Neurogenesis in the 3-month-old rat visual cortex. J Comp Neurol 195:323–338

Kaplan MS (1983) Proliferation of subependymal cells in the adult primate CNS: differential uptake of DNA labelled precursors. J Hirnforsch 24:23–33

Kaplan MS, Bell DH (1983) Neuronal proliferation in the 9-month-old rodent—radioautographic study of granule cells in the hippocampus. Exp Brain Res 52:1–5

Kaplan MS, Bell DH (1984) Mitotic neuroblasts in the 9-day-old and 11-month-old rodent hippocampus. J Neurosci 4:1429–1441

Kaplan MS, Hinds JW (1977) Neurogenesis in the adult rat: electron microscopic analysis of light radioautographs. Science 197:1092–1094

Katchanov J, Harms C, Gertz K, Hauck L, Waeber C, Hirt L, Priller J, von Harsdorf R, Bruck W, Hortnagl H, Dirnagl U, Bhide PG, Endres M (2001) Mild cerebral ischemia induces loss of cyclin-dependent kinase inhibitors and activation of cell cycle machinery before delayed neuronal cell death. J Neurosci 21:5045–5053

Kee N, Sivalingam S, Boonstra R, Wojtowicz JM (2002) The utility of Ki-67 and BrdU as proliferative markers of adult neurogenesis. J Neurosci Methods 115:97–105

Kee NJ, Preston E, Wojtowicz JM (2001) Enhanced neurogenesis after transient global ischemia in the dentate gyrus of the rat. Exp Brain Res 136:313–320

Keynes RG, Garthwaite J (2004) Nitric oxide and its role in ischaemic brain injury. Curr Mol Med 4:179–191

Kirino T (1982) Delayed neuronal death in the gerbil hippocampus following ischemia. Brain Res 239:57–69

Kohda Y, Yamashima T, Sakuda K, Yamashita J, Ueno T, Kominami E, Yoshioka T (1996) Dynamic changes of cathepsins B and L expression in the monkey hippocampus after transient ischemia. Biochem Biophys Res Commun 228:616–622

Kohwi M, Osumi N, Rubenstein JL, Alvarez-Buylla A (2005) Pax6 is required for making specific subpopulations of granule and periglomerular neurons in the olfactory bulb. J Neurosci 25:6997–7003

Kokaia Z, Lindvall O (2003) Neurogenesis after ischaemic brain insults. Curr Opin Neurobiol 13:127–132

Koketsu D, Mikami A, Miyamoto Y, Hisatsune T (2003) Nonrenewal of neurons in the cerebral neocortex of adult macaque monkeys. J Neurosci 23:937–942

Komitova M, Mattsson B, Johansson BB, Eriksson PS (2005a) Enriched environment increases neural stem/progenitor cell proliferation and neurogenesis in the subventricular zone of stroke-lesioned adult rats. Stroke 36:1278–1282

Komitova M, Zhao LR, Gido G, Johansson BB, Eriksson P (2005b) Postischemic exercise attenuates whereas enriched environment has certain enhancing effects on lesion-induced subventricular zone activation in the adult rat. Eur J Neurosci 21:2397–2405

Kornack DR (2000) Neurogenesis and the evolution of cortical diversity: mode, tempo, and partitioning during development and persistence in adulthood. Brain Behav Evol 55:336–344

Kornack DR, Rakic P (1999) Continuation of neurogenesis in the hippocampus of the adult macaque monkey. Proc Natl Acad Sci USA 96:5768–5773

Kornack DR, Rakic P (2001a) The generation, migration, and differentiation of olfactory neurons in the adult primate brain. Proc Natl Acad Sci USA 98:4752–4757

Kornack DR, Rakic P (2001b) Cell proliferation without neurogenesis in adult primate neocortex. Science 294:2127–2130

Kronenberg G, Wang LP, Synowitz M, Gertz K, Katchanov J, Glass R, Harms C, Kempermann G, Kettenmann H, Endres M (2005) Nestin-expressing cells divide and adopt a complex electrophysiologic phenotype after transient brain ischemia. J Cereb Blood Flow Metab 25:1613–1624

Kuan CY, Schloemer AJ, Lu A, Burns KA, Weng WL, Williams MT, Strauss KI, Vorhees CV, Flavell RA, Davis RJ, Sharp FR, Rakic P (2004) Hypoxia-ischemia induces DNA synthesis without cell proliferation in dying neurons in adult rodent brain. J Neurosci 24:10763–10772

Kuhn HG, Dickinson-Anson H, Gage FH (1996) Neurogenesis in the dentate gyrus of the adult rat: age-related decrease of neuronal progenitor proliferation. J Neurosci 16:2027–2033

Kuhn HG, Palmer TD, Fuchs E (2001) Adult neurogenesis: a compensatory mechanism for neuronal damage. Eur Arch Psychiatry Clin Neurosci 251:152–158

Larsson E, Mandel RJ, Klein RL, Muzyczka N, Lindvall O, Kokaia Z (2002) Suppression of insult-induced neurogenesis in adult rat brain by brain-derived neurotrophic factor. Exp Neurol 177:1–8

Lee MK, Rebhun LI, Frankfurter A (1990) Posttranslational modification of class III beta-tubulin. Proc Natl Acad Sci USA 87:7195–7199

Lendahl U, Zimmerman LB, McKay RD (1990) CNS stem cells express a new class of intermediate filament protein. Cell 60:585–595

Levison SW, Rothstein RP, Romanko MJ, Snyder MJ, Meyers RL, Vannucci SJ (2001) Hypoxia/ischemia depletes the rat perinatal subventricular zone of oligodendrocyte progenitors and neural stem cells. Dev Neurosci 23:234–247

Lewis PD (1968) Mitotic activity in the primate subependymal layer and the genesis of gliomas. Nature 217:974–975
Lichtenwalner RJ, Parent JM (2006) Adult neurogenesis and the ischemic forebrain. J Cereb Blood Flow Metab 26:1–20
Lie DC, Song H, Colamarino SA, Ming GL, Gage FH (2004) Neurogenesis in the adult brain: new strategies for central nervous system diseases. Annu Rev Pharmacol Toxicol 44:399–421
Lindvall O, Kokaia Z (2004) Recovery and rehabilitation in stroke: stem cells. Stroke 35(Suppl 1):2691–2694
Lipton P (1999) Ischemic cell death in brain neurons. Physiol Rev 79:1431–1568
Liu J, Solway K, Messing RO, Sharp FR (1998) Increased neurogenesis in the dentate gyrus after transient global ischemia in gerbils. J Neurosci 18:7768–7778
Liu J, Bartels M, Lu A, Sharp FR (2001b) Microglia/macrophages proliferate in striatum and neocortex but not in hippocampus after brief global ischemia that produces ischemic tolerance in gerbil brain. J Cereb Blood Flow Metab 21:361–373
Liu PK, Grossman RG, Hsu CY, Robertson CS (2001a) Ischemic injury and faulty gene transcripts in the brain. Trends Neurosci 24:581–588
Lois C, Garcia-Verdugo JM, Alvarez-Buylla A (1996) Chain migration of neuronal precursors. Science 271:978–981
Lorente de No R (1934) Studies on the structure of the cerebral cortex. II. Continuation of the study of the Ammonic system. J Psychol Neurol 46:113–177
Love S, Barber R, Wilcock GK (1998) Apoptosis and expression of DNA repair proteins in ischaemic brain injury in man. Neuroreport 9:955–959
Love S, Barber R, Wilcock GK (1999) Neuronal accumulation of poly(ADP-ribose) after brain ischaemia. Neuropathol Appl Neurobiol 25:98–103
Luskin MB (1993) Restricted proliferation and migration of postnatally generated neurons derived from the forebrain subventricular zone. Neuron 11:173–189
Magavi SS, Leavitt BR, Macklis JD (2000) Induction of neurogenesis in the neocortex of adult mice. Nature 405:951–955
Maslov AY, Barone TA, Plunkett RJ, Pruitt SC (2004) Neural stem cell detection, characterization, and age-related changes in the subventricular zone of mice. J Neurosci 24:1726–1733
McDermott KW, Lantos PL (1991) Cell proliferation in the subependymal layer of the postnatal marmoset, Callithrix jacchus. Brain Res Dev Brain Res 57:269–277
Messier B, Leblond CP, Smart I (1958) Presence of DNA synthesis and mitosis in the brain of young adult mice. Exp Cell Res 14:224–226
Miller MW, Nowakowski RS (1988) Use of bromodeoxyuridine-immunohistochemistry to examine the proliferation, migration and time of origin of cells in the central nervous system. Brain Res 457:44–52
Miyata T, Ogawa M (1994) Developmental potentials of early telencephalic neuroepithelial cells: a study with microexplant culture. Dev Growth Differ 36:319–331
Mizuguchi M, Qin J, Yamada M, Ikeda K, Takashima S (1999) High expression of doublecortin and KIAA0369 protein in fetal brain suggests their specific role in neuronal migration. Am J Pathol 155:1713–1721
Mullen RJ, Buck CR, Smith AM (1992) NeuN, a neuronal specific nuclear protein in vertebrates. Development 116:201–211
Nakatomi H, Kuriu T, Okabe S, Yamamoto S, Hatano O, Kawahara N, Tamura A, Kirino T, Nakafuku M (2002) Regeneration of hippocampal pyramidal neurons after ischemic brain injury by recruitment of endogenous neural progenitors. Cell 110:429–441

Nemoto EM, Bleyaert AL, Stezoski SW, Moossy J, Rao GR, Safar P (1977) Global brain ischemia: a reproducible monkey model. Stroke 8:558–564

Neubuerger KT (1954) Lesions of the human brain following circulatory arrest. J Neuropathol Exp Neurol 13:144–260

Nottebohm F (2002) Neuronal replacement in adult brain. Brain Res Bull 57:737–749

Nowakowski RS, Hayes NL (2001) Stem cells: the promises and pitfalls. Neuropsychopharmacology 25:799–804

Nunes MC, Roy NS, Keyoung HM, Goodman RR, McKhann G 2nd, Jiang L, Kang J, Nedergaard M, Goldman SA (2003) Identification and isolation of multipotential neural progenitor cells from the subcortical white matter of the adult human brain. Nat Med 9:439–447

Okano HJ, Darnell RB (1997) A hierarchy of Hu RNA binding proteins in developing and adult neurons. J Neurosci 17:3024–3037

Ourednik V, Ourednik J, Flax JD, Zawada WM, Hutt C, Yang C, Park KI, Kim SU, Sidman RL, Freed CR, Snyder EY (2001) Segregation of human neural stem cells in the developing primate forebrain. Science 293:1820–1824

Packard DS, Menzies RA, Skalko DG (1973) Incorporation of thymidine and its analogue, bromodeoxyuridine, into the embryos and maternal tissues of the mouse. Differentiation 1:397–405

Pagano SF, Impagnatiello F, Girelli M, Cova L, Grioni E, Onofri M, Cavallaro M, Etteri S, Vitello F, Giombini S, Solero CL, Parati EA (2000) Isolation and characterization of neural stem cells from the adult human olfactory bulb. Stem Cells 18:295–300

Parent JM (2003) Injury-induced neurogenesis in the adult mammalian brain. Neuroscientist 9:261–272

Parent JM, Vexler ZS, Gong C, Derugin N, Ferriero DM (2002) Rat forebrain neurogenesis and striatal neuron replacement after focal stroke. Ann Neurol 52:802–813

Paton JA, Nottebohm F (1984) Neurons generated in the adult brain are recruited into functional circuits. Science 225:1046–1048

Pencea V, Bingaman KD, Wiegand SJ, Luskin MB (2001a) Infusion of brain-derived neurotrophic factor into the lateral ventricle of the adult rat leads to new neurons in the parenchyma of the striatum, septum, thalamus, and hypothalamus. J Neurosci 21:6706–6717

Pencea V, Bingaman KD, Freedman LJ, Luskin MB (2001b) Neurogenesis in the subventricular zone and rostral migratory stream of the neonatal and adult primate forebrain. Exp Neurol 172:1–16

Petito CK, Feldmann E, Pulsinelli WA, Plum F (1987) Delayed hippocampal damage in humans following cardiorespiratory arrest. Neurology 37:1281–1286

Pevny L, Rao MS (2003) The stem-cell menagerie. Trends Neurosci 26:351–359

Picard-Riera N, Nait-Oumesmar B, Baron-Van Evercooren A (2004) Endogenous adult neural stem cells: limits and potential to repair the injured central nervous system. J Neurosci Res 76:223–231

Plane JM, Liu R, Wang TW, Silverstein FS, Parent JM (2004) Neonatal hypoxic–ischemic injury increases forebrain subventricular zone neurogenesis in the mouse. Neurobiol Dis 16:585–595

Pulsinelli WA, Brierly JB, Plum F (1982) Temporal profile of neuronal damage in a model of transient brain ischemia. Ann Neurol 11:491–498

Quinn CC, Gray GE, Hockfield S (1999) A family of proteins implicated in axon guidance and outgrowth. J Neurobiol 41:158–164

Raber J, Fan Y, Matsumori Y, Liu Z, Weinstein PR, Fike JR, Liu J (2004) Irradiation attenuates neurogenesis and exacerbates ischemia-induced deficits. Ann Neurol 55:381–389

Rakic P (1985a) Limits of neurogenesis in primates. Science 227:1054–1056
Rakic P (1985b) DNA synthesis and cell division in the adult primate brain. Ann N Y Acad Sci 457:193–211
Rakic P (2002a) Adult neurogenesis in mammals: an identity crisis. J Neurosci 22:614–618
Rakic P (2002b) Neurogenesis in adult primate neocortex: an evaluation of the evidence. Nat Rev Neurosci 3:65–71
Ramon y Cajal S (1928) Degeneration and regeneration of the nervous system. vol. 2. Haffner Publishing, New York, p. 750
Rempel-Clower NL, Zola SM, Squire LR, Amaral DG (1996) Three cases of enduring memory impairment after bilateral damage limited to the hippocampal formation. J Neurosci 16:5233–5255
Rich T, Allen RL, Wyllie AH (2000) Defying death after DNA damage. Nature 407:777–783
Roy NS, Wang S, Jiang L, Kang J, Benraiss A, Harrison-Restelli C, Fraser RA, Couldwell WT, Kawaguchi A, Okano H, Nedergaard M, Goldman SA (2000) In vitro neurogenesis by progenitor cells isolated from the adult human hippocampus. Nat Med 6:271–277
Saeger W (2004) Proliferation markers and cell cycle inhibitors in pituitary adenomas. Front Horm Res 32:110–126
Sakakibara S, Okano H (1997) Expression of neural RNA-binding proteins in the postnatal CNS: implications of their roles in neuronal and glial cell development. J Neurosci 17:8300–8312
Sakakibara S, Imai T, Hamaguchi K, Okabe M, Aruga J, Nakajima K, Yasutomi D, Nagata T, Kurihara Y, Uesugi S, Miyata T, Ogawa M, Mikoshiba K, Okano H (1996) Mouse-Musashi1, a neural RNA-binding protein highly enriched in the mammalian CNS stem cell. Dev Biol 176:230–242
Schmidt W, Reymann KG (2002) Proliferating cells differentiate into neurons in the hippocampal CA1 region of gerbils after global cerebral ischemia. Neurosci Lett 334:153–156
Schmued LC, Hopkins KJ (2000) Fluoro–Jade B: a high affinity fluorescent marker for the localization of neuronal degeneration. Brain Res 874:123–130
Schneider A, Kruger C, Steigleder T, Weber D, Pitzer C, Laage R, Aronowski J, Maurer MH, Gassler N, Mier W, Hasselblatt M, Kollmar R, Schwab S, Sommer C, Bach A, Kuhn HG, Schabitz WR (2005) The hematopoietic factor G-CSF is a neuronal ligand that counteracts programmed cell death and drives neurogenesis. J Clin Invest 115:2083–2098
Scholzen T, Gerdes J (2000) The Ki-67 protein: from the known and the unknown. J Cell Physiol 182:311–322
Schultze B, Oehlert W (1960) Autoradiographic investigation of incorporation of H3-thymidine into cells of the rat and mouse. Science 131:737–738
Seki T, Arai Y (1993) Highly polysialylated neural cell adhesion molecule (NCAM-H) is expressed by newly generated granule cells in the dentate gyrus of the adult rat. J Neurosci 13:2351–2358
Seri B, Garcia-Verdugo JM, McEwen BS, Alvarez-Buylla A (2001) Astrocytes give rise to new neurons in the adult mammalian hippocampus. J Neurosci 21:7153–7160
Sharp FR, Liu J, Bernabeu R (2002) Neurogenesis following brain ischemia. Brain Res Dev Brain Res 134:23–30
Shyu WC, Lin SZ, Yang HI, Tzeng YS, Pang CY, Yen PS, Li H (2004) Functional recovery of stroke rats induced by granulocyte colony-stimulating factor-stimulated stem cells. Circulation 110:1847–1854
Smith ML, Auer RN, Siesjo BK (1984) The density and distribution of ischemic brain injury in the rat following 2–10 min of forebrain ischemia. Acta Neuropathol (Berl) 64:319–332
Squire LR, Zola SM (1996) Ischemic brain damage and memory impairment: a commentary. Hippocampus 6:546–552

Squire LR, Zola-Morgan S (1991) The medial temporal lobe memory system. Science 253:1380–1386

Strahl BD, Allis CD (2000) The language of covalent histone modifications. Nature 403:41–45

Streitfeld BD (1980) The fiber connections of the temporal lobe with emphasis on the rhesus monkey. Int J Neurosci 11:51–71

Sugiura S, Kitagawa K, Tanaka S, Todo K, Omura-Matsuoka E, Sasaki T, Mabuchi T, Matsushita K, Yagita Y, Hori M (2005) Adenovirus-mediated gene transfer of heparin-binding epidermal growth factor-like growth factor enhances neurogenesis and angiogenesis after focal cerebral ischemia in rats. Stroke 36:859–864

Sun Y, Jin K, Xie L, Childs J, Mao XO, Logvinova A, Greenberg DA (2003) VEGF-induced neuroprotection, neurogenesis, and angiogenesis after focal cerebral ischemia. J Clin Invest 111:1843–1851

Tabuchi E, Endo S, Ono T, Nishijo H, Kuze S, Kogure K (1992) Hippocampal neuronal damage after transient forebrain ischemia in monkeys. Brain Res Bull 29:685–690

Tabuchi E, Ono T, Nishijo H, Endo S, Kuze S (1995) Ischemic neuronal damage specific to monkey hippocampus: histological investigation. Brain Res Bull 37:73–87

Takagi Y, Nozaki K, Takahashi J, Yodoi J, Ishikawa M, Hashimoto N (1999) Proliferation of neuronal precursor cells in the dentate gyrus is accelerated after transient forebrain ischemia in mice. Brain Res 831:283–287

Takasawa K, Kitagawa K, Yagita Y, Sasaki T, Tanaka S, Matsushita K, Ohstuki T, Miyata T, Okano H, Hori M, Matsumoto M (2002) Increased proliferation of neural progenitor cells but reduced survival of newborn cells in the contralateral hippocampus after focal cerebral ischemia in rats. J Cereb Blood Flow Metab 22:299–307

Tanaka R, Yamashiro K, Mochizuki H, Cho N, Onodera M, Mizuno Y, Urabe T (2004) Neurogenesis after transient global ischemia in the adult hippocampus visualized by improved retroviral vector. Stroke 35:1454–1459

Teramoto T, Qiu J, Plumier JC, Moskowitz MA (2003) EGF amplifies the replacement of parvalbumin-expressing striatal interneurons after ischemia. J Clin Invest 111:1125–1132

Tonchev AB, Yamashima T, Zhao L, Okano HJ, Okano H (2003a) Proliferation of neural and neuronal progenitors after global brain ischemia in young adult macaque monkeys. Mol Cell Neurosci 23:292–301

Tonchev AB, Yamashima T, Zhao L, Okano H (2003b) Differential proliferative response in the postischemic hippocampus, temporal cortex and olfactory bulb of young adult macaque monkeys. Glia 42:209–224

Tonchev AB, Yamashima T, Sawamoto K, Okano H (2005) Enhanced proliferation of progenitor cells in the subventricular zone and limited neuronal production in the striatum and neocortex of adult macaque monkeys after global cerebral ischemia. J Neurosci Res 81:776–788

Tontchev AB, Yamashima T (1999) Ischemic delayed neuronal death: the role of cysteine proteases calpain and cathepsin. Neuropathology 19:356–365

Tsuchiya K, Kohda Y, Yoshida M, Zhao L, Ueno T, Yamashita J, Yoshioka T, Kominami E, Yamashima T (1999) Postictal blockade of ischemic hippocampal neuronal death in primates using selective cathepsin inhibitors. Exp Neurol 155:187–194

Tsukada T, Watanabe M, Yamashima T (2001) Implications of CAD and DNase II in ischemic neuronal necrosis specific for the primate hippocampus. J Neurochem 79:1196–1206

van Hoesen GW (1982) The parahippocampal gyrus: new observations regarding its cortical connections in the monkey. Trends Neurosci 5:345–350

van Praag H, Schinder AF, Christie BR, Toni N, Palmer TD, Gage FH (2002) Functional neurogenesis in the adult hippocampus. Nature 415:1030–1034

Wakamatsu Y, Weston JA (1997) Sequential expression and role of Hu RNA-binding proteins during neurogenesis. Development 124:3449–3460

Wolin LR, Massopust LC Jr, Taslitz N (1971) Tolerance to arrest of cerebral circulation in the rhesus monkey. Exp Neurol 30:103–115

Yagita Y, Kitagawa K, Ohtsuki T, Takasawa KI, Miyata T, Okano H, Hori M, Matsumoto M (2001) Neurogenesis by progenitor cells in the ischemic adult rat hippocampus. Stroke 32:1890–1896

Yamashima T (2000) Implication of cysteine proteases calpain, cathepsin and caspase in ischemic neuronal death of primates. Prog Neurobiol 62:273–295

Yamashima T, Takita M, Akaike S, Hirano M, Miyakawa A, Miyazawa A, Kudo Y, Yoshioka T (1994) Temperature-dependent Ca^{2+} mobilization induced by hypoxia-hypoglycemia in the monkey hippocampal slices. Biochem Biophys Res Commun 205:1843–1849

Yamashima T, Saido TC, Takita M, Miyazawa A, Yamano J, Miyakawa A, Nishijyo H, Yamashita J, Kawashima S, Ono T, Yoshioka T (1996) Transient brain ischaemia provokes Ca^{2+}, PIP2 and calpain responses prior to delayed neuronal death in monkeys. Eur J Neurosci 8:1932–1944

Yamashima T, Kohda Y, Tsuchiya K, Ueno T, Yamashita J, Yoshioka T, Kominami E (1998) Inhibition of ischaemic hippocampal neuronal death in primates with cathepsin B inhibitor CA-074: a novel strategy for neuroprotection based on 'calpain-cathepsin hypothesis'. Eur J Neurosci 10:1723–1733

Yamashima T, Tonchev AB, Vachkov IH, Popivanova BK, Tatsunori Seki T, Sawamoto K, Okano H (2004) Vascular adventitia generates neuronal progenitors in the monkey hippocampus after ischemia. Hippocampus 14:861–875

Yamashima T, Tonchev AB, Tsukada T, Saido TC, Imajoh-Ohmi S, Momoi T, Kominami E (2003) Sustained calpain activation associated with lysosomal rupture executes necrosis of the postischemic CA1 neurons in primates. Hippocampus 13:791–800

Yang Y, Geldmacher DS, Herrup K (2001) DNA replication precedes neuronal cell death in Alzheimer's disease. J Neurosci 21:2661–2668

Yoshida M, Yamashima T, Zhao L, Tsuchiya K, Kohda Y, Tonchev AB, Matsuda M, Kominami E (2002) Primate neurons show different vulnerability to transient ischemia and response to cathepsin inhibition. Acta Neuropathol (Berl) 104:267–272

Yoshimura S, Takagi Y, Harada J, Teramoto T, Thomas SS, Waeber C, Bakowska JC, Breakefield XO, Moskowitz MA (2001) FGF-2 regulation of neurogenesis in adult hippocampus after brain injury. Proc Natl Acad Sci USA 98:5874–5879

Zhang R, Zhang Z, Zhang C, Zhang L, Robin A, Wang Y, Lu M, Chopp M (2004) Stroke transiently increases subventricular zone cell division from asymmetric to symmetric and increases neuronal differentiation in the adult rat. J Neurosci 24:5810–5815

Zhang RL, Zhang ZG, Zhang L, Chopp M (2001) Proliferation and differentiation of progenitor cells in the cortex and the subventricular zone in the adult rat after focal cerebral ischemia. Neuroscience 105:33–41

Zhang RL, Zhang ZG, Chopp M (2005) Neurogenesis in the adult ischemic brain: generation, migration, survival, and restorative therapy. Neuroscientist 11:408–416

Zigova T, Pencea V, Wiegand SJ, Luskin MB (1998) Intraventricular administration of BDNF increases the number of newly generated neurons in the adult olfactory bulb. Mol Cell Neurosci 11:234–245

Zola-Morgan S, Squire LR, Amaral DG (1986) Human amnesia and the medial temporal region: enduring memory impairment following a bilateral lesion limited to field CA1 of the hippocampus. J Neurosci 6:2950–2967

Zola-Morgan S, Squire LR, Rempel NL, Clower RP, Amaral DG (1992) Enduring memory impairment in monkeys after ischemic damage to the hippocampus. J Neurosci 12:2582–2596

Subject Index